2022

EXPERIMENTAL COMPARISON OF TWO SAMPLED-DATA ADAPTIVE CONTROL ALGORITHMS FOR REJECTING SINUSOIDAL DISTURBANCES

William Grayson Woods
University of Kentucky, woods.grayson10@gmail.com
Digital Object Identifier: https://doi.org/10.13023/etd.2022.323

STUDENT AGREEMENT:

I represent that my thesis or dissertation and abstract are my original work. Proper attribution has been given to all outside sources. I understand that I am solely responsible for obtaining any needed copyright permissions. I have obtained needed written permission statement(s) from the owner(s) of each third-party copyrighted matter to be included in my work, allowing electronic distribution (if such use is not permitted by the fair use doctrine) which will be submitted to UKnowledge as Additional File.

I hereby grant to The University of Kentucky and its agents the irrevocable, non-exclusive, and royalty-free license to archive and make accessible my work in whole or in part in all forms of media, now or hereafter known. I agree that the document mentioned above may be made available immediately for worldwide access unless an embargo applies.

I retain all other ownership rights to the copyright of my work. I also retain the right to use in future works (such as articles or books) all or part of my work. I understand that I am free to register the copyright to my work.

REVIEW, APPROVAL AND ACCEPTANCE

The document mentioned above has been reviewed and accepted by the student's advisor, on behalf of the advisory committee, and by the Director of Graduate Studies (DGS), on behalf of the program; we verify that this is the final, approved version of the student's thesis including all changes required by the advisory committee. The undersigned agree to abide by the statements above.

William Grayson Woods, Student

Dr. Jesse Hoagg, Major Professor

Dr. Jesse Hoagg, Director of Graduate Studies

EXPERIMENTAL COMPARISON OF TWO SAMPLED-DATA ADAPTIVE CONTROL ALGORITHMS FOR REJECTING SINUSOIDAL DISTURBANCES

THESIS

A thesis submitted in partial fulfillment of the requirements for the degree of Master of Science in Mechanical Engineering in the College of Engineering at the University of Kentucky

By
William Grayson Woods

Advisor: Jesse B. Hoagg, Professor of Mechanical Engineering

Lexington, Kentucky, August 1, 2022

ABSTRACT OF THESIS

EXPERIMENTAL COMPARISON OF TWO SAMPLED-DATA ADAPTIVE CONTROL ALGORITHMS FOR REJECTING SINUSOIDAL DISTURBANCES

We review two adaptive control algorithms that address the problem of rejecting sinusoids with known frequencies that act on an unknown asymptotically stable linear time-invariant system. We present modifications to the algorithms that address the problems of sensor noise and actuator saturation. We demonstrate the effectiveness of the algorithms and compare the performance of the algorithms via numerical simulation and experimental testings.

KEYWORDS: Adaptive, Disturbance Rejection, Harmonic, Unknown System

Author's signature: William Grayson Woods

Date: August 1, 2022

EXPERIMENTAL COMPARISON OF TWO SAMPLED-DATA ADAPTIVE CONTROL ALGORITHMS FOR REJECTING SINUSOIDAL DISTURBANCES

By
William Grayson Woods

Director of Thesis: Prof. Jesse B. Hoagg

Director of Graduate Studies: Prof. Jesse B. Hoagg

Date: August 1, 2022

To my wife, parents, brother, and sister for their unwavering support.

ACKNOWLEDGMENTS

First, I would like to thank my adviser, Dr. Hoagg, for all of his help and guidance over the years. I first became interested in control theory through an undergraduate controls course Dr. Hoagg taught. This course was the key factor that sparked my interest in the subject of control theory. His engaging and methodical teaching style, along with his ability to communicate complex ideas in simple ways, is something I admire even to this day. I owe Dr. Hoagg an immense dept of gratitude for all of the time, energy, and patience he has provided over the last few years. Accomplishing this goal and dream would not have been possible without his help and support.

In addition, I would like to thank all of my friends and colleagues at the University of Kentucky. Two people in particular that I would like to thank are Dr. Henninger and Dr. Colliver. They allowed me the opportunity to grow and learn under their leadership at the Kentucky Industrial Assessment Center. I have great memories of this program, and I will always look back fondly on the time I spent with the great people there.

Finally, I would like to especially thank my spectacular wife Jenna, my loving parents Mark and Ginny Woods, and my sister Maggie and brother Mark for their unwavering support over the years. Through great times and through difficult times they have always supported me and have had my back. I could not ask for better people in my life.

LIST OF FIGURES

LIST OF TABLES

Chapter 1
Motivation and Introduction

1.1 Motivation

Noise attenuation and vibration control are key problems in engineering. Problems with noise and vibration often arise in buildings, helicopters, computer hard disks, active noise control, spacecrafts, and other areas. While much progress has been made in the field to address this problem, many of the traditional techniques rely on information about the system in order to reject disturbances.

In building design, a common problem is the suppression of noise and vibration that manifest from mechanical equipment and natural phenomina such as wind. For example, very tall buildings are routinely subject to wind-induced vibrations that manifest as sinusoidal disturbances [1]. While methods have been developed to address the problem, they often rely on information about the system dynamics or disturbances. For example, in the case of mechanical equipment generating noise or vibration, a typical solution involves selecting vibration spring isolators which dampen the vibration transmitted to the building. However, selecting a proper vibration spring isolation system requires the engineer to know some physical parameters about the mechanical system in question [2]. Another problem engineers face is the design of air distribution systems in sound sensitive areas (such as auditoriums and learning environments). To attenuate noise that is generated from air traveling through a duct, engineers will often oversize the ductwork to reduce the velocity of the air or add expensive sound attenuators or internal acoustical insulation. While these strategies can be effective, they tend to increase building costs, add complexity to the design, and can also reduce the space that is available to route other above ceiling utilities.

In helicopter design and operation, a key problem engineers seek to address is the suppression of vibration [3]. Vibration typically manifests in the fuselage as a result of the helicopters main rotor blades rotating at high speeds and experiencing unsteady airloads. As a result, mechanical components can degrade and fail over time and crew members can experience uncomfortable rides resulting in fatigue. In fact, in the 1960s, the average cabin floor vibration levels were around 0.3 g, which contributed to an extremely uncomfortable ride experience for the occupants [4]. In

recent years, vibration levels have decreased to 0.1 g to 0.2 g; however, opportunities remain to decrease these levels further. While solutions have been offered to address this problem, most techniques require information about the disturbance or system dynamics to implement.

In computer hard disks, vibration compensation is of great importance to ensure optimized operation. Advances in operating systems and computing power will continue to affect the demand for larger disk drives. In fact, it is estimated that the track density (which significantly affects the capacity of disk drives) will increase from the current 6,000 tracks per inch (tpi) to over 30,000 tpi by the end of the century. Within hard disks, a read/write head positioning servo mechanism is present which is either track seeking or track following. To achieve optimal performance, the head positioning servo mechanism must attenuate vibration, the primary factor contributing to poor accuracy. For this reason, it is critical that solutions are offered to address the problem of vibration within hard disk drives to ensure that performance can keep up with demand [5]. While control solutions are available to attenuate the vibration, most algorithms require an accurate model of the system dynamics or disturbance frequencies and harmonics to implement. For example, in [6], a control was introduced which used information about an open-loop transfer function to design both the control and the structure which resulted in a 55% increase in positioning accuracy. While this increase in head positioning accuracy is significant, the controller requires an accurate model of the system dynamics, which are often unknown or subject to great uncertainty.

With the growth of technology and industry, the presence of acoustic noise has become a concern from both a health and quality of life standpoint. Noisy conditions in manufacturing and travel (such as trains and air planes), and noise generated in busy urban areas are problems engineers are trying to address [7]. One solution is active noise control (ANC). In ANC, an unwanted sound or disturbance is reduced or eliminated by introducing a secondary sound of equal magnitude and opposite phase. In the ideal case, ANC techniques can be implemented to address an unwanted sound or disturbance that may have characteristics that change over time. ANC techniques have been shown to be effective in some applications such as head phone design. For example, in [8], the design and implementation of an ANC system for head phone applications is presented and implemented in an experiment. Results show that the algorithm was capable of achieving high noise cancellation rates, especially for low-frequency harmonics. ANC methods have also been shown to be successful in practice; however, they typically require knowledge about the system or rely on approximations and assumptions about the system to implement effectively. For example, in [9], a controller is presented which is capable of rejecting unknown disturbances acting on a SISO system. However, the controller requires a sufficiently accurate model of the plant as well as a frequency estimator to estimate the frequency of the disturbance for successful implementation.

In flexible spacecraft design, vibration suppression is a key objective. As engineers continue to challenge their designs, spacecrafts continue to get lighter and more flexible which yields susceptibility to unwanted vibration. For example, orbiting spacecrafts often have a rigid body with attached flexible appendages such as

antennas and solar panels for the purpose of communication, remote sensing, and other useful functions. In addition, mission requirements often warrant demanding rotational maneuvers and sudden movements induced by thrust which can induce vibrations [10]. These elements make vibration suppression using traditional control strategies more challenging as the system dynamics often change over time or are subject to uncertainty.

In real world applications, it is not always possible to accurately model the system in question. Developing an accurate system model can be an extremely time intensive process. Many models are designed using assumptions or approximations to reduce the complexity of the modeling process, which can result in models that may not accurately represent the dynamics of the physical system being modeled. However, while it can be difficult to model a system accurately, it is often possible to measure, or estimate, a sinusoidal disturbance (such as noise or vibration) acting on a system. For example, in noise applications, one can determine the frequency content of a disturbance by performing a discrete Fourier transform. In vibration applications, one can analyze the vibration using an accelerometer to understand the disturbance. This is significant because control algorithms have been developed which are capable of asymptotically rejecting the disturbance, with minimal or even no knowledge of the system as discussed in the literature review.

While progress has been made in the development of such control methods, typically these algorithms are implemented in numerical simulations rather than experimental settings for use in verification or validation of the algorithm. Numerical simulations typically constrain the algorithm to optimal conditions which cannot always be guaranteed in practical implementations due to factors including measurement uncertainty, sensor noise, and actuator saturation. Thus, we are motivated to further analyze these algorithms in experimental applications; specifically, we analyze the frequency domain algorithm presented in [11] and the time domain algorithm presented in [12] which are adaptive control algorithms capable of eliminating known disturbances acting on completely unknown systems.

1.2 Literature Review

The internal model principle is a feedback control technique that can be used for tracking references and rejecting sinusoidal disturbances. The internal model principle states that asymptotic disturbance rejection or command following can be achieved by incorporating copies of the exogenous dynamics in the feedback loop [13]. This technique can be effective, but requires information about the disturbance and system which is not always known. For example, in [14], a control is presented which regulates and internally stabilizes a linear time-invariant system in the presence of external signals; however, the control requires information about both the disturbance and the plant to implement.

While the internal model principle requires information about both the system and disturbance to implement, it can be used in scenarios when the disturbance is not known through the use of a model based observer. A model based observer is an observation mechanism designed to estimate disturbances when they are unknown [15].

In [16], an adaptive feedback controller is developed based on the internal model principle which utilizes a frequency estimator, but some information about the system is still required for implementation. In [17], disturbance rejection for a class of nonlinear multi-input multi-ouput (MIMO) systems is presented using a controller that utilizes a disturbance-based observer to estimate the disturbance. However, information about the system is required to implement.

Adaptive feedforward cancellation is a technique that can be implemented to address disturbances acting on an uncertain or unknown system. In general, it works by adding a copy of the disturbance with updated amplitudes and phases to asymptotically reject the disturbance. In the simplest single-input single-output (SISO) case, adaptive feedfoward cancellation cancels the disturbance at the input of the plant by adding a "negative" copy of the disturbance, that is, a copy of the disturbance with a negative amplitude [18]. To asymptotically reject the disturbance, the amplitudes of the "negative" disturbance copy must be adapted to converge to nominal values that completely cancel the disturbance. One shortcoming of this technique is that certain assumptions or model information is required to implement. For example, in [19], an adaptive feedfoward algorithm is presented which is capable of rejecting a disturbance. However, for implementation, it is required that the plant transfer function must be strictly positive real.

Many large scale control applications, such as flexible spacecraft, demand decentralized control strategies in lieu of centralized methods. Decentralized controllers differ from centralized controllers in that each local control is computed using only local measurements. In [20] a decentralized active vibration controller is used to attenuate vibration of solar panel structures. The algorithm uses a H_∞ control scheme but requires precise, optimal, placement of actuators to implement. In [21], a decentralized adaptive controller is presented that is capable of rejecting known disturbances acting on unknown systems. The adaptive algorithm utilizes a discrete Fourier transform (DFT) to identify the frequency of the disturbance, which is then used to construct a controls update. The algorithm has the advantage of being completely decentralized. One potential short coming of this algorithm is the use of the DFT, which can slow convergence times due to the nature of batch data processing.

Higher harmonic control (HHC) is another strategy which was developed in the helicopter vibration reduction [22–24] and active rotor balancing [25] communities. In the case of helicopter vibration reduction this is typically referred to as higher harmonic control. In the case of active rotor balancing, this is often referred to as convergent control. HHC works by using the amplitude and phase information from the measurement to update the amplitude and the phase of a sinusoidal control. While this strategy can be effective, implementation typically requires an estimate of the control-to-performance transfer function (for non-adaptive algorithms). HHC can also be implemented with adaption to address known disturbances acting on unknown systems. For example, in [26], a controller is introduced that addresses the problem of a known disturbance acting on an unknown system. The controller works by implementing a recursive least squares (RLS) procedure to estimate the secondary path transfer function used in the control update. One shortcoming of this algorithm, however, is that persistent excitation is required to ensure convergence of the RLS

estimate. However, there are adaptive implementations of HCC that address these shortcomings.

One such strategy is called frequency-domain adaptive higher harmonic control (FD-AHHC) introduced in [11]. In contrast to the previously discussed HHC methods, FD-AHHC does not require an estimate of the control-to-performance transfer function, an external excitation signal to ensure stability, or the use of averaging theory to approximate the closed-loop system response. The only information required is the frequencies of the sinusoidal disturbance. FD-AHHC is a frequency domain algorithm that utilizes a DFT to extract the response at the disturbance frequencies. Using only the information from the DFT, the algorithm computes an estimate of the control-to-performance transfer function which is then used to construct a control update. One limitation of this approach is the need to utilize a DFT, which requires batch data processing that can increase the time required to eliminate disturbances. Another drawback is that the algorithm relies on the assumption that the update period T_{s} is sufficiently large relative to that of the settling time of the system. If this assumption is invalid, then instabilities can manifest in the closed-loop response. One way to ensure stability of the closed-loop system is to increase the update period T_{s}. However, this also increases the time it takes to eliminate the disturbance. An extension of this algorithm is presented in [27] which is capable of rejecting unknown disturbances acting on unknown systems. The algorithm works similarly to FD-AHHC, except that a frequency estimator is implemented to estimate the frequency content of the disturbance.

In contrast to frequency-domain control methods, an adaptive time-domain HHC algorithm was introduced in [28]. This method is similar FD-AHHC in that it is in adaptive algorithm that estimates the control-to-performance transfer function at each time step, but it operates entirely in the time domain without the use of a DFT. In addition, larger control update gains can be implemented compared to FD-AHHC without introducing instabilities. However, similar to FD-AHHC, instabilities can manifest in the closed-loop system if the assumption that the update period T_{s} is sufficiently large relative to the settling time of the system is not valid. In addition, another shortcoming of this algorithm is that it requires the use of online matrix inversion, which can be computationally expensive as the number of sensors and actuators are increased. To address this short coming, a new adaptive time-domain algorithm was introduced in [12].

1.3 Summary of Contributions

Chapter 2 reviews the frequency-domain algorithm presented in [11]. This chapter also presents a new modified version of the algorithm, which addresses the problems of actuator saturation and sensor noise. In this thesis, we refer to the method in [11] as frequency-domain adaptive harmonic control (FDAHC).

Chapter 3 reviews the time-domain algorithm presented in [12]. This chapter also presents a new modified version of the algorithm which addresses the problem of sensor noise. The modified version of the algorithm also includes a modification

which addresses actuator saturation, which is based on previous work in [12]. In this thesis, we refer to the method in [12] as time-domain adaptive harmonic control (TDAHC).

The main contribution in this thesis is presented in Ch. 4. In Ch. 4, results from active noise control experiments are presented where we compare the modified FDAHC algorithm and modified TDAHC algorithm under different scenarios. The experiments are used to explore the strengths and weaknesses of each algorithm and to explore optimal parameters to use when implementing in real world applications. The items investigated in this work are presented in the list below:

i) An implementation of each algorithm for a single-input single-output (SISO) system is presented in an experimental setting to illustrate, and compare, how the initial estimate of the control-to-performance transfer function will determine the transient response of the performance for each algorithm.

ii) The algorithms are compared under conditions where the system is first subject to a single-tone disturbance and then subject to a multi-tone disturbance using different initial conditions. The comparison provides insight into multi-tone disturbance rejection.

iii) The performance of the algorithms are compared under conditions where the frequency of the disturbance that is acting on the system is not known with complete certainty. Insight is gained into how robust each algorithm is to uncertainty in the frequency of the disturbance.

iv) The convergence speed (i.e., speed to attenuate the disturbance and reach steady-state) of each algorithm is compared using optimal parameters tuned to deliver the fastest possible convergence speed.

The experiments conducted in Ch. 4 reveal the following trade-offs between the algorithms:

1) FDAHC is less susceptible to measurement noise due to the DFT. Since the DFT performs batch processing, it has the effect of filtering out some sensor noise. In contrast, TDAHC does not utilize a DFT and is, thus, more susceptible to measurement noise.

2) FDHAC is less influenced by the transient response due to the averaging properties of the DFT. In contrast, TDAHC is generally more sensitive to the transient response.

3) TDAHC can be implemented with larger control gains which can yield faster steady-state performance convergence times compared to that of FDAHC. In

practice, TDAHC control gains can be selected higher to yield faster convergence times compared to that of FDAHC.

Chapter 2
Review of Frequency-Domain Adaptive Harmonic Control

In this chapter, we review frequency-domain adaptive harmonic control (FDAHC), which addresses the problem of rejecting sinusoidal disturbances with known frequencies that act on a completely unknown asymptotically stable linear time-invariant (LTI) system. The review of FDAHC is based on [11], which introduced this method. This chapter also presents modifications of the FDAHC algorithm to address sensor noise and actuator saturation.

2.1 Notation

Let $\mathbb{F}$ be $\mathbb{R}$ or $\mathbb{C}$. Let $\|\cdot\|$ be the 2-norm on $\mathbb{F}^n$, and let $\|\cdot\|_\infty$ be the infinity norm on $\mathbb{F}^n$. Let A^* denote the complex conjugate transpose of $A \in \mathbb{F}^{m\times n}$, and define the Frobenius norm of $A \in \mathbb{F}^{m\times n}$ as $\|A\|_{\mathrm{F}} \triangleq \sqrt{\mathrm{trA^*A}}$. Define the *open ball radius* $r \geq 0$ *centered at* $C \in \mathbb{C}^{m\times n}$ by $\mathcal{B}_r(C) \triangleq \{X \in \mathbb{C}^{m\times n} \colon \|X - C\|_{\mathrm{F}} \leq r\}$. Let $\lambda_{\min}(A)$ denote the minimum eigenvalue of the Hermitian positive-semidefinite matrix $A \in \mathbb{F}^{n\times n}$.

Let $\angle\lambda$ denote the argument of $\lambda \in \mathbb{C}$ defined on the interval $(-\pi, \pi]$ rad. Let $\mathbb{N} \triangleq \{0, 1, 2, \dots\}$ and $\mathbb{Z}^+ \triangleq \mathbb{N} \setminus \{0\}$.

2.2 Problem Formulation

Consider the LTI system

$$\dot{x}(t) = Ax(t) + Bu(t) + D_1 d(t), \tag{2.1}$$
$$y(t) = Cx(t) + Du(t) + D_2 d(t), \tag{2.2}$$

where $t \geq 0$, $x(t) \in \mathbb{R}^n$ is the state, $x(0) = x_0 \in \mathbb{R}^n$ is the initial condition, $u(t) \in \mathbb{R}^m$ is the control, $y(t) \in \mathbb{R}^\ell$ is the measured performance, $d(t) \in \mathbb{R}^{\ell_d}$ is the unmeasured disturbance, and $A \in \mathbb{R}^{n\times n}$ is asymptotically stable. Consider the tonal disturbance

$$d(t) = \sum_{i=1}^{q} d_{\mathrm{c},i} \cos \omega_i t + d_{\mathrm{s},i} \sin \omega_i t, \tag{2.3}$$

where $\omega_1, \omega_2, \ldots, \omega_q > 0$ and $d_{\mathrm{c},1}, d_{\mathrm{c},2}, \ldots, d_{\mathrm{c},q}, d_{\mathrm{s},1}, d_{\mathrm{s},2}, \ldots, d_{\mathrm{s},q} \in \mathbb{R}^{\ell_d}$ determine the disturbance amplitude and phase at each disturbance frequency. Define the transfer functions $G_{yu}\colon \mathbb{C} \to \mathbb{C}^{\ell \times m}$ and $G_{yd}\colon \mathbb{C} \to \mathbb{C}^{\ell \times \ell_d}$ by

$$G_{yu}(s) \triangleq C(sI - A)^{-1}B + D, \tag{2.4}$$

$$G_{yd}(s) \triangleq C(sI - A)^{-1}D_1 + D_2. \tag{2.5}$$

We make the following assumptions:

(A2.1) For all $i \in Q \triangleq \{1, 2, \ldots, q\}$, rank $G_{yu}(\jmath\omega_i) = \ell$.

(A2.2) $\omega_1, \cdots, \omega_q$ are known.

Assumption (A2.1) implies that the number of actuators is at least as large as the number of performance measures (i.e., $m \geq \ell$). Assumption (A2.2) implies that the disturbance frequencies ω_i are known; however, the disturbance amplitudes $d_{\mathrm{c},i}$ and $d_{\mathrm{s},i}$ and the system model A, B, C, D, D_1, and D_2 are completely unknown.

The goal is to design a control u that eliminates the effect of the disturbance d on the performance y. We desire a control that relies on no model information regarding the system (2.1) and (2.2), and requires knowledge of only the disturbance frequencies $\omega_1, \ldots, \omega_q$. Unless otherwise stated, all statements in this chapter that involve the subscript i are for all $i \in Q$.

2.3 Ideal Control

For the moment, assume that $G_{yu}(\jmath\omega_i)$, $G_{yd}(\jmath\omega_i)$, $d_{\mathrm{c},i}$, and $d_{\mathrm{s},i}$ are known. Let $u_{\mathrm{c},i}$, $u_{\mathrm{s},i} \in \mathbb{R}^m$, and consider the harmonic control

$$u(t) = \sum_{i=1}^{q} u_{\mathrm{c},i} \cos \omega_i t + u_{\mathrm{s},i} \sin \omega_i t. \tag{2.6}$$

Define $\hat{u}_i \triangleq u_{\mathrm{c},i} - \jmath u_{\mathrm{s},i}$, which is the discrete Fourier transform (DFT) at frequency ω_i obtained from a sampling of u. In addition, define

$$G_{i,*} \triangleq G_{yu}(\jmath\omega_i) \in \mathbb{C}^{\ell \times m}, \tag{2.7}$$

$$d_{i,*} \triangleq G_{yd}(\jmath\omega_i)(d_{\mathrm{c},i} - \jmath d_{\mathrm{s},i}) \in \mathbb{C}^{\ell}. \tag{2.8}$$

The harmonic steady-state (HSS) performance of (2.1) and (2.2) with disturbance (2.3) and control (2.6) is

$$\begin{aligned} y_{\mathrm{hss}}(t, \hat{u}_1, \ldots, \hat{u}_q) &\triangleq \sum_{i=1}^{q} \mathrm{Re}\Big(G_{yu}(\jmath\omega_i)\hat{u}_i + G_{yd}(\jmath\omega_i)(d_{\mathrm{c},i} - \jmath d_{\mathrm{s},i})\Big)e^{\jmath\omega_i t} \\ &= \sum_{i=1}^{q} \mathrm{Re}\Big(G_{i,*}\hat{u}_i + d_{i,*}\Big) \cos \omega_i t - \mathrm{Im}\Big(G_{i,*}\hat{u}_i + d_{i,*}\Big) \sin \omega_i t. \end{aligned} \tag{2.9}$$

Define

$$\hat{y}_{\mathrm{hss},i}(\hat{u}_i) \triangleq G_{i,*}\hat{u}_i + d_{i,*}, \tag{2.10}$$

which is the DFT at frequency ω_i obtained from a sampling of y_{hss}. Consider the cost function

$$J(\hat{u}_1, \ldots, \hat{u}_q) \triangleq \lim_{t\to\infty} \frac{1}{t}\int_0^t \|y_{\mathrm{hss}}(\tau, \hat{u}_1, \ldots, \hat{u}_q)\|^2 \mathrm{d}\tau, \tag{2.11}$$

which is the average power of y_{hss}. Substituting (2.9) and (2.10) into (2.11), it follows that

$$\begin{aligned}
J(\hat{u}_1, \ldots, \hat{u}_q) &= \lim_{t\to\infty} \frac{1}{t}\int_0^t \left\| \sum_{i=1}^{q} \mathrm{Re}\ \hat{y}_{\mathrm{hss},i}(\hat{u}_i)\cos\omega_i\tau - \mathrm{Im}\ \hat{y}_{\mathrm{hss},i}(\hat{u}_i)\sin\omega_i\tau \right\|^2 \mathrm{d}\tau \\
&= \sum_{i=1}^{q} \begin{bmatrix} \mathrm{Re}\ \hat{y}_{\mathrm{hss},i}(\hat{u}_i) \\ \mathrm{Im}\ \hat{y}_{\mathrm{hss},i}(\hat{u}_i) \end{bmatrix}^{\mathrm{T}} \left(\lim_{t\to\infty} \frac{1}{t}\int_0^t \begin{bmatrix} \cos^2\omega_i\tau & -(\cos\omega_i\tau)(\sin\omega_i\tau) \\ -(\cos\omega_i\tau)(\sin\omega_i\tau) & \sin^2\omega_i\tau \end{bmatrix} \mathrm{d}\tau \right) \\
&\quad \times \begin{bmatrix} \mathrm{Re}\ \hat{y}_{\mathrm{hss},i}(\hat{u}_i) \\ \mathrm{Im}\ \hat{y}_{\mathrm{hss},i}(\hat{u}_i) \end{bmatrix} \\
&= \frac{1}{2}\sum_{i=1}^{q} \hat{y}^*_{\mathrm{hss},i}(\hat{u}_i)\hat{y}_{\mathrm{hss},i}(\hat{u}_i).
\end{aligned} \tag{2.12}$$

It follows from (2.12) that J is minimized by finding $\hat{u}_i$ that minimizes $\frac{1}{2}\hat{y}^*_{\mathrm{hss},i}(\hat{u}_i)\times \hat{y}_{\mathrm{hss},i}(\hat{u}_i)$, which is equal to the average power of y_{hss} at frequency ω_i. The following result provides an expression for the control that minimizes J. This result is presented in [11, Theorem 1].

Theorem 2.1. Assume that (A2.1) holds. For all $i \in Q$, define $u_{i,*} \triangleq -G^*_{i,*}\times (G_{i,*}G^*_{i,*})^{-1}d_{i,*}$. Then, $J(u_{1,*}, \ldots, u_{q,*}) = 0$.

Theorem 2.1 provides the ideal control parameters $u_{i,*}$, but $u_{i,*}$ requires knowledge of $G_{i,*}$ and $d_{i,*}$, which are unknown.

2.4 Review of FDAHC

FDAHC uses a sinusoidal control with frequencies ω_i, and amplitudes and phases that are updated at discrete times. Let $T_{\mathrm{s}} > 0$ denote the update period, and for each $k \in \mathbb{N}$ and for all $t \in [kT_{\mathrm{s}}, (k+1)T_{\mathrm{s}})$, consider the control

$$u(t) = \sum_{i=1}^{q} \mathrm{Re}\ u_{i,k}\cos\omega_i t - \mathrm{Im}\ u_{i,k}\sin\omega_i t, \tag{2.13}$$

where $u_{i,k} \in \mathbb{C}^m$ is determined from update equations presented in this section. Thus, the control (2.13) is a piecewise-continuous sinusoid.

For each $k \in \mathbb{Z}^+$, let $y_{i,k} \in \mathbb{C}^\ell$ denote the DFT at ω_i obtained from a sampling of y on the interval $[(k-1)T_{\mathrm{s}}, kT_{\mathrm{s}})$. The DFT data $y_{i,k}$ is the feedback used by FDAHC.

Note that if $T_{\rm s}$ is sufficiently large relative to the settling time of (2.1) and (2.2), then for all $k \in \mathbb{N}$, $y((k+1)T_{\rm s}) \approx y_{\rm hss}((k+1)T_{\rm s}, u_{1,k}, \ldots, u_{q,k})$. In this case, for all $k \in \mathbb{N}$, $y_{i,k+1} \approx \hat{y}_{{\rm hss},i}(u_{i,k})$. In Section 2.5, we invoke the HSS assumption that for all $k \in \mathbb{N}$, $y_{i,k+1} = \hat{y}_{{\rm hss},i}(u_{i,k})$; however, this assumption is used only for the stability analysis in Section 2.5.

Let $\mu_i \in (0,1]$, $\sigma_i > 0$, and $u_{i,0} \in \mathbb{C}^m$. Then, for all $k \in \mathbb{N}$, consider the control

$$u_{i,k+1} = u_{i,k} - \frac{\mu_i}{\sigma_i + \|G_{i,k}\|_{\rm F}^2} G_{i,k}^* y_{i,k+1}, \tag{2.14}$$

where $G_{i,k} \in \mathbb{C}^{\ell \times m}$ is an estimate of $G_{i,*}$ obtained from the adaptive equation developed below.

To determine the adaptive equation for $G_{i,k}$, note that if $y_{i,k+1} = \hat{y}_{{\rm hss},i}(u_{i,k})$, then it follows from (2.10) that $G_{i,*}(u_{i,k} - u_{i,k-1}) - (y_{i,k+1} - y_{i,k}) = 0$. Thus, we consider the cost function $\mathcal{J}_{k,i} : \mathbb{R}^{\ell \times m} \times \mathbb{R}^{\ell \times m} \to [0, \infty)$ defined by

$$\mathcal{J}_{k,i}(G_{\rm r}, G_{\rm i}) \triangleq \frac{1}{2} \|(G_{\rm r} + \jmath G_{\rm i})(u_{i,k} - u_{i,k-1}) - (y_{i,k+1} - y_{i,k})\|^2. \tag{2.15}$$

Note that $\mathcal{J}_{k,i}(\mathrm{Re}\ G_{i,*}, \mathrm{Im}\ G_{i,*}) = 0$, that is, $G_{i,*}$ minimizes $\mathcal{J}_{k,i}$. Define the complex gradient

$$\begin{aligned} \nabla \mathcal{J}_{k,i}(G_{\rm r}, G_{\rm i}) &\triangleq \frac{\partial \mathcal{J}(G_{\rm r}, G_{\rm i})}{\partial G_{\rm r}} + \jmath \frac{\mathcal{J}(G_{\rm r}, G_{\rm i})}{\partial G_{\rm i}} \\ &= [(G_{\rm r} + \jmath G_{\rm i})(u_{i,k} - u_{i,k-1}) - (y_{i,k+1} - y_{i,k})](u_{i,k} - u_{i,k-1})^*, \end{aligned} \tag{2.16}$$

which is the direction of the maximum rate of change of $\mathcal{J}_{k,i}$ with respect to $G_{\rm r} + \jmath G_{\rm i}$. See [Eq. (17)] [11]. Let $G_{i,0} \in \mathbb{C}^{\ell \times m} \setminus \{0\}$,$\gamma_i \in (0,1]$, and $\nu_i > 0$. Then, for all $k \in \mathbb{Z}^+$, consider the adaptive equation

$$G_{i,k} = G_{i,k-1} - \eta_{i,k} \nabla \mathcal{J}_{k,i}(\mathrm{Re}\ G_{i,k-1}, \mathrm{Im}\ G_{i,k-1}), \tag{2.17}$$

where

$$\eta_{i,k} \triangleq \frac{\gamma_i (\sigma_i + \|G_{i,k-1}\|_{\rm F}^2)^2}{\nu_i \mu_i^2 + (\sigma_i + \|G_{i,k-1}\|_{\rm F}^2)^2 \|u_{i,k} - u_{i,k-1}\|^2}. \tag{2.18}$$

Thus, it follows from (2.16)–(2.18) that for all $k \in \mathbb{Z}^+$,

$$\begin{aligned} G_{i,k} = G_{i,k-1} &- \frac{\gamma_i (\sigma_i + \|G_{i,k-1}\|_{\rm F}^2)^2}{\nu_i \mu_i^2 + (\sigma_i + \|G_{i,k-1}\|_{\rm F}^2)^2 \|u_{i,k} - u_{i,k-1}\|^2} \\ &\times \Big[G_{i,k-1}(u_{i,k} - u_{i,k-1}) - (y_{i,k+1} - y_{i,k}) \Big] (u_{i,k} - u_{i,k-1})^*. \end{aligned} \tag{2.19}$$

Thus, FDAHC is given by (2.13), (2.14), and (2.19). The FDAHC architecture is presented in Fig. 2.1.

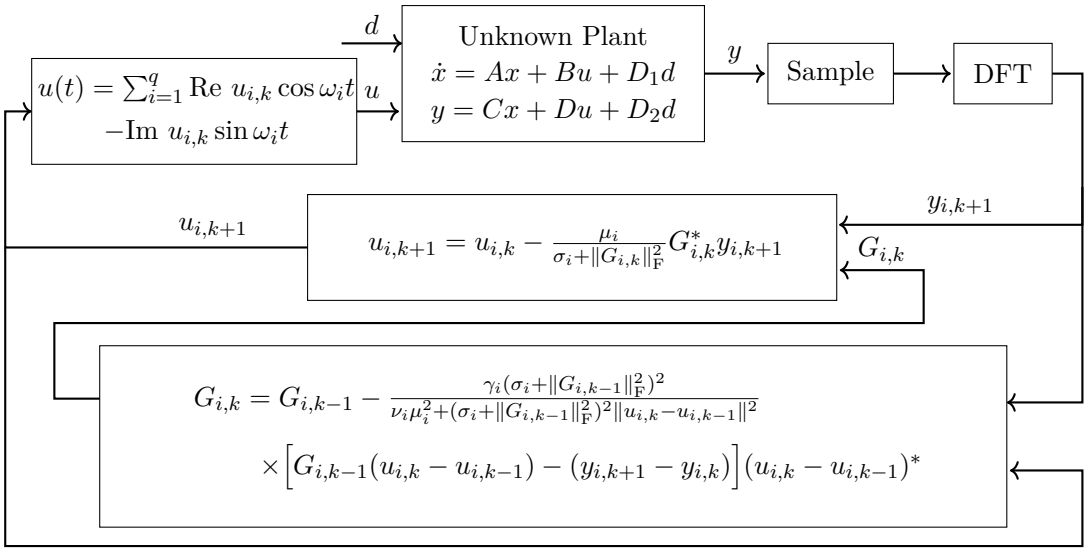

Figure 2.1: Control architecture for FDAHC

2.5 Stability Analysis

If T_{s} is sufficiently large relative to the settling time of (2.1) and (2.2), then for all $k \in \mathbb{N}$, $y_{i,k+1} \approx \hat{y}_{\mathrm{hss,i}}(u_{i,k})$. Thus, we make the HSS assumption:

(A2.3) For all $i \in Q$ and for all $k \in \mathbb{N}$, $y_{i,k+1} = \hat{y}_{\mathrm{hss},i}(u_{i,k})$.

In this case, (2.10) implies that for all $k \in \mathbb{N}$,

$$y_{i,k+1} = G_{i,*} u_{i,k} + d_{i,*}. \tag{2.20}$$

Assumption (A2.3) is used to analyze the stability of the closed-loop system consisting of (2.14), (2.19) and (2.20). The next result is the main result on the stability and performance of FDAHC. This result is given in [11, Corollary 2].

Theorem 2.2. Assume $m = \ell$, and consider the closed-loop system (2.14), (2.19), and (2.20), where $\mu_i \in (0, 1]$, $\gamma_i \in (0, 1]$, $\sigma_i > 0$, and $\nu_i > 0$, and (A2.1)–(A2.3) are satisfied. Then, the following statements hold:

i) For all $i \in Q$, $(y_{i,k}, G_{i,k-1}) \equiv (0, G_{i,*})$ is a Lyapunov stable equilibrium of (2.14),(2.19), and (2.20).

ii) There exists $r > 0$ such that for $i \in Q$ and for all $(u_{i,0}, G_{i,0}) \in \mathbb{C}^{\ell} \times \mathbb{B}_r(G_{i,*})$, $\lim_{k \to \infty} u_{i,k} = u_{i,*}$ and $\lim_{k \to \infty} y_{i,k} = 0$.

iii) For all $i \in Q$, let $u_{i,0} \in \mathbb{C}^{\ell}$, and let $G_{i,0} \in \mathbb{C}^{\ell \times \ell}$ be nonsingular. Assume that there exists $k_{\mathrm{s}} \geq 0$ and $\varepsilon > 0$ such that for all $i \in Q$ and all $k \geq k_{\mathrm{s}}$, $\lambda_{\min}(G_{i,k}^* G_{i,k}) \geq \varepsilon$. Then, for all $i \in Q$, $\lim_{k \to \infty} u_{i,k} = u_{i,*}$ and $\lim_{k \to \infty} y_{i,k} = 0$.

The following result provides the single-input single-output (SISO) stability properties. This result is given in [11, Corollary 3].

Theorem 2.3. Assume $m = \ell = 1$, and consider the closed-loop system (2.14), (2.19), and (2.20), where $\mu_i \in (0, 1]$, $\gamma_i \in (0, 1]$, $\sigma_i > 0$, and $\nu_i > 0$, and (A2.1)–(A2.3) are satisfied. Then, for all $i \in Q$, $(y_{i,k}, G_{i,k-1}) \equiv (0, G_{i,*})$ is a Lyapunov stable equilibrium of (2.14),(2.19), and (2.20). Furthermore, for $i \in Q$ and for all initial conditions $u_{i,0} \in \mathbb{C}$ and $G_{i,0} \in \mathbb{C} \setminus \{x \in \mathbb{C} : \ x = 0 \text{ or } |\angle x - \angle G_{i,*}| = \pi\}$, $G_{i,k}$ is bounded, $\lim_{k\to\infty} u_{i,k} = u_{i,*}$, and $\lim_{k\to\infty} y_{i,k} = 0$.

2.6 FDAHC Modification

Numerical testing demonstrates that actuator saturation and sensor noise can prevent optimal (or even acceptable) disturbance rejection. To address this shortcoming, we present a modified version of FDAHC. Specifically, we present a modification to the update equation for u_k to address the problem of actuator saturation. We also present a modification to the update equation for $G_{i,k}$ to address the problem of sensor noise.

2.6.1 FDAHC Modification to Address Actuator Saturation

Let $u_{\max} > 0$ be the maximum allowable magnitude of each entry of the control u. In other words, we aim to enforce the constraint that for all $t \geq 0$, $\|u(t)\|_\infty \leq u_{\max}$. For all $k \in \mathbb{N}$, consider the update equation for $u_{i,k}$ given by

$$u_{i,k+1} = \begin{cases} \dfrac{u_{\max}}{\alpha_{k+1}} v_{i,k+1}, & \text{if } \alpha_{k+1} > u_{\max}, \\ v_{i,k+1}, & \text{otherwise,} \end{cases} \tag{2.21}$$

where

$$\alpha_{k+1} \triangleq \max_{j\in\{1,\ldots,m\}} \sum_{i=1}^{q} |e_j v_{i,k+1}|, \tag{2.22}$$

$$v_{i,k+1} \triangleq u_{i,k} - \frac{\mu_i}{\sigma_i + \|G_{i,k}\|_{\mathrm{F}}^2} G_{i,k}^* y_{i,k+1}, \tag{2.23}$$

and for all $j \in \{1, 2, \ldots, m\}$, $e_j \in \mathbb{R}^{1\times m}$ denotes the jth row of I_m. The modified update (2.21)–(2.23) is used in place of (2.14).

Note that (2.13) and (2.21)–(2.23) imply

$$\begin{aligned} \max_{t\in[kT_{\mathrm{s}},(k+1)T_{\mathrm{s}})} |e_j u(t)| &= \max_{t\in[kT_{\mathrm{s}},(k+1)T_{\mathrm{s}})} \left| \sum_{i=1}^{q} e_j \mathrm{Re}\ u_{i,k} \cos\omega_i t - e_j \mathrm{Im}\ u_{i,k} \sin\omega_i t \right| \\ &= \max_{t\in[kT_{\mathrm{s}},(k+1)T_{\mathrm{s}})} \left| \sum_{i=1}^{q} \begin{bmatrix} e_j \mathrm{Re}\ u_{i,k} & e_j \mathrm{Im}\ u_{i,k} \end{bmatrix} \begin{bmatrix} \cos\omega_i t \\ \sin\omega_i t \end{bmatrix} \right| \end{aligned}$$

$$
\begin{aligned}
&\leq \max_{t\in[kT_{\mathrm{s}},(k+1)T_{\mathrm{s}})} \sum_{i=1}^{q} \left| \begin{bmatrix} e_j\mathrm{Re}\ u_{i,k} & e_j\mathrm{Im}\ u_{i,k} \end{bmatrix} \begin{bmatrix} \cos\omega_i t \\ \sin\omega_i t \end{bmatrix} \right| \\
&\leq \max_{t\in[kT_{\mathrm{s}},(k+1)T_{\mathrm{s}})} \sum_{i=1}^{q} \left\| \begin{bmatrix} e_j\mathrm{Re}\ u_{i,k} \\ e_j\mathrm{Im}\ u_{i,k} \end{bmatrix} \right\| \left\| \begin{bmatrix} \cos\omega_i t \\ \sin\omega_i t \end{bmatrix} \right\| \\
&= \sum_{i=1}^{q} \left\| \begin{bmatrix} e_j\mathrm{Re}\ u_{i,k} \\ e_j\mathrm{Im}\ u_{i,k} \end{bmatrix} \right\| \\
&= \sum_{i=1}^{q} |e_j u_{i,k}| \\
&= \begin{cases} \dfrac{u_{\max}}{\alpha_k} \displaystyle\sum_{i=1}^{q} |e_j v_{i,k}|, & \text{if } \alpha_k > u_{\max} \\ \displaystyle\sum_{i=1}^{q} |e_j v_{i,k}|, & \text{otherwise} \end{cases} \\
&\leq \frac{u_{\max}}{\alpha_k} \sum_{i=1}^{q} |e_j v_{i,k}| \\
&\leq \frac{u_{\max}}{\alpha_k} \alpha_k \\
&= u_{\max},
\end{aligned}
$$

which demonstrates that (2.21)–(2.23) ensures that for all $t \geq 0$, $\|u(t)\|_\infty < u_{\max}$.

2.6.2 FDAHC Modification to Address Sensor Noise

Let $R_{\mathrm{m}} \in \mathbb{R}$ denote an upper bound on $\|G_{i,k}\|_{\mathrm{F}}$. For all $k \in \mathbb{Z}^+$ consider the update equation for $G_{i,k}$ given by

$$
G_{i,k} = \begin{cases} \dfrac{R_{\mathrm{m}}}{\|\Theta_{i,k}\|_{\mathrm{F}}} \Theta_{i,k}, & \text{if } \|\Theta_{i,k}\|_{\mathrm{F}} \geq R_{\mathrm{m}}, \\ \Theta_{i,k}, & \text{otherwise,} \end{cases} \tag{2.24}
$$

where

$$
\begin{aligned}
\Theta_{i,k} \triangleq G_{i,k-1} &- \frac{\gamma_i(\sigma_i + \|G_{i,k-1}\|_{\mathrm{F}}^2)^2}{\nu_i\mu_i^2 + (\sigma_i + \|G_{i,k-1}\|_{\mathrm{F}}^2)^2 \|u_{i,k} - u_{i,k-1}\|^2} \\
&\times \Big[G_{i,k-1}(u_{i,k} - u_{i,k-1}) - (y_{i,k+1} - y_{i,k}) \Big] (u_{i,k} - u_{i,k-1})^*.
\end{aligned} \tag{2.25}
$$

The modified update (2.24) and (2.25) is used in place of (2.19). Note that (2.24) and (2.25) imply that $\|G_{i,k}\|_{\mathrm{F}} \leq R_{\mathrm{m}}$.

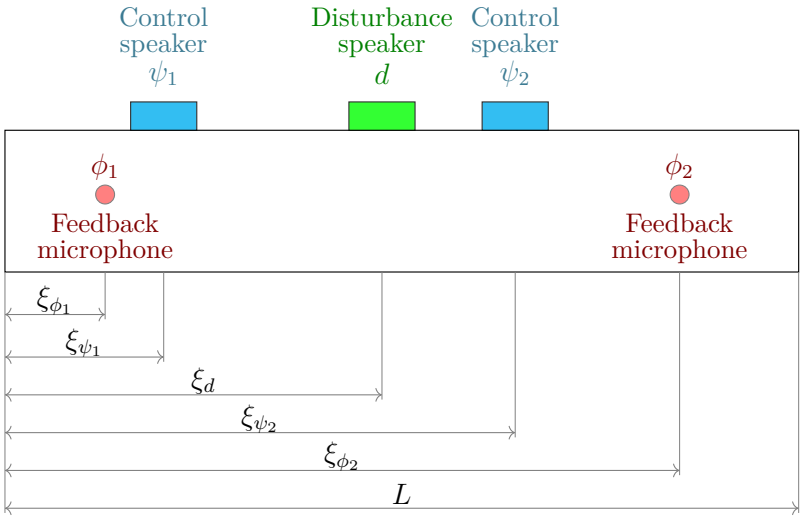

Figure 2.2: Acoustic duct.

2.7 Numerical Examples

In this section, we present numerical examples of FDAHC. Examples 2.1–2.3 illustrate the application of FDAHC to an acoustic duct. Examples 2.4–2.6 illustrate the application of FDAHC and modified FDAHC to a 2-mass structure. For all examples, the DFT is performed using a 1 kHz sampling frequency.

2.7.1 Acoustic Duct

Consider the acoustic duct of length $L = 3$ m shown in Fig. 2.2, where all measurements are from the left end of the duct. A disturbance speaker is at $\xi_d = 1.5$ m, while 2 control speakers are at $\xi_{\psi_1} = 0.6$ m and $\xi_{\psi_2} = 1.35$ m. All speakers have cross-sectional area $A_\mathrm{s} = 0.0025$ m^2. Two feedback microphones are in the duct at $\xi_{\phi_1} = 0.5$ m and $\xi_{\phi_2} = 2.7$ m, and they measure the acoustic pressures $\phi_1(t) = p(\xi_{\phi_1}, t)$ and $\phi_2(t) = p(\xi_{\phi_2}, t)$, respectively. Thus, for $i \in \{1, 2\}$, $\phi_i(t) = C_i x(t)$, where $C_i = \frac{\rho_0}{A_\mathrm{s}}[\ 0 \quad V_1(\xi_{\phi_i}) \quad \cdots \quad 0 \quad V_r(\xi_{\phi_i})\ ]$. The equation for the acoustic duct is given by

$$\frac{1}{c^2}\frac{\partial^2 p(\xi,t)}{\partial t^2} = \frac{\partial^2 p(\xi,t)}{\partial \xi^2} + \rho_0 \dot{\psi}_1(t)\delta(\xi - \xi_{\psi_1}) + \rho_0 \dot{\psi}_2(t)\delta(\xi - \xi_{\psi_2}) + \rho_0 \dot{d}(t)\delta(\xi - \xi_d), \tag{2.26}$$

where $p(\xi, t)$ is the acoustic pressure, δ is the Dirac delta, $c = 343$ m/s is the phase speed of the acoustic wave, ψ_1 and ψ_2 are the speaker cone velocities of the control speakers, d is the speaker cone velocity of the disturbance speaker, and $\rho_0 = 1.21$ kg/m^2 is the equilibrium density of air at room conditions. Refer to [29] for more details. Using separation of variables and retaining r modes, the solution $p(\xi, t)$ can

be approximated by

$$p(\xi,t)=\sum_{i=0}^{r}q_i(t)V_i(\xi),$$

where for $i\in\{1,2,\cdots,r\}$,

$$V_i(\xi)\triangleq c\sqrt{\frac{2}{L}}\sin\frac{i\pi\xi}{L},$$

$\omega_{\mathrm{n},i}\triangleq i\pi c/L$ is the natural frequency of the ith mode, $\zeta_i=0.2$ is the assumed damping ratio of the ith mode, and q_i satisfies the differential equation (2.1), where

$$x(t)=\begin{bmatrix}\int_0^t q_1(\sigma)\mathrm{d}\sigma\\ q_1(t)\\ \vdots\\ \int_0^t q_r(\sigma)\mathrm{d}\sigma\\ q_r(t)\end{bmatrix},\quad A=\mathrm{diag}\left(\begin{bmatrix}0&1\\-\omega_{\mathrm{n}1}^2&-2\zeta_1\omega_{\mathrm{n}1}^2\end{bmatrix}\cdots\begin{bmatrix}0&1\\-\omega_{\mathrm{n}1}^2&-2\zeta_1\omega_{\mathrm{n}1}^2\end{bmatrix}\right),$$

$$B=\frac{\rho_0}{A_{\mathrm{s}}}\begin{bmatrix}0&V_1(\xi_{\psi_1})&\cdots&0&V_r(\xi_{\psi_1})\\0&V_1(\xi_{\psi_2})&\cdots&0&V_r(\xi_{\psi_2})\end{bmatrix}^{\mathrm{T}},\quad D_1=\frac{\rho_0}{A_{\mathrm{s}}}\begin{bmatrix}0&V_1(\xi_d)&\cdots&0&V_r(\xi_d)\end{bmatrix}^{\mathrm{T}},$$

Let $\omega_1=200\pi$ rad/s, $\omega_2=160\pi$ rad/s, $r=5$, $T_{\mathrm{s}}=0.1$ s, $\nu_1=\sigma_1=1\times10^{-6}$, and $x_0=0$. The initial estimate G_0 and disturbance d is given in each example. For each example, the control turns on at $t=1$ s.

In the following example, we show that FDAHC is able to asymptotically reject a single-tone disturbance acting on a SISO system. Note that the non-adaptive version of the algorithm requires a sufficiently accurate estimate of $G_{1,*}$ for stability. Specifically, as shown in [11, Theorem 3], the estimate $G_{1,k}$ must be within 90° of $G_{1,*}$ for stability. In contrast, the adaptive version of the algorithm reviewed in this chapter is stable even if the initial estimate $G_{1,k}$ is not within 90° of $G_{1,*}$ as shown in [11, Theorem 4]. Thus, in this example, we first use an initial condition $G_{1,0}$ which is within 90° of $G_{1,*}$. We then use an initial condition for $G_{1,0}$ which is not within 90° of $G_{1,*}$ to illustrate the effect that the initial estimate $G_{i,k}$ has on the transient response of y.

Example 2.1. Consider the SISO ($\ell=m=1$) system, where we let $u=\psi_1$, $y=\phi_1$, $\psi_2=0$, and $d(t)=2\sin\omega_1t+0.2\cos\omega_1t$. Let $\mu_1=\gamma_1=0.15$. First, consider the case where $G_{1,0}$ is within 90° of $G_{1,*}$, specifically, let $G_{1,0}=0.75e^{\jmath\frac{3\pi}{7}}G_{1,*}$. Figure 2.3 presents the response y and control u. Figure 2.4 presents the trajectory of the estimate $G_{1,k}$ which approaches $G_{1,*}$. FDAHC yields asymptotic disturbance rejection.

Next, consider the case where $G_{1,0}$ is not within 90° of $G_{1,*}$, specifically, let $G_{1,0}=-0.75e^{\jmath\frac{3\pi}{7}}G_{1,*}$. Figure 2.5 presents the response y and control u. Figure 2.6 presents the trajectory of the estimate $G_{1,k}$ which approaches $G_{1,*}$. In contrast to the first initial condition, this initial condition yielded a larger transient response, but FDAHC

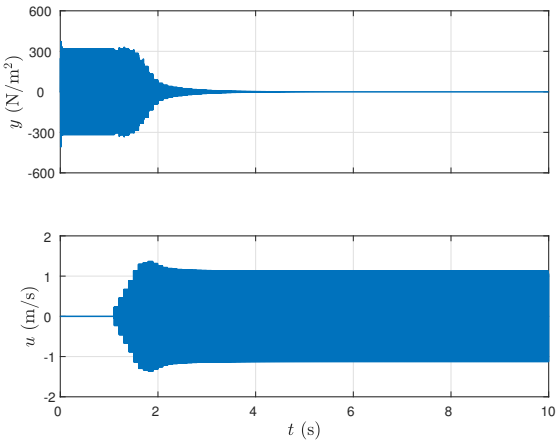

Figure 2.3: FDAHC for a SISO system where $|\angle G_{1,0}/G_{1,*}| < \frac{\pi}{2}$. The response $y(t) \to 0$ as $t \to \infty$.

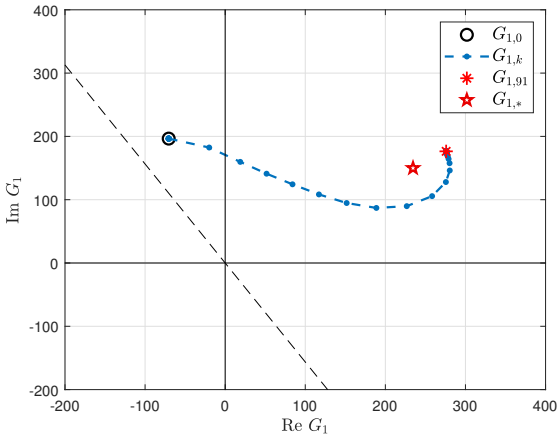

Figure 2.4: Trajectory of $G_{1,k}$ with FDAHC for a SISO system where $|\angle G_{1,0}/G_{1,0}| < \frac{\pi}{2}$. The dashed lines show the locus of G such that $|\angle G_{1,0}/G_{1,*}| = \frac{\pi}{2}$.

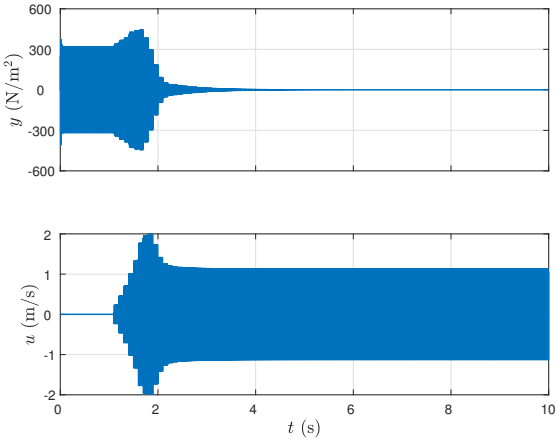

Figure 2.5: FDAHC for a SISO system where $|\angle G_{1,0}/G_{1,*}| > \frac{\pi}{2}$. The response $y(t) \to 0$ as $t \to \infty$.

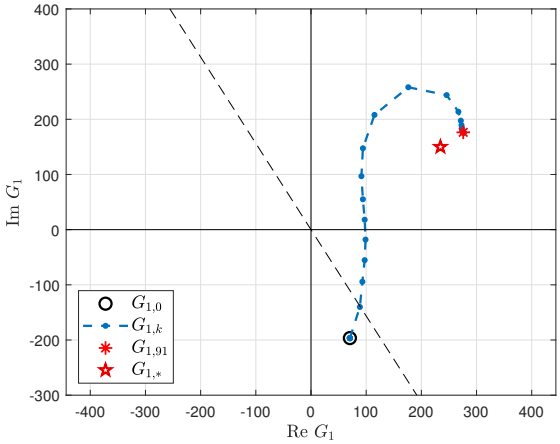

Figure 2.6: Trajectory of $G_{1,k}$ with FDAHC for a SISO system where $|\angle G_{1,0}/G_{1,0}| > \frac{\pi}{2}$. The dashed lines show the locus of G such that $|\angle G_{1,0}/G_{1,*}| = \frac{\pi}{2}$.

was still able to yield asymptotic disturbance rejection. This shows that the HSS stability condition determines the transient response of y. △

Next, we address MIMO systems using FDAHC. In the following example, we show that FDAHC is able to asymptotically reject a single-tone disturbance acting on a MIMO ($\ell = m = 2$) system. We implement FDAHC using two initial conditions to illustrate that the initial condition $G_{1,0}$ affects the transient response of y.

Example 2.2. Consider the MIMO ($\ell = m = 2$) system where we let $u = \begin{bmatrix}\psi_1 & \psi_2\end{bmatrix}^{\mathrm{T}}$, $y = \begin{bmatrix}\phi_1 & \phi_2\end{bmatrix}^{\mathrm{T}}$, and $d(t) = 2\sin\omega_1 t + 0.2\cos\omega_1 t$. Let $\mu_1 = \gamma_1 = 0.3$ and let $G_{1,0} = 0.5e^{\jmath\frac{\pi}{5}}G_{1,*}$ denote the initial estimate of $G_{1,*}$ which satisfies the non-adaptive stability requirement presented in [11, Theorem 2]. Figure 2.7 presents the

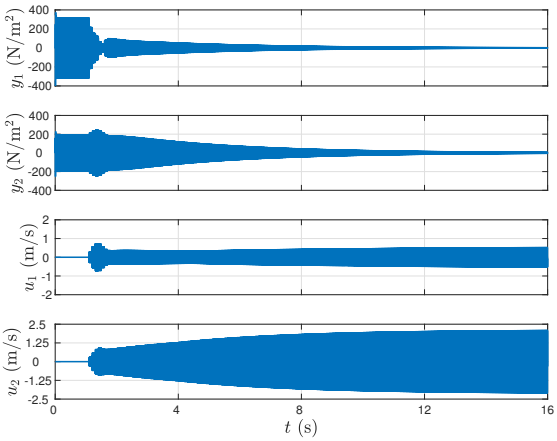

Figure 2.7: FDAHC for a MIMO system where $G_{1,0} = 0.5e^{\jmath\frac{\pi}{5}}G_{1,*}$. The response $y(t) \to 0$ as $t \to \infty$.

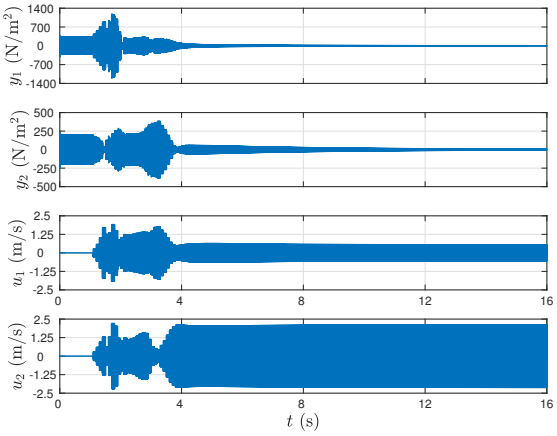

Figure 2.8: FDAHC for a MIMO system where $G_{1,0} = 0.5e^{\jmath\frac{6\pi}{5}}G_{1,*}$. The response $y(t) \to 0$ as $t \to \infty$.

response y and control u. FDAHC yields asymptotic disturbance rejection.

Next, we consider the initial estimate $G_{1,0} = 0.5e^{\jmath\frac{6\pi}{5}}G_{1,*}$ which does not satisfy the non-adaptive stability requirement presented in [11, Theorem 2]. Figure 2.8 presents the response y and control u. In contrast to the first initial condition, this initial condition yielded a larger transient response, but FDAHC was still able to yield asymptotic disturbance rejection. This shows that the HSS stability condition determines the transient response of y. △

Example 2.3. Consider the MIMO ($\ell = m = 2$) system where we let $u = \begin{bmatrix}\psi_1 & \psi_2\end{bmatrix}^{\mathrm{T}}$, $y = \begin{bmatrix}\phi_1 & \phi_2\end{bmatrix}^{\mathrm{T}}$, and

$$d(t) = 2\sin\omega_1 t + 0.2\cos\omega_1 t + 2\sin\omega_2 t + 0.2\cos\omega_2 t,$$

which is a 2-tone disturbance. Let $\mu_1 = \gamma_1 = 0.3$. Let $G_{1,0} = 1e^{\jmath\frac{\pi}{3}}G_{1,*}$ and $G_{2,0} = 0.75e^{\jmath\frac{\pi}{6}}G_{2,*}$ denote the initial estimates of $G_{1,*}$ and $G_{2,*}$, respectively, which satisfy the non-adaptive stability requirement presented in [11, Theorem 2]. Figure 2.9 presents the response y and control u. FDAHC yields asymptotic disturbance rejection. △

2.7.2 Two-Mass Structure

Consider the 2-mass structure shown in Fig. 2.10, where ψ_1 and ψ_2 are the control forces, d_1 and d_2 are disturbance forces, ξ_1 and ξ_2 are displacements of masses m_1 and m_2. This system is modeled by (2.1), where

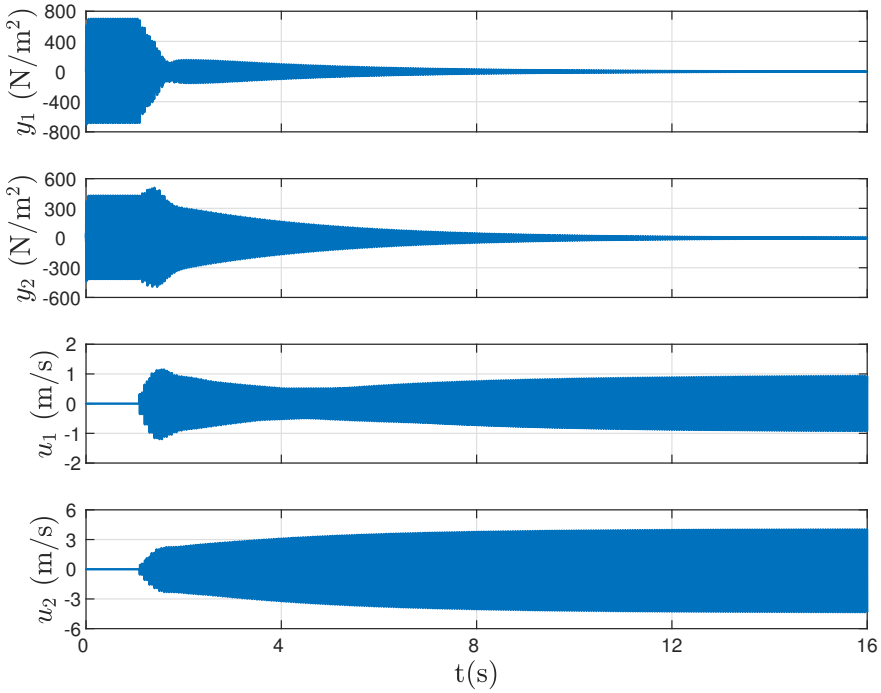

Figure 2.9: FDAHC for a multi-tone disturbance acting on a MIMO system. The response $y(t) \to 0$ as $t \to \infty$.

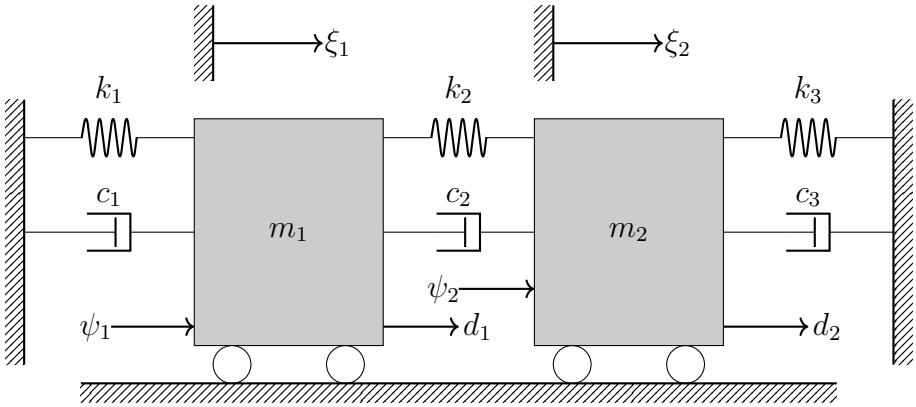

Figure 2.10: Two-Mass Structure.

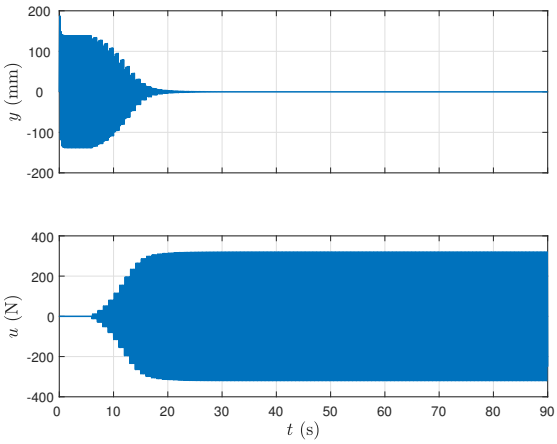

Figure 2.11: FDAHC for a SISO system in the absence of sensor noise. The response $y(t) \to 0$ as $t \to \infty$.

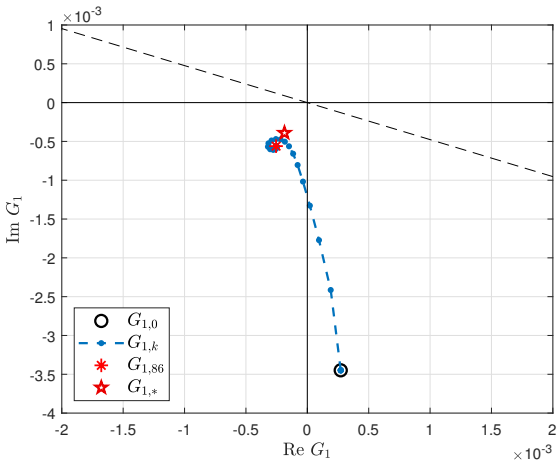

Figure 2.12: Trajectory of $G_{1,k}$ with FDAHC for a SISO system in the absence of sensor noise. The dashed lines show the locus of G such that $|\angle G_{1,0}/G_{1,*}| = \frac{\pi}{2}$.

$$A = \begin{bmatrix} 0 & 1 & 0 & 0 \\ \frac{-(k_1+k_2)}{m_1} & \frac{-(c_1+c_2)}{m_1} & \frac{k_2}{m_1} & \frac{c_2}{m_1} \\ \frac{k_2}{m_2} & \frac{c_2}{m_2} & \frac{-(k_2+k_3)}{m_2} & \frac{-(c_2+c_3)}{m_2} \end{bmatrix}, \quad B = \begin{bmatrix} 0 & 0 \\ \frac{1}{m_1} & 0 \\ 0 & 0 \\ 0 & \frac{1}{m_2} \end{bmatrix}, \quad D_1 = B,$$

$$x(t) = \begin{bmatrix} \xi_1(t) \\ \dot{\xi}_1(t) \\ \xi_2(t) \\ \dot{\xi}_2(t) \end{bmatrix}, \quad u(t) = \begin{bmatrix} \psi_1 \\ \psi_2 \end{bmatrix}, \quad d(t) = \begin{bmatrix} d_1(t) \\ d_2(t) \end{bmatrix},$$

where $m_1 = 2$ kg, $m_2 = 1$ kg, $c_1 = 60$ kg/s, $c_2 = 50$ kg/s, $c_3 = 40$ kg/s, $k_1 = 300$ N/m, $k_2 = 200$ N/m, and $k_3 = 400$ N/m. The initial conditions are $x(0) = 0$ and $d(0) = 0$.

For all examples, let $T_s = 1$ s, and $\sigma_1 = \nu_1 = 1 \times 10^{-12}$. For each example, the control turns on at $t = 5$ s. The disturbance forces d_1 and d_2 and adaptive gains μ_1 and γ_1 are identified in each example.

Example 2.4. Consider the SISO system where $y = \xi_1$, $\psi_1 = u$, $\psi_2 = 0$, $d_1(t) = 200 \sin \omega_1 t + 250 \cos \omega_1 t$ and $d_2(t) = 0$, where $\omega_1 = 8\pi$ rad/s. Let $G_{1,0} = \mathrm{e}^{\jmath \frac{\pi}{6}} G_{1,*}$, which is 30° away from $G_{1,*}$ and let $\mu_1 = \gamma_1 = 0.3$. Figure 2.11 presents the response y and control u. Figure 2.12 presents the trajectory of the estimate $G_{1,k}$ which approaches $G_{1,*}$. FDAHC yields asymptotic disturbance rejection. △

In the following examples, we show that actuator saturation and sensor noise can prevent optimal (or even acceptable) disturbance rejection using FDAHC. Despite this shortcoming, we show that modified FDAHC is able to address these problems. In the following example, we show that modified FDAHC is able to address the problem of actuator saturation.

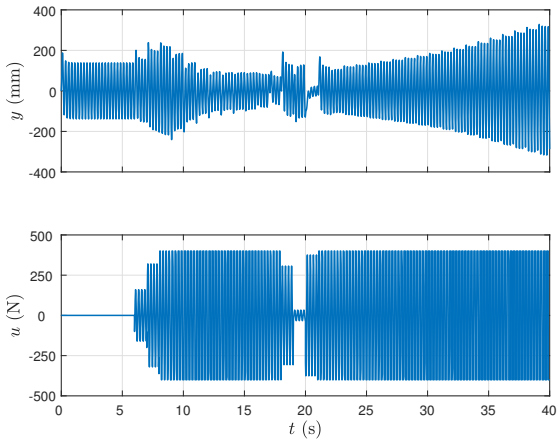

Figure 2.13: FDAHC for a SISO system with actuator saturation. Due to the effects of actuator saturation, asymptotic disturbance rejection is not achieved.

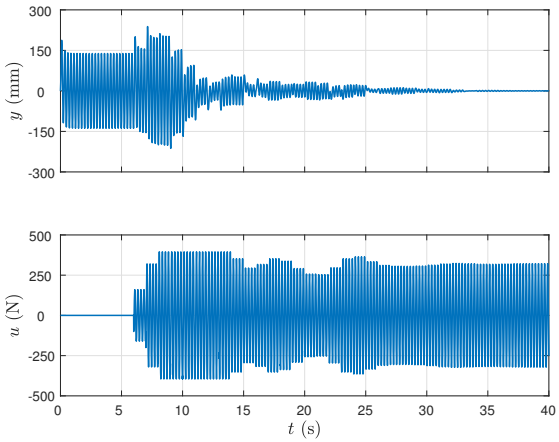

Figure 2.14: Modified FDAHC for a SISO system with actuator saturation. Asymptotic disturbance rejection is achieved despite actuator saturation.

Example 2.5. We reconsider Example 2.4 but let the gains $\mu_1 = 0.4$ and $\gamma_1 = 0.2$ and initial estimate $G_{1,0} = 0.8\mathrm{e}^{\jmath\frac{3\pi}{2}} G_{1,*}$. We impose actuator saturation at $u_{\mathrm{m}} = 400$ N, which is the maximum allowable magnitude of $u_{1,k}$. First, we use FDAHC to investigate the effects of actuator saturation. Figure 2.13 presents the response y and control u. At approximately $t = 8$ s, u saturates and asymptotic disturbance rejection is not achieved.

Next, we revisit the simulation but implement modified FDAHC. Let $u_{\max} = 395$ N, which was selected to ensure $|u_{1,k}|$ does not exceed u_{m}. Figure 2.14 presents the response y and control u. In contrast to FDAHC, modified FDAHC prevents actuator saturation and yields asymptotic disturbance rejection. △

In the following example, we show that in the presence sensor noise, the estimate $G_{i,k}$ can experience drift and diverge from $G_{i,*}$.

Example 2.6. We reconsider Example 2.4 but introduce Gaussian white noise with a mean of 0 and variance of 8×10^{-6} m. Figure 2.15 presents the response y and control u. Fig. 2.16 presents the trajectory of the estimate $G_{1,k}$. Note that due to the presence of sensor noise, the estimate $G_{1,k}$ diverges significantly from $G_{1,*}$. Despite this effect, FDAHC yields asymptotic disturbance rejection.

Next, we revisit the simulation but implement modified FDAHC to address the problem of sensor noise. Let $R_{\mathrm{m}} = 4 \times 10^{-3}$ which bounds $G_{i,k}$ and ensures that $|G_{i,k}| < R_{\mathrm{m}}$. Figure 2.17 presents the response y and control u. Figure 2.18 presents the trajectory of the estimate $G_{1,k}$. Note that despite the presence of sensor noise, modified FDAHC constrains the estimate $G_{1,k}$ by R_{m} which mitigates the affect of drift. Modified FDAHC yields asymptotic disturbance rejection. △

In the next example, we implement modified FDAHC on a system acted on by a multi-tone disturbance that is subject to both actuator saturation and sensor noise.

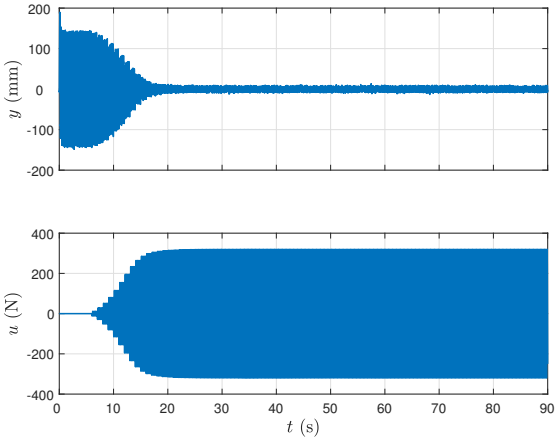

Figure 2.15: FDAHC for a SISO system in the presence of sensor noise. Despite the presence of drift in the estimate $G_{1,k}$, the response $y(t) \to 0$ as $t \to \infty$.

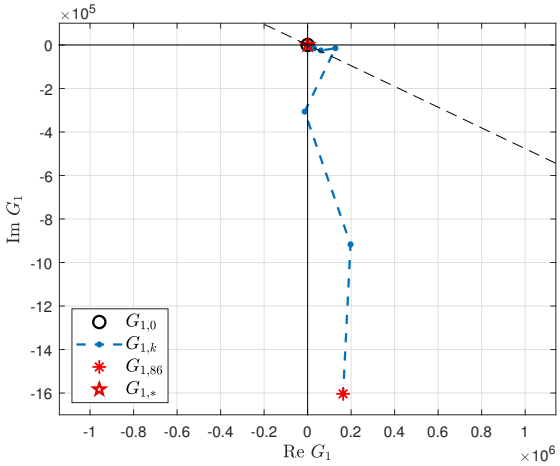

Figure 2.16: Trajectory of $G_{1,k}$ with FDAHC for a SISO system in the presence of sensor noise. The dashed lines show the locus of G such that $|\angle G_{1,0}/G_{1,*}| = \frac{\pi}{2}$. Due to the presence of sensor noise, the estimate $G_{1,k}$ diverges significantly from $G_{1,*}$.

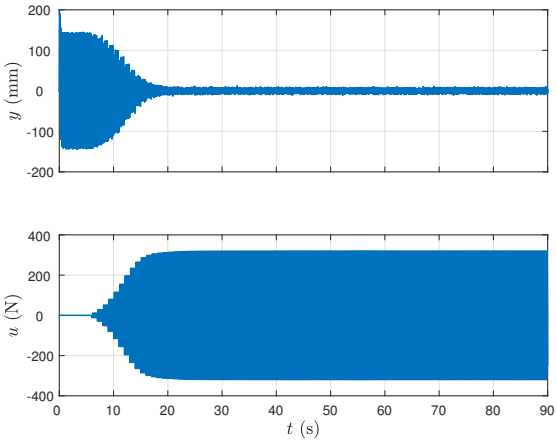

Figure 2.17: Modified FDAHC for a SISO system in the presence of sensor noise. Despite the presence of drift in the estimate $G_{1,k}$, the response $y(t) \to 0$ as $t \to \infty$.

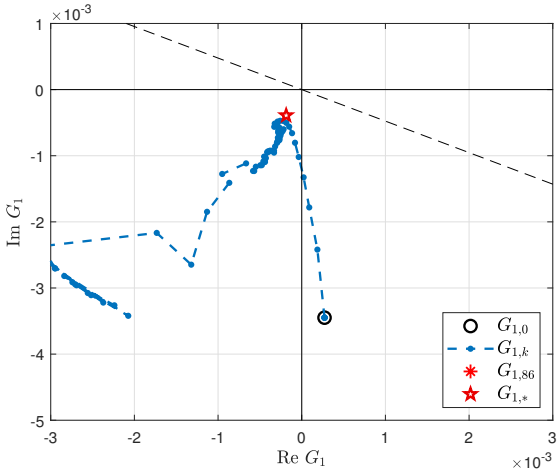

Figure 2.18: Trajectory of $G_{1,k}$ with Modified FDAHC for a SISO system in the presence of sensor noise. The dashed lines show the locus of G such that $|\angle G_{1,0}/G_{1,*}| = \frac{\pi}{2}$. Despite the presence of sensor noise, modified FDAHC constrains the estimate $G_{1,k}$ by R_{m} which mitigates the affect of drift.

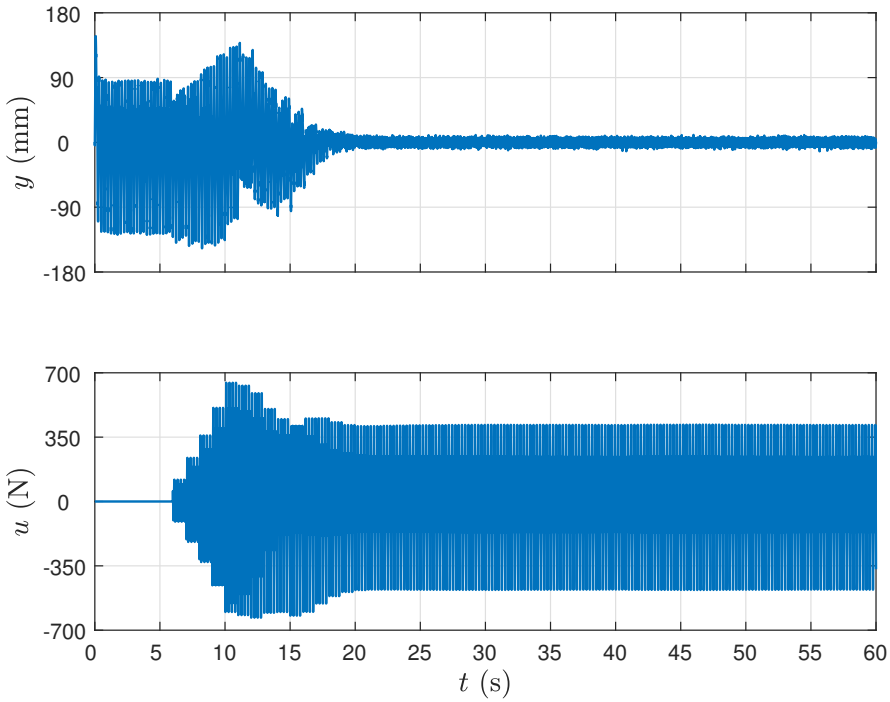

Figure 2.19: Modified FDAHC for a SISO system acted on by a multi-tone disturbance that is subject to actuator saturation and sensor noise. Asymptotic disturbance rejection is achieved.

Example 2.7. Consider the SISO system where $y = \xi_1$, $\psi_1 = u$, $\psi_2 = 0$,

$$d_1(t) = 200 \sin \omega_1 t + 250 \cos \omega_1 t, \quad d_2(t) = 200 \sin \omega_2 t + 250 \cos \omega_2 t,$$

where $\omega_1 = 16\pi$ rad/s and $\omega_2 = 8\pi$ rad/s. Let $G_{1,0} = 0.75\mathrm{e}^{\jmath \frac{5\pi}{2}} G_{1,*}$ and let $G_{2,0} = 3.5\mathrm{e}^{\jmath \frac{3\pi}{2}} G_{2,*}$. Let $\mu_1 = \gamma_1 = 0.25$. We impose actuator saturation at $u_{\mathrm{m}} = 655$ N, which is the maximum allowable magnitude of $u_{i,k}$. To ensure actuator saturation does not occur, we let $u_{\max} = 650$ N, which was selected to ensure $|u_{i,k}|$ does not exceed u_{m}. We also introduce Gaussian white noise with a mean of 0 and variance of 8×10^{-6} m. To mitigate the effect of drift in $G_{i,k}$ caused by the Gaussian white noise, we select $R_{\mathrm{m}} = 4 \times 10^{-3}$ which bounds $G_{i,k}$ and ensures that $|G_{i,k}| < R_{\mathrm{m}}$. Figure 2.19 presents the response y and control u. Modified FDAHC yields asymptotic disturbance rejection. △

2.8 Conclusion

First, this chapter reviewed FDAHC, which is introduced in [11]. Next, we noted that sensor noise and actuator saturation can negatively impact the performance of FDAHC. To address this shortcoming, we presented a modification to FDAHC to alleviate the problems of sensor noise and actuator saturation.

Chapter 3
Review of Time-Domain Adaptive Harmonic Control

In this chapter, we review time-domain adaptive harmonic control (TDAHC), which addresses the problem of rejecting sinusoidal disturbances with known frequencies that act on a completely unknown asymptotically stable linear time-invariant (LTI) system. The review of TDAHC is based on [12], which introduced this method. This chapter also presents modifications of the TDAHC algorithm to address sensor noise and actuator saturation.

3.1 Notation

Let $\mathbb{F}$ be $\mathbb{R}$ or $\mathbb{C}$, and let $x_{(i)}$ denote the ith element of $x \in \mathbb{F}^n$. Let $\|\cdot\|$ be the 2-norm on $\mathbb{F}^n$, and let $\|\cdot\|_\infty$ be the infinity norm on $\mathbb{F}^n$. Let A^* denote the complex conjugate transpose of $A \in \mathbb{F}^{m\times n}$ and define the Frobenius norm of $A \in \mathbb{F}^{m\times n}$ as $\|A\|_{\mathrm{F}} \triangleq \sqrt{\mathrm{trA^*A}}$. Define the *open ball radius* $r \geq 0$ *centered at* $C \in \mathbb{C}^{m\times n}$ by $\mathbb{B}_r(C) \triangleq X \in \mathbb{C}^{m\times n} \colon \|X - C\|_{\mathrm{F}} < r$.

Let $\mathrm{spec}(A) \triangleq \{\lambda \in \mathbb{C} : \det(\lambda I - A) = 0\}$ denote the spectrum of $A \in \mathbb{F}^{n\times n}$, and let $\mathrm{sprad}(A) \triangleq \max_{\lambda\in\mathrm{spec(A)}}|\lambda|$ denote the spectral radius of $A \in \mathbb{F}^{n\times n}$. Let $\lambda_{\min}(A)$ denote the minimum eigenvalue of the symmetric positive-semi definite matrix $A \in \mathbb{F}^{n\times n}$. Let $\sigma_{\min}(A)$ denote the minimum eigenvalue of the symmetric positive-semidefinite matrix $A \in \mathbb{F}^{m\times n}$ and let $\sigma_{\max}(A)$ denote the maximum singular value of $A \in \mathbb{F}^{m\times n}$.

The Moore-Penrose generalized inverse [30, Chap. 8.1] of $A \in \mathbb{R}^{m\times n}$ is denoted by $A^+ \in \mathbb{R}^{n\times m}$. Note that if $A \in \mathbb{R}^{m\times n}$ is right invertible (i.e., rank $A = m$), then $A^+ = A^{\mathrm{T}}(AA^{\mathrm{T}})^{-1}$.

Let $\angle\lambda$ denote the argument of $\lambda \in \mathbb{C}$ defined on the interval $(-\pi, \pi]$ rad. Let ORHP and OUD denote the open-left-half plane and open unit disk in $\mathbb{C}$, respectively. Define $\mathbb{N} \triangleq \{0, 1, 2, \dots\}$ and $\mathbb{Z}^+ \triangleq \mathbb{N} \setminus \{0\}$.

3.2 Problem Formulation

Consider the LTI system

$$\dot{x}(t) = Ax(t) + Bu(t) + D_1 d(t), \tag{3.1}$$
$$y(t) = Cx(t) + Du(t) + D_2 d(t), \tag{3.2}$$

where $t \geq 0$, $x(t) \in \mathbb{R}^n$ is the state, $x(0) = x_0 \in \mathbb{R}^n$ is the initial condition, $u(t) \in \mathbb{R}^m$ is the control, $y(t) \in \mathbb{R}^\ell$ is the measured performance, $d(t) \in \mathbb{R}^{\ell_d}$ is the unmeasured disturbance, and $A \in \mathbb{R}^{n \times n}$ is asymptotically stable. Consider the tonal disturbance

$$d(t) = \sum_{i=1}^{q} d_{\mathrm{c},i} \cos \omega_i t + d_{\mathrm{s},i} \sin \omega_i t, \tag{3.3}$$

where $\omega_1, \omega_2, \ldots, \omega_q > 0$ and $d_{\mathrm{c},1}, d_{\mathrm{c},2}, \ldots, d_{\mathrm{c},q}, d_{\mathrm{s},1}, d_{\mathrm{s},2}, \ldots, d_{\mathrm{s},q} \in \mathbb{R}^{\ell_d}$ determine the disturbance amplitude and phase at each disturbance frequency. Define the transfer functions $G_{yu} \colon \mathbb{C} \to \mathbb{C}^{\ell \times m}$ and $G_{yd} \colon \mathbb{C} \to \mathbb{C}^{\ell \times \ell_d}$ by

$$G_{yu}(s) \triangleq C(sI - A)^{-1}B + D, \tag{3.4}$$
$$G_{yd}(s) \triangleq C(sI - A)^{-1}D_1 + D_2. \tag{3.5}$$

We make the following assumptions:

(A3.1) For all $i \in Q \triangleq \{1, 2, \ldots, q\}$, rank $G_{yu}(\jmath\omega_i) = \ell$.

(A3.2) $\omega_i, \ldots, \omega_q$ are known.

Assumption (A3.1) implies that the number of actuators is at least as large as the number of performance measures (i.e., $m \geq \ell$). Assumption (A3.2) implies that the disturbance frequencies ω_i are known; however, the disturbance amplitudes $d_{\mathrm{c},i}$ and $d_{\mathrm{s},i}$ and the system model A, B, C, D, D_1, and D_2 are completely unknown.

The goal is to design a control u that eliminates the effect of the disturbance d on the performance y. We desire a control that relies on no model information regarding the system (3.1) and (3.2), and requires knowledge of only the disturbance frequencies $\omega_1, \ldots, \omega_q$. Unless otherwise stated, all statements in this chapter that involve the subscript i are for all $i \in Q$.

3.3 Ideal Control

For the moment, assume that $G_{yu}(\jmath\omega_i)$, $G_{yd}(\jmath\omega_i)$, $d_{\mathrm{c},i}$, and $d_{\mathrm{s},i}$ are known. Let $u_{\mathrm{c},i}, u_{\mathrm{s},i} \in \mathbb{R}^m$, and consider the harmonic control

$$\begin{aligned} u(t) &= \sum_{i=1}^{q} u_{\mathrm{c},i} \cos \omega_i t + u_{\mathrm{s},i} \sin \omega_i t \\ &= \sum_{i=1}^{q} \Big(f_i^{\mathrm{T}}(t) \otimes I_m \Big) \hat{u}_i, \end{aligned} \tag{3.6}$$

where $\otimes$ is the Kronecker product, and

$$\hat{u}_i \triangleq \begin{bmatrix} u_{\mathrm{c},i} \\ u_{\mathrm{s},i} \end{bmatrix} \in \mathbb{R}^{2m}, \tag{3.7}$$

$$f_i(t) \triangleq \begin{bmatrix} \cos \omega_i t \\ \sin \omega_i t \end{bmatrix} \in \mathbb{R}^2. \tag{3.8}$$

Define

$$G_{i,*} \triangleq G_{yu}(\jmath\omega_i) \in \mathbb{C}^{\ell \times m}, \tag{3.9}$$

$$d_{i,*} \triangleq \begin{bmatrix} \operatorname{Re} G_{yd}(\jmath\omega_i) & \operatorname{Im} G_{yd}(\jmath\omega_i) \\ -\operatorname{Im} G_{yd}(\jmath\omega_i) & \operatorname{Re} G_{yd}(\jmath\omega_i) \end{bmatrix} \begin{bmatrix} d_{\mathrm{c},i} \\ d_{\mathrm{s},i} \end{bmatrix} \in \mathbb{R}^{2\ell}. \tag{3.10}$$

The harmonic steady-state (HSS) performance of (3.1) and (3.2) with disturbance (3.3) and control (3.6) is

$$\begin{aligned} y_{\mathrm{hss}}(t, \hat{u}_1, \ldots, \hat{u}_q) &\triangleq \sum_{i=1}^{q} \operatorname{Re} \Big(G_{yu}(\jmath\omega_i)(u_{\mathrm{c},i} - \jmath u_{\mathrm{s},i}) + G_{yd}(\jmath\omega_i)(d_{\mathrm{c},i} - \jmath d_{\mathrm{s},i}) \Big) e^{\jmath\omega_i t} \\ &= \sum_{i=1}^{q} \Big(f_i^{\mathrm{T}}(t) \otimes I_\ell \Big) \Big(H(G_{i,*}) \hat{u}_{i,} + d_{i,*} \Big), \end{aligned} \tag{3.11}$$

where $H \colon \mathbb{C}^{\ell \times m} \to \mathbb{R}^{2\ell \times 2m}$ is defined by

$$H(G) \triangleq \begin{bmatrix} \operatorname{Re} G & \operatorname{Im} G \\ -\operatorname{Im} G & \operatorname{Re} G \end{bmatrix} \in \mathbb{R}^{2\ell \times 2m}. \tag{3.12}$$

Consider the cost function

$$J(\hat{u}_1, \ldots, \hat{u}_q) \triangleq \lim_{t \to \infty} \frac{1}{t} \int_0^t \| y_{\mathrm{hss}}(\tau, \hat{u}_1, \ldots, \hat{u}_q) \|^2 \mathrm{d}\tau, \tag{3.13}$$

which is the average power of y_{hss}. Substituting (3.11) into (3.13) yields

$$\begin{aligned} J(\hat{u}_1, \ldots, \hat{u}_q) &= \lim_{t \to \infty} \frac{1}{t} \int_0^t \left\| \sum_{i=1}^{q} \Big(f_i^{\mathrm{T}}(\tau) \otimes I_\ell \Big) \Big(H(G_{i,*}) \hat{u}_{i,} + d_{i,*} \Big) \right\|^2 \mathrm{d}\tau \\ &= \sum_{i=1}^{q} \sum_{j=1}^{q} (H(G_{i,*}) \hat{u}_i + d_{i,*})^{\mathrm{T}} \Big(\lim_{t \to \infty} \frac{1}{t} \int_0^t \Big(f_i(\tau) f_j^{\mathrm{T}}(\tau) \Big) \otimes I_\ell \, \mathrm{d}\tau \Big) \\ &\qquad \times (H(G_{j,*}) \hat{u}_j + d_{j,*}) \\ &= \sum_{i=1}^{q} (H(G_{i,*}) \hat{u}_i + d_{i,*})^{\mathrm{T}} \Big(\lim_{t \to \infty} \frac{1}{t} \int_0^t \Big(f_i(\tau) f_i^{\mathrm{T}}(\tau) \Big) \otimes I_\ell \, \mathrm{d}\tau \Big) \\ &\qquad \times (H(G_{i,*}) \hat{u}_i + d_{i,*}) \\ &= \frac{1}{2} \sum_{i=1}^{q} \| H(G_{i,*}) \hat{u}_i + d_{i,*} \|^2. \end{aligned} \tag{3.14}$$

It follows from (3.14) that J is minimized by finding $\hat{u}_i$ that minimizes $\frac{1}{2}\|H(G_{i,*})\hat{u}_i + d_{i,*}\|^2$, which is equal to the average power of $y_{\rm hss}$ at frequency ω_i. Since (A3.1) implies that rank $G_{i,*} = \ell$, it follows that rank $H(G_{i,*}) = 2\ell$, which implies that $H(G_{i,*})$ is right invertible. The following result provides an expression for the control that minimizes J. This result is presented in [12, Theorem 1].

Theorem 3.1. Assume that (A3.1) holds. For all $i \in Q$, define $u_{i,*} \triangleq -H^+(G_{i,*})d_{i,*}$. Then, $J(u_{1,*}, \ldots, u_{q,*}) = 0$.

Theorem 3.1 provides the ideal control parameter $u_{i,*}$, but $u_{i,*}$ requires knowledge of $G_{i,*}$ and $d_{i,*}$, which are unknown.

3.4 Review of TDAHC

TDAHC uses a sinusoidal control with frequencies ω_i, and amplitudes and phases that are updated at discrete times. Let $T_{\rm s}$ denote the update period, and for each $k \in \mathbb{N}$ and for all $t \in [kT_{\rm s}, (k+1)T_{\rm s})$, consider the control

$$u(t) = \sum_{i=1}^{q} \Big(f_i^{\rm T}(t) \otimes I_m\Big) u_{i,k}, \tag{3.15}$$

where $u_{i,k} \in \mathbb{R}^{2m}$ is determined from the update equations presented in this section. Thus, the control (3.15) is a piecewise-continuous sinusoid. We make the following technical assumptions:

(A3.3) For all $i \in Q$ and for all $j \in Q\backslash\{i\}$, $e^{\jmath\omega_j T_{\rm s}} \neq e^{\jmath\omega_i T_{\rm s}}$ and $e^{-\jmath\omega_j T_{\rm s}} \neq e^{\jmath\omega_i T_{\rm s}}$.

(A3.4) For all $i \in Q$, $\angle e^{\jmath\omega_i T_{\rm s}} \notin \{0, \pi\}$.

Assumption (A3.3) implies that the disturbance frequencies are distinct. Assumption (A3.4) implies that $\omega_i T_{\rm s}$ is not an integer multiple of π. Assumptions (A3.3) and (A3.4) involve disturbance frequencies ω_i and the update period $T_{\rm s}$. Since $\omega_i, \ldots, \omega_q$ are known, it follows that $T_{\rm s}$ can be selected to satisfy (A3.3) and (A3.4).

For each $k \in \mathbb{Z}^+$, define the sampled performance

$$y_k \triangleq y(kT_{\rm s}), \tag{3.16}$$

which is the feedback used by TDAHC. Note that if $T_{\rm s}$ is sufficiently large relative to the settling time of (3.1) and (3.2), then for all $k \in \mathbb{Z}^+$, $y_k \approx y_{\rm hss}(kT_{\rm s}, u_{1,k-1}, \ldots, u_{q,k-1})$. In Section 3.5, we invoke the HSS assumption that for all $k \in Z^+$, $y_k = y_{\rm hss}(kT_{\rm s}, u_{1,k-1}, \ldots, u_{q,k-1})$; however, this assumption is used only for the stability analysis in Section 3.5.

For all $\alpha \in \mathbb{Z}^+ \setminus \{1, 2, \ldots, 2q-1\}$, define the Vandermonde matrix

$$V_\alpha \triangleq \begin{bmatrix} 1 & e^{-\jmath\omega_1 T_\mathrm{s}} & e^{-\jmath 2\omega_1 T_\mathrm{s}} & \ldots & e^{-\jmath(\alpha-1)\omega_1 T_\mathrm{s}} \\ 1 & e^{\jmath\omega_1 T_\mathrm{s}} & e^{\jmath 2\omega_1 T_\mathrm{s}} & \ldots & e^{\jmath(\alpha-1)\omega_1 T_\mathrm{s}} \\ \vdots & \vdots & \vdots & & \vdots \\ 1 & e^{-\jmath\omega_q T_\mathrm{s}} & e^{-\jmath 2\omega_q T_\mathrm{s}} & \ldots & e^{-\jmath(\alpha-1)\omega_q T_\mathrm{s}} \\ 1 & e^{\jmath\omega_q T_\mathrm{s}} & e^{\jmath 2\omega_q T_\mathrm{s}} & \ldots & e^{\jmath(\alpha-1)\omega_q T_\mathrm{s}} \end{bmatrix} \in \mathbb{C}^{2q\times\alpha}. \tag{3.17}$$

The following lemma concerns right invertibility of V_α. The proof follows from [30, Fact 7.18.5].

Lemma 3.1. Assume that (A3.3) and (A3.4) hold. Then, for all $\alpha \in \mathbb{Z}^+\setminus\{1, 2, \ldots, 2q-1\}$, V_α is right invertible.

Let $r \in \mathbb{Z}^+$ be such that $r \geq 2q$, and for all $k \in \mathbb{Z}^+$, define

$$f_{i,k} \triangleq f_i(kT_\mathrm{s}) \in \mathbb{R}^2, \tag{3.18}$$

$$\psi_k \triangleq \begin{bmatrix} f_{1,k}^\mathrm{T} & \ldots & f_{q,k}^\mathrm{T} \end{bmatrix}^\mathrm{T} \in \mathbb{R}^{2q}, \tag{3.19}$$

$$\Psi_k \triangleq \begin{bmatrix} \psi_k & \ldots & \psi_{k-r+1} \end{bmatrix} \in \mathbb{R}^{2q\times r}. \tag{3.20}$$

The choice of r affects the performance of TDAHC. The following result from [12, Lemma 2] concerns the right inverse of Ψ_k, and provides an expression for Ψ_k^+.

Lemma 3.2. Assume that (A3.3) and (A3.4) are satisfied. Then, for all $k \in \mathbb{N}$, Ψ_k is invertible, and

$$\Psi_k^+ = \Psi_k^\mathrm{T} S_k^\mathrm{T} (V_r V_r^\mathrm{T})^{-1} S_k, \tag{3.21}$$

where

$$S_k \triangleq \mathrm{diag}(S_{1,k}, \ldots, S_{q,k}) \in \mathbb{C}^{2q\times 2q}, \tag{3.22}$$

$$S_{i,k} \triangleq \begin{bmatrix} e^{-\jmath k\omega_i T_\mathrm{s}} & \jmath e^{-\jmath k\omega_i T_\mathrm{s}} \\ e^{\jmath k\omega_i T_\mathrm{s}} & -\jmath e^{\jmath k\omega_i T_\mathrm{s}} \end{bmatrix} \in \mathbb{C}^{2\times 2}. \tag{3.23}$$

Lemma 3.2 provides an expression for Ψ_k^+ that can be computed without an online matrix inversion. In particular, $(V_r V_r^\mathrm{T})^{-1}$ can be computed offline, and Ψ_k^+ can be computed from (3.20).

Let $\mu \in (0, 2)$, $\sigma_i > 0$, and $u_{i,0} \in \mathbb{R}^{2m}$. Then, for all $k \in \mathbb{N}$, consider the control

$$u_{i,k+1} = u_{i,k} - \frac{\mu}{\sigma_i + \sum_{i=1}^q \|G_{i,k}\|_\mathrm{F}^2} H^\mathrm{T}(G_{i,k})(f_{i,k+1} \otimes I_\ell) y_{k+1}, \tag{3.24}$$

where $G_{i,k} \in \mathbb{C}^{\ell\times m}$ is an estimate of $G_{i,*}$ and is obtained from the update equations presented below.

For all $k \geq r$, consider $d_{i,k} : \mathbb{C}^{\ell\times m} \times \cdots \times \mathbb{C}^{\ell\times m} \to \mathbb{R}^{2\ell}$ defined by

$$d_{i,k}(\hat{G}_1, \ldots, \hat{G}_q) \triangleq (e_i \otimes I_{2\ell})\Big((\Psi_k^+)^\mathrm{T} \otimes I_\ell\Big)$$

$$\times \begin{bmatrix} y_k - \sum_{j=1}^{q} \Big(f_{j,k}^{\mathrm{T}} \otimes I_\ell\Big) H(\hat{G}_j) u_{j,k-1} \\ \vdots \\ y_{k-r+1} - \sum_{j=1}^{q} \Big(f_{j,k-r+1}^{\mathrm{T}} \otimes I_\ell\Big) H(\hat{G}_j) u_{j,k-r} \end{bmatrix}, \tag{3.25}$$

where $e_i \in \mathbb{R}^{1\times q}$ is the ith row of I_q. Next, for all $k > r$, consider $\hat{y}_k : \mathbb{C}^{\ell\times m} \times \cdots \times \mathbb{C}^{\ell\times m} \to \mathbb{R}^\ell$ defined by

$$\hat{y}_k(\hat{G}_1, \ldots, \hat{G}_q) \triangleq \sum_{i=1}^{q} (f_{i,k}^{\mathrm{T}} \otimes I_\ell)\Big(H(\hat{G}_i) u_{i,k-1} + d_{i,k-1}(\hat{G}_1, \ldots, \hat{G}_q)\Big). \tag{3.26}$$

To determine the update equation for $G_{i,k}$, consider the cost $\mathcal{J}_k : \mathbb{C}^{\ell\times m} \times \cdots \times \mathbb{C}^{\ell\times m} \to [0, \infty)$ defined by

$$\mathcal{J}_k(\hat{G}_1, \ldots, \hat{G}_q) \triangleq \frac{1}{2} \Big\| y_{k+1} - \hat{y}_{k+1}(\hat{G}_1, \ldots, \hat{G}_q) \Big\|^2,$$

which is a measure of how well $\hat{y}_{k+1}(\hat{G}_1, \ldots, \hat{G}_q)$ approximates the measurement y_{k+1}, which itself is approximately equal to $y_{\mathrm{hss}}((k+1)T_{\mathrm{s}}, u_{1,k}, \ldots, u_{q,k}) = \sum_{i=1}^{q} (f_{i,k+1}^{\mathrm{T}} \otimes I_\ell)(H(G_{i,*})u_{i,k} + d_{i,*})$. Thus, if the HSS assumption and (A3.3)–(A3.4) are satisfied, then $\hat{y}_{k+1}(G_{1,*}, \ldots, G_{q,*}) = y_{k+1}$ and $\mathcal{J}_k(G_{1,*}, \ldots, G_{q,*}) = 0$, that is, $\mathcal{J}_k$ is minimized by $\hat{G}_i = G_{i,*}$.

For all $k \geq r$, define the complex gradient

$$\begin{aligned} \nabla \mathcal{J}_{i,k}(\hat{G}_1, \ldots, \hat{G}_q) &\triangleq \left[\tfrac{\partial \mathcal{J}_k(\hat{G}_1, \ldots, \hat{G}_q)}{\partial(\mathrm{Re}\ \hat{G}_i)} + \jmath \tfrac{\partial \mathcal{J}_k(\hat{G}_1, \ldots, \hat{G}_q)}{\partial(\mathrm{Im}\ \hat{G}_i)} \right]^{\mathrm{T}} \\ &= \Big[I_\ell \quad -\jmath I_\ell \Big] \Gamma_{i,k}(\hat{G}_1, \ldots, \hat{G}_q) \begin{bmatrix} I_m \\ \jmath I_m \end{bmatrix}, \end{aligned} \tag{3.27}$$

where $\Gamma_{i,k} : \mathbb{C}^{\ell\times m} \times \cdots \times \mathbb{C}^{\ell\times m} \to \mathbb{R}^{2\ell\times 2m}$ is defined by

$$\begin{aligned} \Gamma_{i,k}(\hat{G}_1, \ldots, \hat{G}_q) \triangleq \mathrm{vec}^{-1}\Big(F_{i,k}\Big[y_{k+1} - \hat{y}_{k+1}(\hat{G}_1, \ldots, \hat{G}_q)\Big]\Big) \\ - (f_{i,k+1} \otimes I_\ell)\Big[y_{k+1} - \hat{y}_{k+1}(\hat{G}_1, \ldots, \hat{G}_q)\Big] u_{i,k}^{\mathrm{T}}, \end{aligned} \tag{3.28}$$

where $F_{i,k} \in \mathbb{R}^{4\ell m\times \ell}$ is defined by

$$F_{i,k} \triangleq \Big[u_{i,k-1} \otimes f_{i,k} \quad \ldots \quad u_{i,k-r} \otimes f_{i,k-r+1}\Big] \Psi_k^{+} \psi_{k+1}, \tag{3.29}$$

and $\mathrm{vec}^{-1}\colon \mathbb{R}^{4\ell \mathrm{m}} \to \mathbb{R}^{2\ell\times 2\mathrm{m}}$ is the inverse vec operator, that is, for all $X \in \mathbb{R}^{2\ell\times 2m}$, $\mathrm{vec}^{-1}\mathrm{vec}\ \mathrm{X} = \mathrm{X}$. Note that $\nabla\mathcal{J}_{i,k}$ is the direction of the maximum rate of change of $\mathcal{J}_k$ with respect to $\hat{G}_i$. Let $G_{i,0} \in \mathbb{C}^{\ell\times m}$, and for all $k \in \{1, 2, \ldots, r-1\}$, let $G_{i,k} = G_{i,0}$. For all $k \geq r$, consider the update equation

$$G_{i,k} = G_{i,k-1} - \eta_k \nabla \mathcal{J}_{i,k}(G_{1,k-1}, \ldots, G_{q,k-1}), \tag{3.30}$$

where

$$\eta_k \triangleq \frac{\gamma}{\nu + \sum_{j=1}^{q} \|F_{i,k} - u_{i,k} \otimes f_{i,k+1}\|_{\mathrm{F}}^2}, \tag{3.31}$$

where $\gamma \in (0,1)$, and $\nu > 0$. Thus, TDAHC is given by (3.15) and (3.24)–(3.31). The TDAHC architecture is presented in Fig. 3.1.

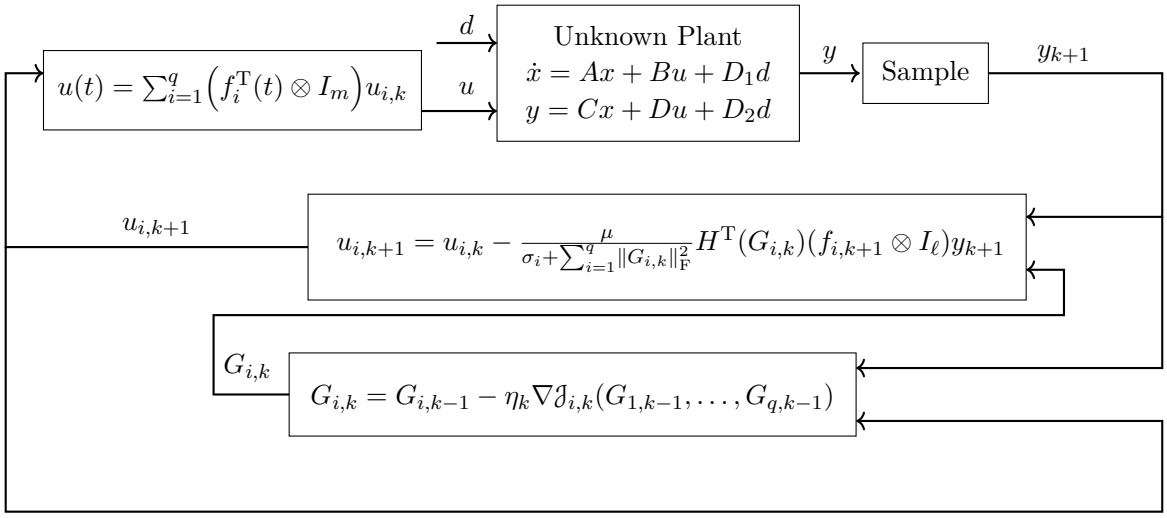

Figure 3.1: Control architecture for TDAHC

3.5 Stability Analysis

If T_{s} is sufficiently large relative to the settling time of (3.1) and (3.2), then for all $k \in \mathbb{Z}^+$, $y_k \approx y_{\mathrm{hss}}(kT_{\mathrm{s}}, u_{1,k-1}, \ldots, u_{q,k-1})$. Thus, we make the HSS assumption:

(A3.5) For all $k \in \mathbb{Z}^+$, $y_k = y_{\mathrm{hss}}(kT_{\mathrm{s}}, u_{1,k-1}, \ldots, u_{q,k-1})$

In this case, (3.11) implies that for all $k \in \mathbb{N}$,

$$y_{k+1} = \sum\nolimits_{i=1}^{q} (f_{i,k+1}^{\mathrm{T}} \otimes I_\ell)(H(G_{i,*})u_{i,k} + d_{i,*}). \tag{3.32}$$

Assumption (A3.5) is used to analyze the stability of the closed loop system consisting of (3.24)–(3.32).

The following result provides the stability properties of the closed-loop system consisting of (3.24)–(3.32) for the case where $q = 1$ and $m \geq \ell = 1$. This result is given in [12, Theorem 4].

Theorem 3.2. Consider the closed-loop system consisting of (3.24)–(3.32), where $q = 1, m \geq \ell = 1$, and (A3.1)–(A3.5) are satisfied. Let $\mu \in (0,2), \gamma \in (0,1), \sigma > 0, \nu > 0, r = 2$, and let $u_{1,0} \in \mathbb{R}^{2m}$ and $G_{1,0} \in \mathbb{C}^{\ell \times m}$. Assume that there exists $k_{\mathrm{s}} \in \mathbb{N}$ and $\varepsilon > 0$ such that for all $k \geq k_{\mathrm{s}}$, $|\mathrm{Im}\, G_{1,*} G_{1,k}^*| \geq \varepsilon$. Then, $\lim_{k\to\infty} y_k = 0$.

3.6 TDAHC Modification

Numerical testing demonstrates that actuator saturation and sensor noise can prevent optimal (or even acceptable) disturbance rejection. To address this shortcoming, we present a modified version of TDAHC. Specifically, we present a modification to the update equation for u_k to address the problem of actuator saturation. We also present a modification to the update equation for $G_{i,k}$ to address the problem of sensor noise.

3.6.1 TDAHC Modification to Address Actuator Saturation

Let $u_{\max} > 0$ be the maximum allowable magnitude of each entry of the control u. In other words, we aim to enforce the constraint that for all $t \geq 0$, $\|u(t)\|_\infty \leq u_{\max}$. For all $k \in \mathbb{N}$, consider the update equation for $u_{i,k}$ given by

$$u_{i,k+1} = \begin{cases} \dfrac{u_{\max}}{\alpha_{k+1}} v_{i,k+1}, & \text{if } \alpha_{k+1} > u_{\max}, \\ v_{i,k+1}, & \text{otherwise,} \end{cases} \tag{3.33}$$

where

$$\alpha_{k+1} \triangleq \max_{j \in \{1,\ldots,m\}} \sum_{i=1}^{q} \|E_j v_{i,k+1}\|, \tag{3.34}$$

$$v_{i,k+1} \triangleq u_{i,k} - \frac{\mu}{\sigma_i + \sum_{i=1}^{q} \|G_{i,k}\|_{\mathrm{F}}^2} H^{\mathrm{T}}(G_{i,k})(f_{i,k+1} \otimes I_\ell) y_{k+1}, \tag{3.35}$$

and for all $j \in \{1, 2, \ldots, m\}$,

$$E_j \triangleq \begin{bmatrix} e_j & 0_{1\times m} \\ 0_{1\times m} & e_j \end{bmatrix}, \tag{3.36}$$

where $e_j \in \mathbb{R}^{1\times m}$ denotes the jth row of I_m. The modified update (3.33)–(3.36) is used in place of (3.24). Note that (3.15) and (3.33)–(3.35) imply that

$$\begin{aligned} \max_{t\in[kT_{\mathrm{s}},(k+1)T_{\mathrm{s}})} |e_j u(t)| &= \max_{t\in[kT_{\mathrm{s}},(k+1)T_{\mathrm{s}})} \left| \sum_{i=1}^{q} e_j \Big(f_i^{\mathrm{T}}(t) \otimes I_m \Big) u_{i,k} \right| \\ &= \max_{t\in[kT_{\mathrm{s}},(k+1)T_{\mathrm{s}})} \left| \sum_{i=1}^{q} f_i^{\mathrm{T}}(t) E_j u_{i,k} \right| \\ &\leq \max_{t\in[kT_{\mathrm{s}},(k+1)T_{\mathrm{s}})} \sum_{i=1}^{q} \left| f_i^{\mathrm{T}}(t) E_j u_{i,k} \right| \\ &\leq \max_{t\in[kT_{\mathrm{s}},(k+1)T_{\mathrm{s}})} \sum_{i=1}^{q} \|f_i(t)\| \|E_j u_{i,k}\| \end{aligned}$$

$$
\begin{aligned}
&= \sum_{i=1}^{q} \|E_j u_{i,k}\| \\
&= \begin{cases} \dfrac{u_{\max}}{\alpha_k} \displaystyle\sum_{i=1}^{q} \|E_j v_{i,k}\|, & \text{if } \alpha_k > u_{\max} \\ \displaystyle\sum_{i=1}^{q} \|E_j v_{i,k}\|, & \text{otherwise} \end{cases} \\
&\leq \frac{u_{\max}}{\alpha_k} \sum_{i=1}^{q} \|E_j v_{i,k}\| \\
&\leq \frac{u_{\max}}{\alpha_k} \alpha_k \\
&= u_{\max},
\end{aligned}
$$

which demonstrates that (3.33)–(3.36) ensures that for all $t \geq 0$, $\|u(t)\|_\infty < u_{\max}$.

3.6.2 TDAHC Modification to Address Sensor Noise

Let $R_{\mathrm{m}} \in \mathbb{R}$ denote an upper bound on $\|G_{i,k}\|_{\mathrm{F}}$. For all $k \in \mathbb{Z}^+$, consider the update equation for $G_{i,k}$ given by

$$
G_{i,k} = \begin{cases} \dfrac{R_{\mathrm{m}}}{\|\Theta_{i,k}\|_{\mathrm{F}}} \Theta_{i,k}, & \text{if } \|\Theta_{i,k}\|_{\mathrm{F}} \geq R_{\mathrm{m}}, \\ \Theta_{i,k}, & \text{otherwise,} \end{cases} \tag{3.37}
$$

where

$$
\Theta_{i,k} \triangleq G_{i,k-1} - \eta_k \nabla \mathcal{J}_{i,k}(G_{1,k-1}, \ldots, G_{q,k-1}). \tag{3.38}
$$

The modified update (3.37) and (3.38) is used in place of (3.30). Note that (3.37) and (3.38) imply that $\|G_{i,k}\|_{\mathrm{F}} \leq R_m$.

3.7 Numerical Examples

In this section, we present numerical examples of TDAHC. Examples 3.1–3.3 illustrate the application of TDAHC to an acoustic duct system. Examples 3.4–3.6 illustrate the application of TDAHC and modified TDAHC to a 2-mass structure.

3.7.1 Acoustic Duct

Consider the acoustic duct shown in Fig. 2.2 and described in Section 2.7.1. All parameters for the acoustic duct are the same as those considered in Section 2.7.1.

Let $\omega_1 = 200\pi$ rad/s, $\omega_2 = 160\pi$ rad/s, $r = 5$, $T_{\mathrm{s}} = 0.091$ s, $\nu_1 = \sigma_1 = 1 \times 10^{-6}$, and $x_0 = 0$. The initial estimate G_0 and disturbance d is given in each example. For each example, the control turns on at $t = 1$ s.

In the following example, we show that TDAHC is able to asymptotically reject a single-tone disturbance acting on a SISO system. Note that the non-adaptive

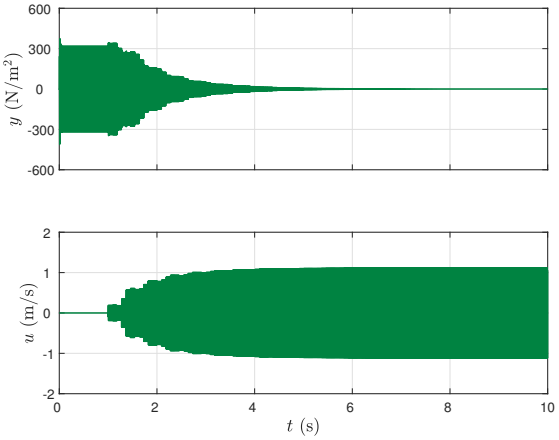

Figure 3.2: TDAHC for a SISO system where $|\angle G_{1,0}/G_{1,*}| < \frac{\pi}{2}$. The response $y(t) \to 0$ as $t \to \infty$.

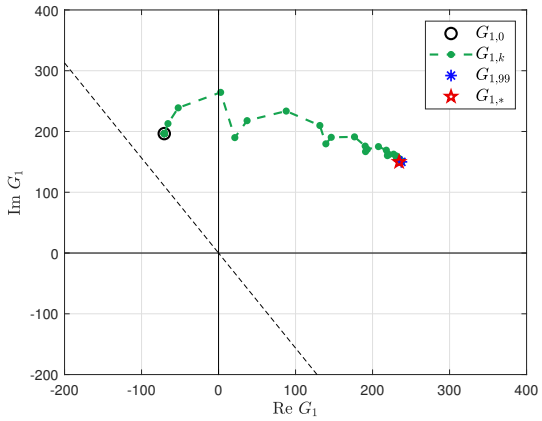

Figure 3.3: Trajectory of $G_{1,k}$ with TDAHC for a SISO system where $|\angle G_{1,0}/G_{1,0}| < \frac{\pi}{2}$. The dashed lines show the locus of G such that $|\angle G_{1,0}/G_{1,*}| = \frac{\pi}{2}$.

version of the algorithm requires a sufficiently accurate estimate of $G_{1,*}$ for stability. Specifically, as shown in [12, Theorem 2], the estimate $G_{1,k}$ must be within 90° of $G_{1,*}$ for stability. In contrast, the adaptive version of the algorithm reviewed in this chapter is stable even if the initial estimate $G_{1,k}$ is not within 90° of $G_{1,*}$ as shown in [11, Theorem 3]. Thus, in this example, we first use an initial condition $G_{1,0}$ which is within 90° of $G_{1,*}$. We then use an initial condition for $G_{1,0}$ which is not within 90° of $G_{1,*}$ to illustrate the effect that the initial estimate $G_{i,k}$ has on the transient response of y.

Example 3.1. Consider the SISO ($\ell = m = 1$) system, where we let $u = \psi_1$, $y = \phi_1$, $\psi_2 = 0$, and $d(t) = 2\sin\omega_1 t + 0.2\cos\omega_1 t$. Let $\mu_1 = \gamma_1 = 0.35$. First, consider the case where $G_{1,0}$ is within 90° of $G_{1,*}$, specifically, let $G_{1,0} = 0.75e^{j\frac{3\pi}{7}}G_{1,*}$. Figure 3.2 presents the response y and control u. Figure 3.3 presents the trajectory of the estimate $G_{1,k}$ which approaches $G_{1,*}$. TDAHC yields asymptotic disturbance rejection.

Next, consider the case where $G_{1,0}$ is not within 90° of $G_{1,*}$, specifically, let $G_{1,0} = -0.75e^{j\frac{3\pi}{7}}G_{1,*}$. Figure 3.4 presents the response y and control u. Figure 3.5 presents the trajectory of the estimate $G_{1,k}$ which approaches $G_{1,*}$. TDAHC yields asymptotic disturbance rejection. In contrast to the first initial condition, this initial condition yielded a larger transient response, but TDAHC was still able to yield asymptotic disturbance rejection. This shows that the HSS stability condition determines the transient response of y. △

Next, we address MIMO systems using TDAHC. In the following example, we show that TDAHC is able to asymptotically reject a single-tone disturbance acting on a MIMO ($\ell = m = 2$) system. We implement TDAHC using two initial conditions to illustrate that the initial condition $G_{1,0}$ affects the transient response of y.

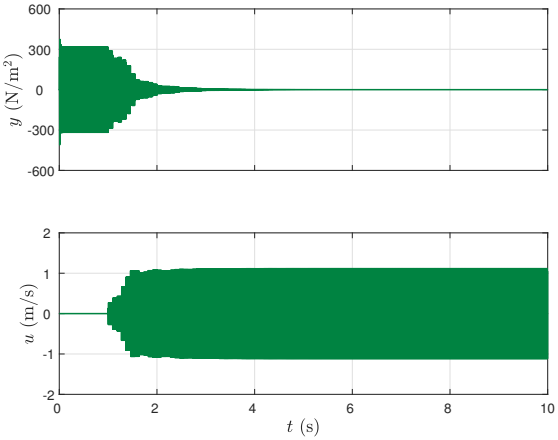

Figure 3.4: TDAHC for a SISO system where $|\angle G_{1,0}/G_{1,*}| > \frac{\pi}{2}$. The response $y(t) \to 0$ as $t \to \infty$.

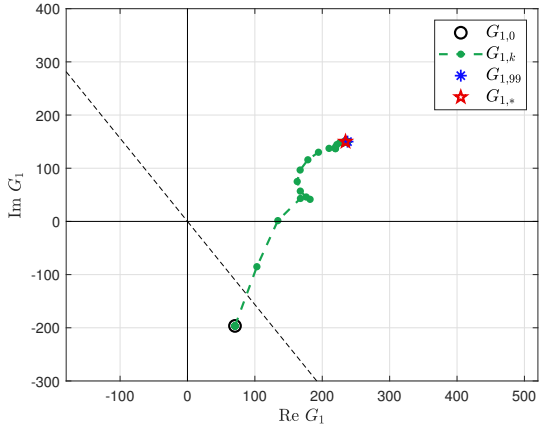

Figure 3.5: Trajectory of $G_{1,k}$ with TDAHC for a SISO system where $|\angle G_{1,0}/G_{1,0}| > \frac{\pi}{2}$. The dashed lines show the locus of G such that $|\angle G_{1,0}/G_{1,*}| = \frac{\pi}{2}$.

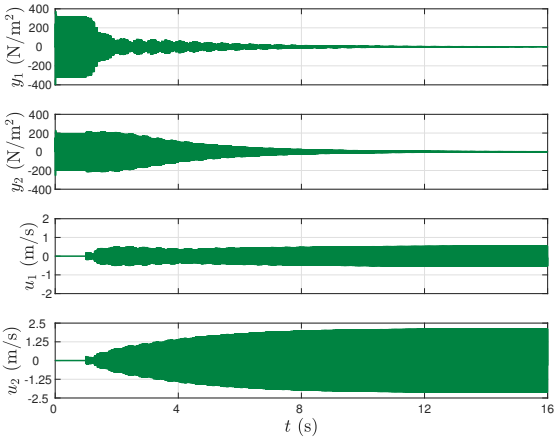

Figure 3.6: TDAHC for a MIMO system where $G_{1,0} = 0.5e^{\jmath\frac{\pi}{5}}G_{1,*}$. The response $y(t) \to 0$ as $t \to \infty$.

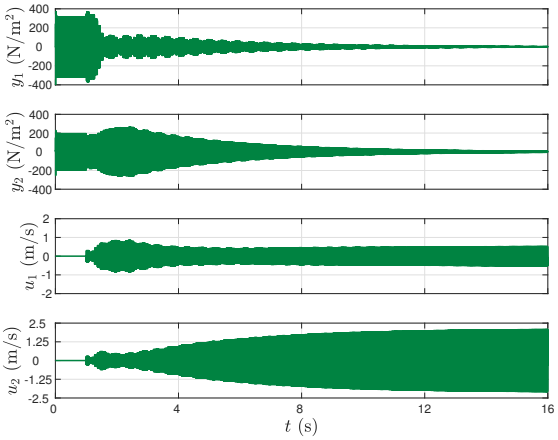

Figure 3.7: TDAHC for a MIMO system where $G_{1,0} = 0.5e^{\jmath\frac{6\pi}{5}}G_{1,*}$. The response $y(t) \to 0$ as $t \to \infty$.

Example 3.2. Consider the MIMO ($\ell = m = 2$) system where we let $u = \begin{bmatrix}\psi_1 & \psi_2\end{bmatrix}^{\mathrm{T}}$, $y = \begin{bmatrix}\phi_1 & \phi_2\end{bmatrix}^{\mathrm{T}}$, and $d(t) = 2\sin\omega_1 t + 0.2\cos\omega_1 t$. Let $\mu_1 = \gamma_1 = 0.7$ and let $G_{1,0} = 0.5e^{\jmath\frac{\pi}{5}}G_{1,*}$ denote the initial estimate of $G_{1,*}$ which satisfies the non-adaptive stability requirement presented in [12, Theorem 2]. Figure 3.6 presents the response y and control u. TDAHC yields asymptotic disturbance rejection.

Next, we consider the initial estimate $G_{1,0} = 0.5e^{\jmath\frac{6\pi}{5}}G_{1,*}$ which does not satisfy the non-adaptive stability requirement presented in [12, Theorem 2]. Figure 3.7 presents the response y and control u. In contrast to the first initial condition, this initial condition yielded a larger transient response, but TDAHC was still able to yield asymptotic disturbance rejection. This shows that the HSS stability condition determines the transient response of y. △

Next, we consider a multi-tone disturbance acting on a MIMO system.

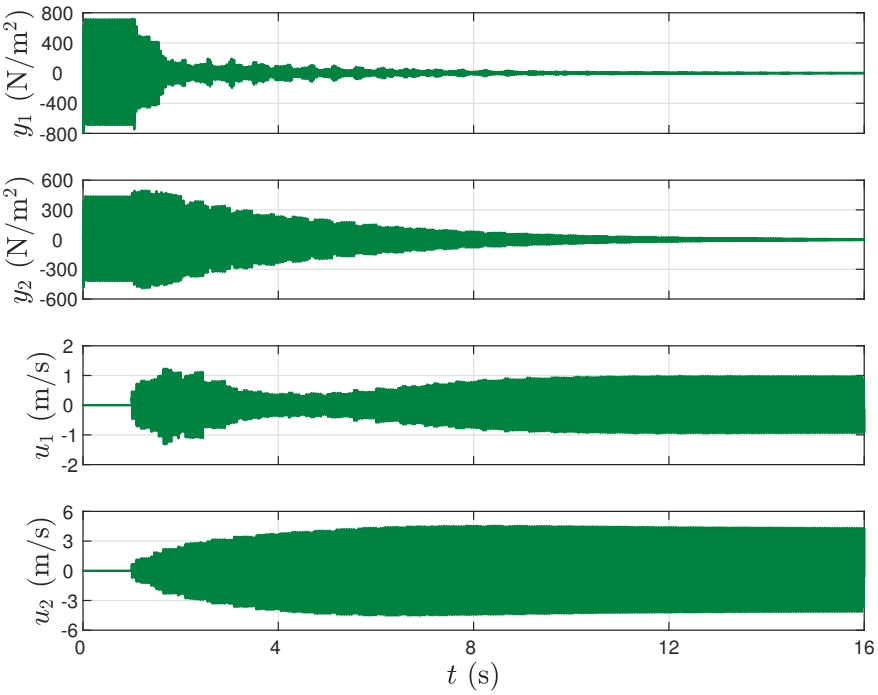

Figure 3.8: TDAHC for a multi-tone disturbance acting on a MIMO system. The response $y(t) \to 0$ as $t \to \infty$.

Example 3.3. Consider the MIMO ($\ell = m = 2$) system where we let $u = \begin{bmatrix}\psi_1 & \psi_2\end{bmatrix}^{\mathrm{T}}$, $y = \begin{bmatrix}\phi_1 & \phi_2\end{bmatrix}^{\mathrm{T}}$, and

$$d(t) = 2\sin\omega_1 t + 0.2\cos\omega_1 t + 2\sin\omega_2 t + 0.2\cos\omega_2 t,$$

which is a 2-tone disturbance. Let $\mu_1 = \gamma_1 = 1.6$. Let $G_{1,0} = 1e^{\jmath\frac{\pi}{3}}G_{1,*}$ and $G_{2,0} = 0.75e^{\jmath\frac{\pi}{6}}G_{2,*}$ denote the initial estimates of $G_{1,*}$ and $G_{2,*}$, respectively, which satisfy the non-adaptive stability requirement presented in [12, Theorem 2]. Figure 3.8 presents the response y and control u. TDAHC yields asymptotic disturbance rejection. $\triangle$

3.7.2 Two-Mass Structure

Consider the 2-mass structure shown in Fig. 2.10 and described in Section 2.7.2. All parameters for the 2-mass structure are the same as those considered in Section 2.7.2.

For all examples, let $T_\mathrm{s} = 0.97$ s, and $\sigma_1 = \nu_1 = 1 \times 10^{-12}$. For each example, the control turns on at $t = 5$ s. The disturbance forces d_1 and d_2 and adaptive gains μ_1 and γ_1 are identified in each example.

Example 3.4. Consider the SISO system where $y = \xi_1$, $\psi_1 = u$, $\psi_2 = 0$, $d_1(t) = 200\sin\omega_1 t + 250\cos\omega_1 t$ and $d_2 = 0$, where $\omega_1 = 8\pi$ rad/s. Let $G_{1,0} = \mathrm{e}^{\jmath\frac{\pi}{6}}G_{1,*}$, which is 30° away from $G_{1,*}$ and let $\mu_1 = \gamma_1 = 0.5$. Figure 3.9 presents the response y and

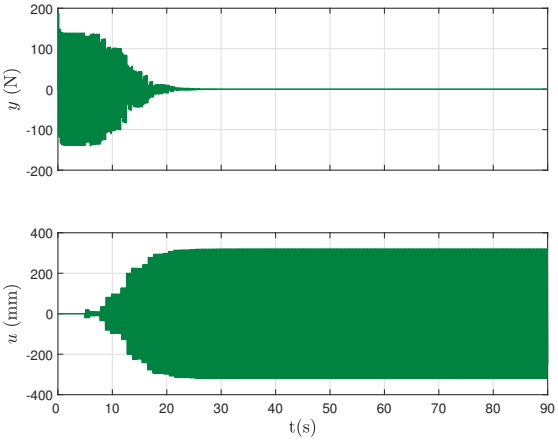

Figure 3.9: TDAHC for a SISO system in the absence of sensor noise. The response $y(t) \to 0$ as $t \to \infty$.

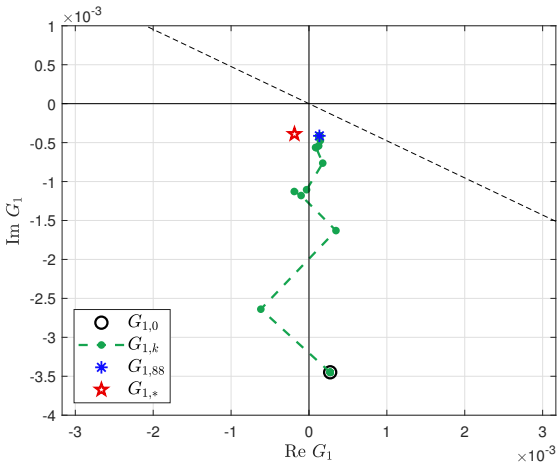

Figure 3.10: Trajectory of $G_{1,k}$ with TDAHC for a SISO system in the absence of sensor noise where $|\angle G_{1,0}/G_{1,0}| < \frac{\pi}{2}$. The dashed lines show the locus of G such that $|\angle G_{1,0}/G_{1,*}| = \frac{\pi}{2}$.

control u. Figure 3.10 presents the trajectory of the estimate $G_{1,k}$ which approaches $G_{1,*}$. TDAHC yields asymptotic disturbance rejection. △

In the following examples, we show that actuator saturation and sensor noise can prevent optimal (or even acceptable) disturbance rejection using TDAHC. Despite this shortcoming, we show that modified TDAHC is able to address these problems.

In the following example, we show that modified TDAHC is able to address the problem of actuator saturation.

Example 3.5. We reconsider Example 3.4 but let the adaptive gains $\mu_1 = 0.5$ and $\gamma_1 = 0.2$ and initial estimate $G_{1,0} = 0.8\mathrm{e}^{\jmath\frac{3\pi}{2}} G_{1,*}$. We impose actuator saturation at $u_{\mathrm{m}} = 400$ N, which is the maximum allowable magnitude of $u_{1,k}$. First, we use TDAHC to investigate the effects of actuator saturation. Figure 3.11 presents the response y and control u. At approximately $t = 8.5$ s, u saturates. Despite saturation occurring, asymptotic disturbance rejection is achieved.

Next, we revisit the simulation but implement modified TDAHC. Let $u_{\max} = 395$ N, which was selected to ensure $|u_{1,k}|$ does not exceed u_{m}. Figure 3.12 presents the response y and control u. In contrast to TDAHC, modified TDAHC prevents actuator saturation and yields asymptotic disturbance rejection. △

In the following example, we show that in the presence sensor noise, the estimate $G_{i,k}$ can experience drift and diverge from $G_{i,*}$.

Example 3.6. We reconsider Example 3.4 but introduce Gaussian white noise with a mean of 0 and variance of 8×10^{-6} m. Figure 3.13 presents the response y and control u. Figure 3.14 presents the trajectory of the estimate $G_{1,k}$. Note that due to the presence of sensor noise, the estimate $G_{1,k}$ diverges significantly from $G_{1,*}$.

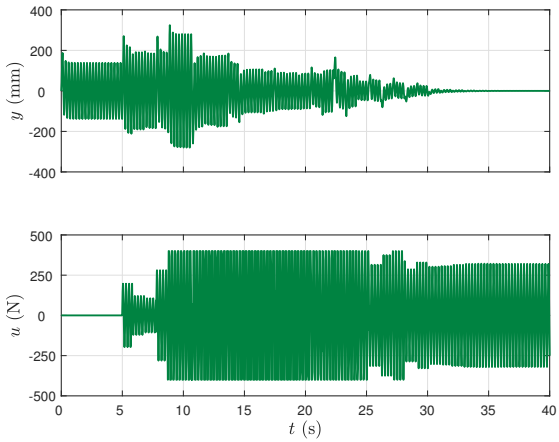

Figure 3.11: TDAHC for a SISO system with actuator saturation. Despite the effects of actuator saturation, asymptotic disturbance rejection is achieved.

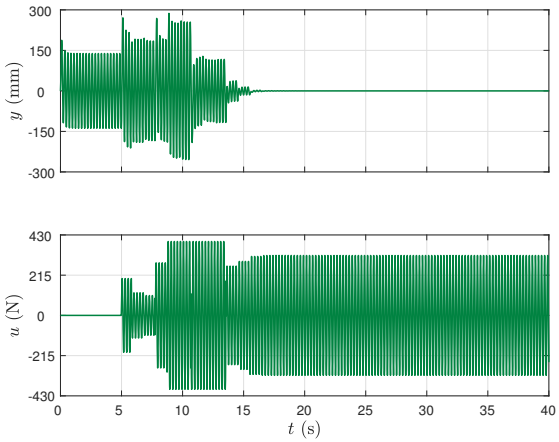

Figure 3.12: Modified TDAHC for a SISO system with actuator saturation. Asymptotic disturbance rejection is achieved despite actuator saturation.

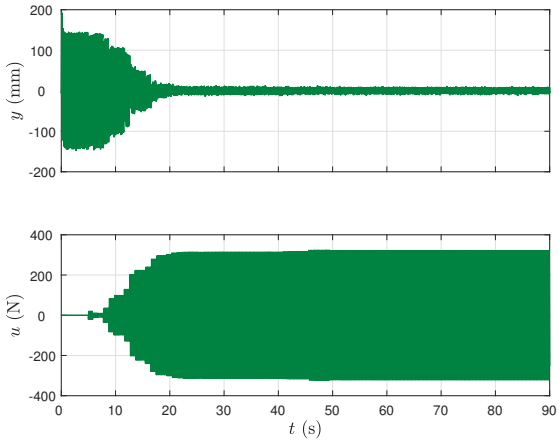

Figure 3.13: TDAHC for a SISO system in the presence of sensor noise. Despite the presence of drift in the estimate $G_{1,k}$, the response $y(t) \to 0$ as $t \to \infty$.

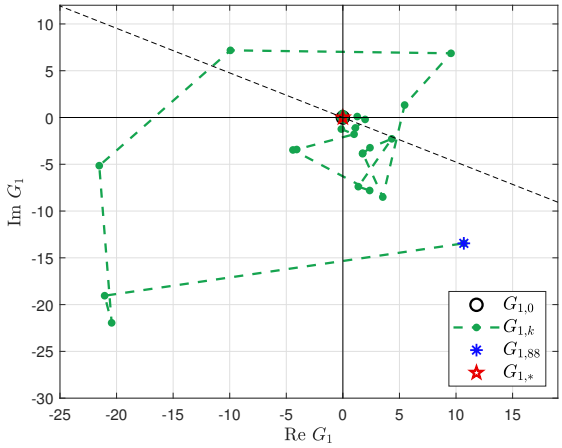

Figure 3.14: Trajectory of $G_{1,k}$ with TDAHC for a SISO system in the presence of sensor noise. The dashed lines show the locus of G such that $|\angle G_{1,0}/G_{1,*}| = \frac{\pi}{2}$. Due to the presence of sensor noise, the estimate $G_{1,k}$ diverges significantly from $G_{1,*}$.

Despite this effect, TDAHC yields asymptotic disturbance rejection.

Next, we revisit the simulation but implement modified TDAHC to address the problem of sensor noise. Let $R_{\mathrm{m}} = 4 \times 10^{-3}$ which bounds $G_{i,k}$ and ensures that $|G_{i,k}| < R_{\mathrm{m}}$. Figure 3.15 presents the response y and control u. Figure 3.16 presents the trajectory of the estimate $G_{1,k}$. Note that despite the presence of sensor noise, modified TDAHC constrains the estimate $G_{1,k}$ by R_{m} which mitigates the affect of drift. Modified TDAHC yields asymptotic disturbance rejection. △

In the next example, we implement modified TDAHC on a system acted on by a multi-tone disturbance that is subject to both actuator saturation and sensor noise.

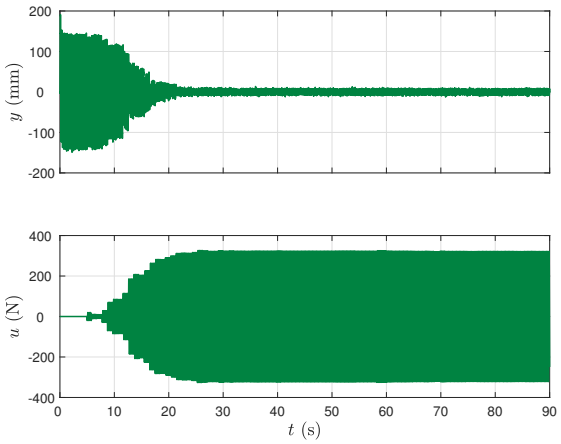

Figure 3.15: Modified TDAHC for a SISO system in the presence of sensor noise. Despite the presence of drift in the estimate $G_{1,k}$, the response $y(t) \to 0$ as $t \to \infty$.

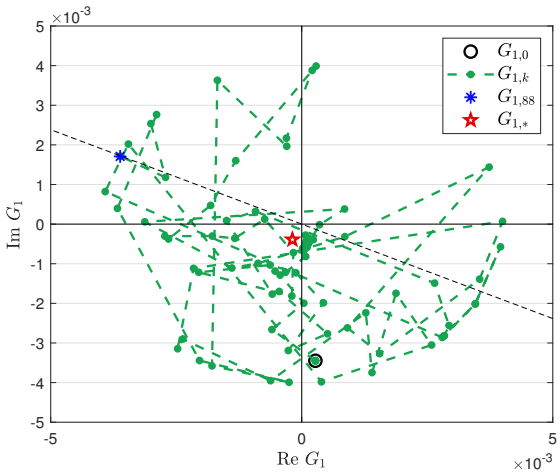

Figure 3.16: Trajectory of $G_{1,k}$ with Modified TDAHC for a SISO system in the presence of sensor noise. The dashed lines show the locus of G such that $|\angle G_{1,0}/G_{1,*}| = \frac{\pi}{2}$. Despite the presence of sensor noise, modified TDAHC constrains the estimate $G_{1,k}$ by R_{m} which mitigates the affect of drift.

Example 3.7. Consider the SISO system where $y = \xi_1$, $\psi_1 = u$, $\psi_2 = 0$,

$$d_1(t) = 200 \sin \omega_1 t + 250 \cos \omega_1 t, \quad d_2(t) = 200 \sin \omega_2 t + 250 \cos \omega_2 t,$$

where $\omega_1 = 16\pi$ rad/s and $\omega_2 = 8\pi$ rad/s. Let $G_{1,0} = 0.75\mathrm{e}^{\jmath \frac{5\pi}{2}} G_{1,*}$ and let $G_{2,0} = 3.5\mathrm{e}^{\jmath \frac{3\pi}{2}} G_{2,*}$. Let $\mu_1 = \gamma_1 = 0.6$. We impose actuator saturation at $u_{\mathrm{m}} = 655$ N, which is the maximum allowable magnitude of $u_{i,k}$. To ensure actuator saturation does not occur, we let $u_{\max} = 650$ N, which was selected to ensure $|u_{i,k}|$ does not exceed u_{m}. We also introduce Gaussian white noise with a mean of 0 and variance of 8×10^{-6} m. To mitigate the effect of drift in $G_{i,k}$ caused by the Gaussian white noise, we select $R_{\mathrm{m}} = 4 \times 10^{-3}$ which bounds $G_{i,k}$ and ensures that $|G_{i,k}| < R_{\mathrm{m}}$. Figure 3.17 presents the response y and control u. Modified TDAHC yields asymptotic disturbance rejection. △

3.8 Conclusion

First, this chapter reviewed TDAHC, which is introduced in [12]. Next, we noted that sensor noise and actuator saturation can negatively impact the performance of TDAHC. To address this shortcoming, we presented a modification to TDAHC to alleviate the problems of sensor noise and actuator saturation.

A comparison of between the examples using FDAHC in Ch. 2 to the examples presented in this chapter which utilized TDAHC reveals a few key trade-offs between the algorithms:

1) FDAHC is less susceptible to measurement noise due to properties of the DFT.

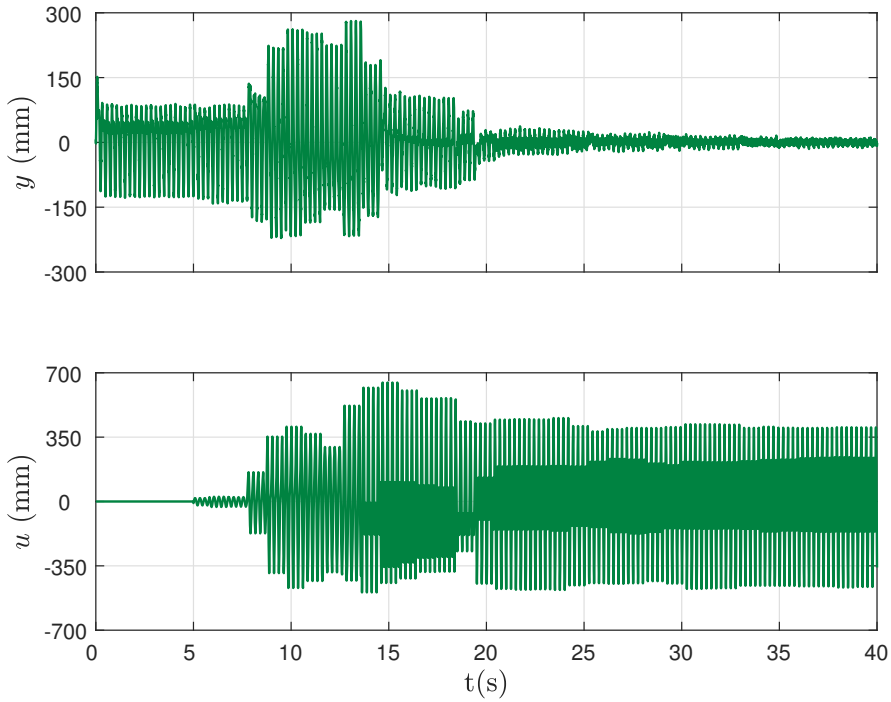

Figure 3.17: Modified TDAHC for a SISO system acted on by a multi-tone disturbance that is subject to actuator saturation and sensor noise. Asymptotic disturbance rejection is achieved.

Since the DFT performs batch processing, it is able to average the data and filter out some of the sensor noise. In contrast, TDAHC does not utilize a DFT and is, thus, more susceptible to measurement noise. For example, by comparing the average power of Fig. 2.17 using FDAHC to Fig. 3.13 using TDAHC, we see that FDAHC has an average power that is about 10% lower than TDAHC (i.e., 0.0011 mm^2 compared to 0.0012 mm^2). These effects are observed in greater detail in Ch. 4 where real world experiments are presented that draw a greater contrast between the algorithms.

2) FDHAC is less influenced by the transient response of y due to the averaging properties of the DFT. In contrast, TDAHC is generally more sensitive to the transient response of y. For example, compare Fig. 2.16, which has a peak transient response of 200 mm (FDAHC) to Fig. 3.12, which has a peak transient response of 298 mm (TDAHC). This effect can also be observed by comparing Fig. 2.19, which has a peak transient response of 150 mm (FDAHC) to Fig. 3.17, which has a peak transient response of 285 mm (TDAHC).

3) TDAHC can be implemented with larger control gains which can yield faster steady-state performance convergence times compared to that of FDAHC. In addition, TDAHC also does not require the use of a DFT which eliminates the need of batch processing. Note that in this chapter, we implemented TDAHC and FDAHC using parameters that were selected to yield similar performance.

However, in practice, TDAHC parameters can be selected higher to yield faster convergence times compared to that of FDAHC. This concept is explored further in Ch. 4 where real world experiments are presented.

Chapter 4
Active Noise Control Experiments

In this chapter, we present experimental results that compare modified FDAHC to modified TDAHC. Each experiment aims to answer the following questions:

- Experiment 4.1: How does the initial estimate $G_{i,k}$ affect the performance and transient response for SISO systems?
- Experiment 4.2: How do FDAHC and TDAHC perform if there is an error in the estimate of the disturbance frequency?
- Experiment 4.3: What are the optimal values of T_s, γ_i, and μ_i for a specific experimental setup? What trade-offs in performance exist between FDAHC and TDAHC when the algorithms are tuned to yield the fastest convergence speed?
- Experiment 4.4: What are the trade-offs in performance when rejecting a multi-tone disturbance (i.e., $q \geq 2$) versus a single-tone (i.e., $q = 1$) disturbance?

4.1 Experiment Design

This section reviews the design of the experiments. A photo of the general experimental setup is shown in Fig. 4.1. However, multiple configurations of the performance microphone, control speaker, and disturbance speaker are used. Thus, each experiment provides a schematic identifying the configuration of these elements. The performance measurement signal from the microphone is amplified by a SM Pro Audio PR8E microphone pre-amplifier. Each speaker is an M-Audio AV42 2-way 4-in monitor. The microphone is an Audio2000 1064BL vocal microphone. The controller is implemented on a dSPACE DS1103 controller board. Note that no system information is required to implement FDAHC or TDAHC, and we do not use any knowledge of the characteristics or locations of the components of the experiments to implement FDAHC and TDAHC.

All data is sampled at 10,000 Hz. Let $u_m > 0$ be the maximum allowable magnitude for each control input. For all control speakers, $u_m = 447 \times 10^{-3}$ V. Thus, we select $u_{max} = 400 \times 10^{-3}$ V for implementation of FDAHC and TDAHC to ensure

Figure 4.1: General experiment configuration.

actuator saturation does not occur.

For all experiments, TDAHC is implemented with $r = 4$. The values for the gains μ_i, γ_i, σ_i, ν_i; the update time T_s; and the projection radius R_m are provided in each experiment. In Experiments 4.1, 4.2, and 4.4 the control is turned on after 5 s of open-loop operation. In Experiment 4.3, the control is turned on after 1 s of open-loop operation.

4.2 Results from Active Noise Control Experiments

We present results from four active noise control experiments that were conducted to compare FDAHC and TDAHC.

Experiment 4.1. This experiment shows that FDAHC and TDAHC are capable of asymptotically rejecting a single-tone ($q = 1$) disturbance acting on an unknown SISO system regardless of the initial estimate $G_{1,0}$. We examine two initial conditions $G_{1,0}$, which have angles that are 180° apart. The 180° difference guarantees that one of the initial conditions satisfies the higher-harmonic control (HHC) stability condition (i.e., $G_{1,0}$ is within 90° of $G_{yu}(\jmath\omega_1)$), whereas the other initial condition does not satisfy the stability condition.

The configuration for this experiment is in Fig. 4.2. In this configuration, one microphone measures the response y, one speaker provides the control u, and one speaker provides the disturbance d. The disturbance is $d(t) = 0.1 \sin \omega_1 t$, where $\omega_1 = 250\pi$ rad/s (i.e., 125 Hz). We consider the initial condition $0.1 - \jmath 0.2$ and $-0.1 + \jmath 0.2$, which have angles that are 180° apart.

Next, we discuss the selection of the update time T_s; implementation of the DFT; choice of gains μ_i, γ_i, ρ_i, ν_i; and the projection radius R_m. These values are shown in Table 4.1.

The settling time of the system at frequency ω_1 is experimentally determined to

Table 4.1: Control parameters for Experiment 4.1.

Parameter	FDAHC	TDAHC
T_{s}	0.064 s	0.055 s
μ_1	0.3	0.65
γ_1	0.3	0.4
σ_1	10^{-7}	10^{-5}
ν_1	10^{-7}	10^{-5}
R_{m}	10	10

be approximately $T_{\mathrm{HSS}} = 0.05$ s. FDAHC requires that the update period satisfy $T_{\mathrm{s}} \geq T_{\mathrm{HSS}} + 2\pi/\omega_1$, while TDAHC requires that the update period satisfy $T_{\mathrm{s}} \geq T_{\mathrm{HSS}}$. In addition, FDAHC requires that $\omega_1 T_{\mathrm{s}} = 2\pi n$ where $n \in \mathbb{Z}^+$ (that is, T_{s} is an integer multiple of $2\pi/\omega_1$), and TDAHC requires that $\omega_1 T_{\mathrm{s}} \neq n\pi$ where $n \in \mathbb{Z}^+$ (that is, T_{s} is not an integer multiple of π/ω_1). With these constraints in mind, the control update periods are chosen to be $T_{\mathrm{s}} = 0.064$ s for FDAHC and $T_{\mathrm{s}} = 0.055$ s for TDAHC.

The discrete Fourier transform (DFT) used with FDAHC is implemented using the last $2\pi/\omega_1 = 0.0008$ s of data from each update period. Since the data is sampled at 10 kHz, it follows that at each update the DFT is computed from the final 80 data points sampled over that interval.

The gains gains μ_1, γ_1, ρ_1, ν_1 are selected based on empirical testing to obtain good convergence speed (i.e., the time required to reach steady state) without large peak transients.

The projection radius R_{m} is selected to be large enough to allow $G_{1,k}$ to adapt over a large region.

The system response y and u, and trajectory of $G_{1,k}$ are presented in Figs. 4.3–4.10 for FDAHC and TDAHC with $G_{1,0} = 0.1 - \jmath 0.2$ and $G_{1,0} = -0.1 + \jmath 0.2$. Both FDAHC and TDAHC attenuate the disturbance yielding near-zero steady-state performance as shown in Figs. 4.3, 4.5, 4.7, and 4.9. Both algorithms also adapt the estimate $G_{1,k}$ regardless of the initial condition as shown in Figs. 4.4, 4.6, 4.8, and 4.10. In general, the initial condition that is within 90° of $G_{yu}(\jmath\omega_1)$ results in a smaller peak transient response. For this reason, it is likely that the initial condition $0.1 - \jmath 0.2$ satisfies the HHC stability condition whereas the initial condition $-0.1 + \jmath 0.2$ does not.

Experiment 4.2. In practice, the frequency of the disturbance may not be known exactly. This experiment examines which algorithm is more robust to uncertainty in the disturbance frequency.

The configuration for this experiment is shown in Fig. 4.11. In this configuration, one microphone measures the response y, one speaker provides the control u, and one speaker provides the disturbance d. We use the initial condition $0.05 - \jmath 0.25$.

For all results, the control algorithms are implemented to attenuate a disturbance

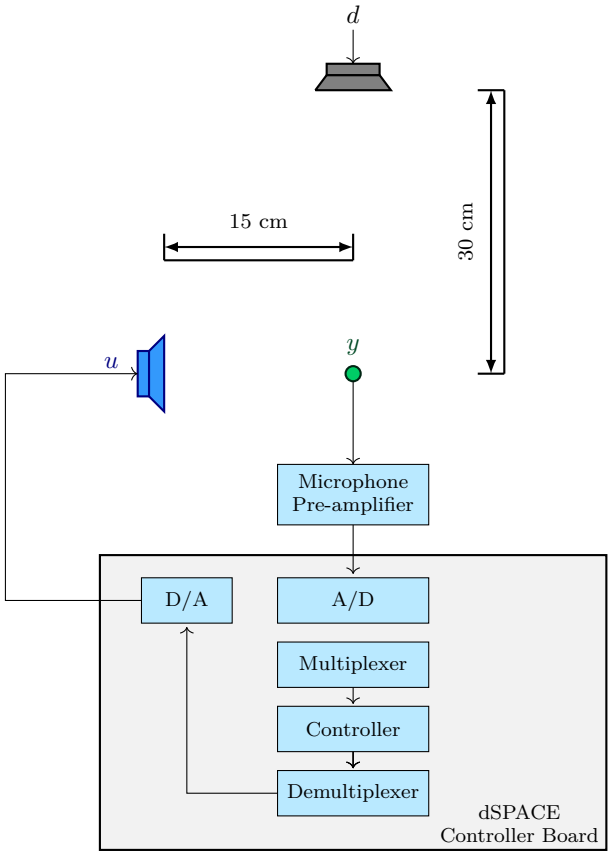

Figure 4.2: Experiment 4.1 configuration.

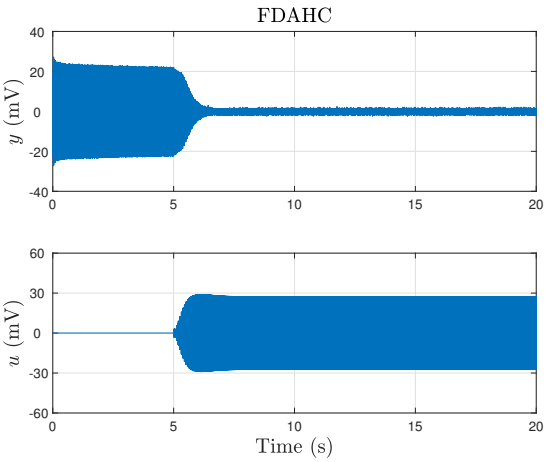

Figure 4.3: FDAHC with $G_{1,0} = 0.1 - \jmath 0.2$.

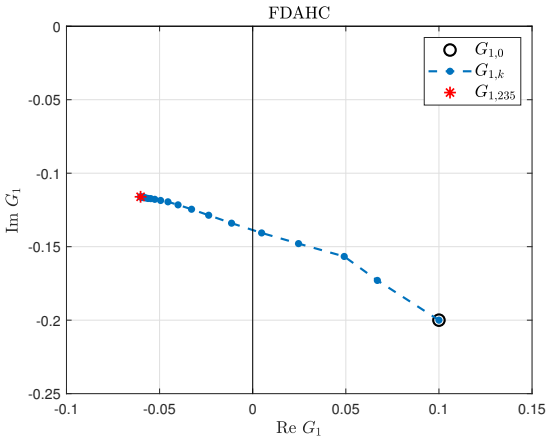

Figure 4.4: Trajectory of $G_{1,k}$ for FDAHC with $G_{1,0} = 0.1 - \jmath 0.2$.

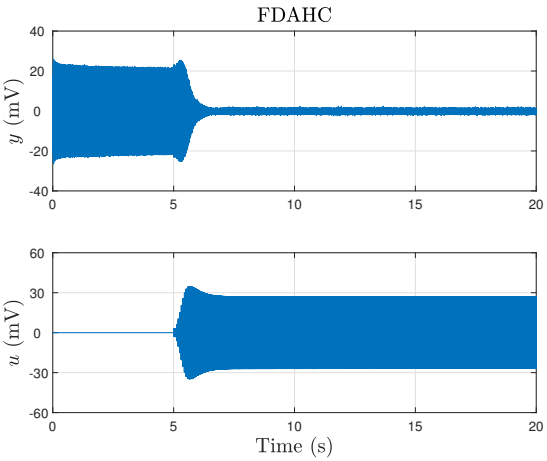

Figure 4.5: FDAHC with $G_{1,0} = -0.1 + \jmath 0.2$.

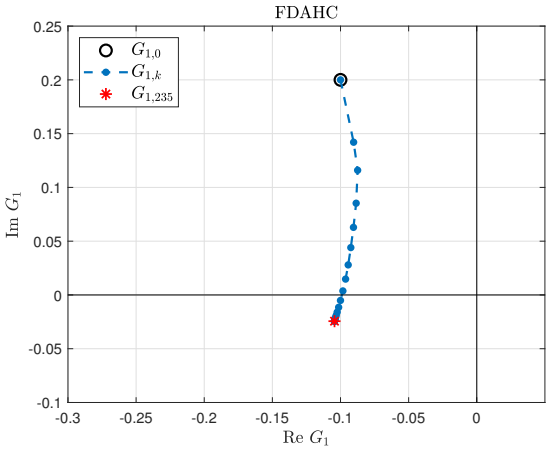

Figure 4.6: Trajectory of $G_{1,k}$ for FDAHC with $G_{1,0} = -0.1 + \jmath 0.2$.

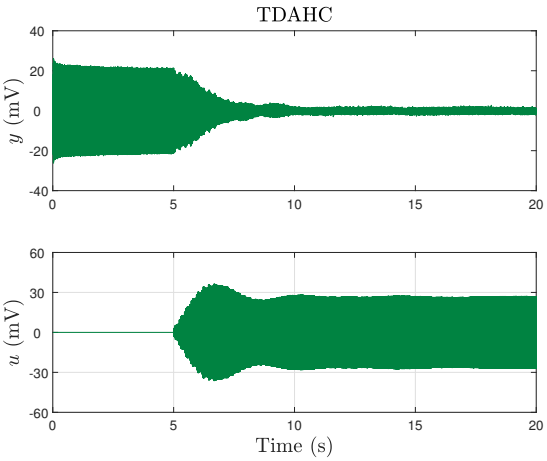

Figure 4.7: TDAHC with $G_{1,0} = 0.1 - \jmath 0.2$.

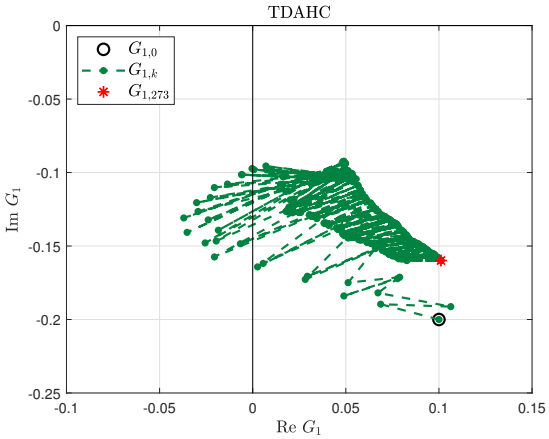

Figure 4.8: Trajectory of $G_{1,k}$ for TDAHC with $G_{1,0} = 0.1 - \jmath 0.2$.

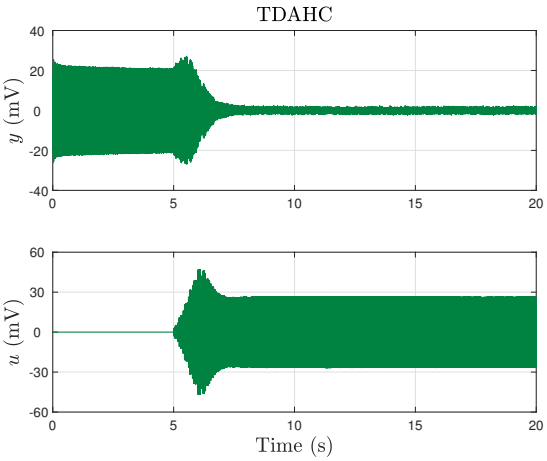

Figure 4.9: TDAHC with $G_{1,0} = -0.1 + \jmath 0.2$.

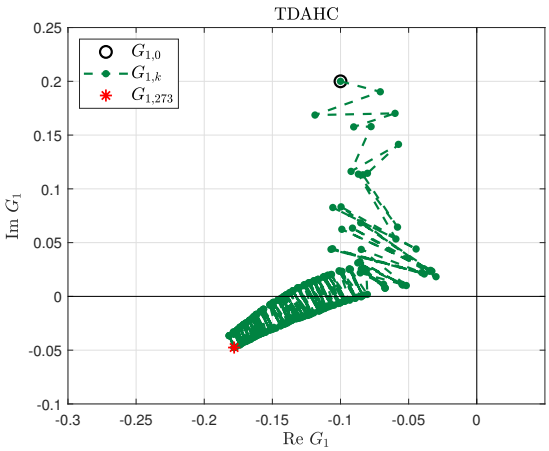

Figure 4.10: Trajectory of $G_{1,k}$ for TDAHC with $G_{1,0} = -0.1 + \jmath 0.2$.

Table 4.2: Control parameters for Experiment 4.2.

Parameter.	FDAHC	TDAHC
T_s	0.064	0.055
μ_1	0.2	0.4
γ_1	0.5	0.9
σ_1	10^{-7}	10^{-4}
ν_1	10^{-7}	10^{-4}
R_m	100	100

with a frequency of $\omega_1 = 250\pi$ rad/s (i.e., $f = 125$ Hz). However, the true frequency f_d of the disturbance is not necessarily 125 Hz. Each algorithm is tested at 19 different values of f_d from 124.55 Hz to 125.45 Hz changing in 0.05 Hz increments. In particular, $d(t) = 0.1 \sin 2\pi f_\mathrm{d} t$.

The algorithm parameters used in this experiment are in Table 4.2. The update time T_s and the DFT implementation in this experiment are the same as in Experiment 4.1.

The gains μ_1, γ_1, σ_1, and ν_1 are selected based on empirical testing to obtain similar convergence speeds between FDAHC and TDAHC for the nominal case where $f_\mathrm{d} = f = 125$ Hz. The adaptive gains of $\mu_1 = 0.2$ and $\gamma_1 = 0.5$ are selected for FDAHC. Numerical simulations demonstrate that a reasonable rule of thumb for determining FDAHC and TDAHC gains that yield similar convergence speed is to select μ_1/T_s and γ_1/T_s for TDAHC as double that for FDAHC. Using this relationship as a starting point, combined with experimental testing, results in $\mu_1 = 0.4$ and $\gamma_1 = 0.9$ for TDAHC.

For FDAHC, numerical and empirical testing demonstrates that the normalization gains σ_1 and ν_1 should be small relative to the squared Frobenius norm of $G_{1,0}$, that is, $\sigma_1 \ll \|G_{1,0}\|_\mathrm{F}^2$ and $\nu_1 \ll \|G_{1,0}\|_\mathrm{F}^2$. Using this metric as a guideline, we select $\sigma_1 = \nu_1 = 10^{-7}$ for FDAHC. For TDAHC, we select $\sigma_1 = \nu_1 = 10^{-4}$ to obtain similar performance to FDAHC.

The system response for the nominal case where $f = f_\mathrm{d} = 125$ Hz is shown in Figs. 4.12–4.13. For the nominal case, FDAHC and TDAHC attenuate the disturbance yielding a near-zero steady-state response.

Figures 4.14 and 4.15 show the average power of y using FDAHC and TDAHC for each of the 19 disturbance frequencies tested. The average power of y for each case is computed using 150 s of data, specifically,

$$J \triangleq \frac{1}{N+1} \sum_{k=0}^{N} \|y(10^{-4}k)\|^2,$$

where $N = 150 \times 10^4$ data points. The average among trials is 42.6 mV^2 for FDAHC compared to 19.7 mV^2 for TDAHC. This difference is due primarily to trials where

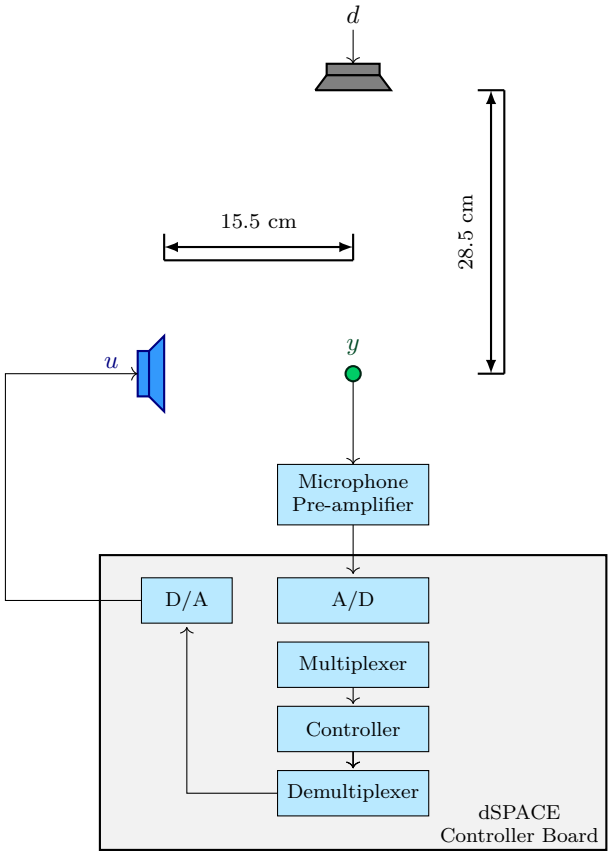

Figure 4.11: Experiment 4.2 configuration.

$f - f_{\mathrm{d}} \in \{-0.45, -0.4, 0.4, 0.45\}$. For these trials, the average power with FDAHC is higher than that without control (i.e., open-loop). In contrast, TDAHC achieves significant attenuation on these trials. However, for trials where $f - f_{\mathrm{d}} \in (-0.35, 0.35)$, the average power with FDAHC is less than that with TDAHC.

Figures 4.16 and 4.17 show the magnitude of peak response of y using FDAHC and TDAHC for each of the 19 disturbance frequencies tested. The magnitude of the peak response is

$$P \triangleq \max_{k \in \{0,\ldots,N\}} |y(10^{-4}k)|,$$

where $N = 150 \times 10^4$ data points. Figures 4.16 and 4.17 show that the magnitude of the peak response is generally smaller with FDAHC than with TDAHC. The magnitude of the peak response averaged over all 19 disturbance frequencies is 24.5 mV with FDAHC and 29.0 mV with TDAHC. However, there are disturbance frequencies (e.g.,124.55 Hz, 124.6 Hz, 125.4 Hz, and 125.45 Hz) where TDAHC outperforms FDAHC.

Figures 4.18–4.53 show the system response with FDAHC and TDAHC for each of the 18 off nominal cases for f_{d}. Note that in general, the response with FDAHC is more smooth than that with TDAHC. This property is most likely a result of the

fact that FDAHC uses the DFT, which can have an averaging effect.

Based on the results in Figs. 4.14–4.53, we conclude that FDAHC tends to perform better than TDAHC if there is uncertainty in the disturbance frequency. However, this trend does not hold at all frequencies. For example, Figs. 4.14 and 4.15 show that TDAHC outperforms FDAHC if the frequency error $|f - f_{\mathrm{d}}|$ exceeds 0.35 Hz.

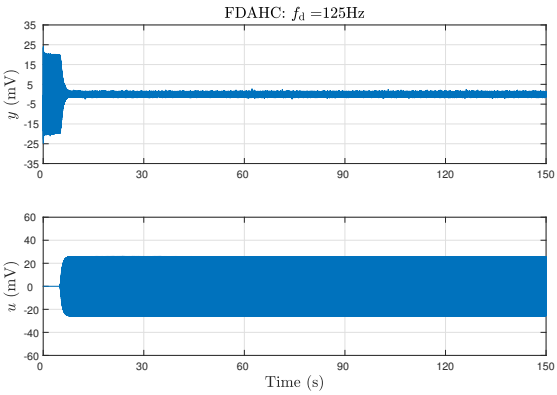

Figure 4.12: FDAHC for $f_{\mathrm{d}} = 125$ Hz.

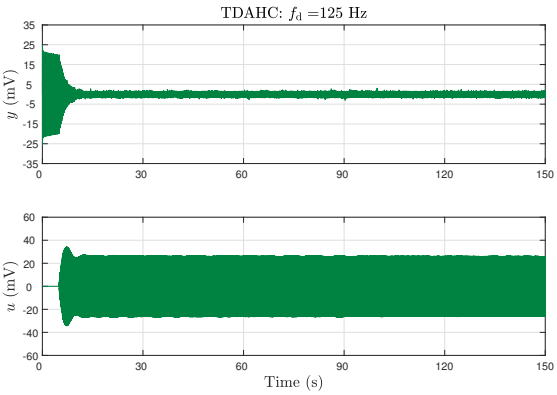

Figure 4.13: TDAHC for $f_{\mathrm{d}} = 125$ Hz.

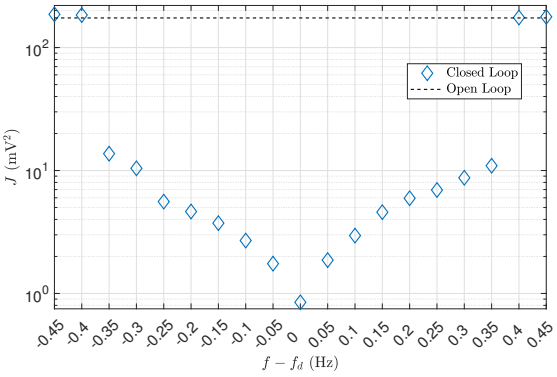

Figure 4.14: Average power for FDAHC.

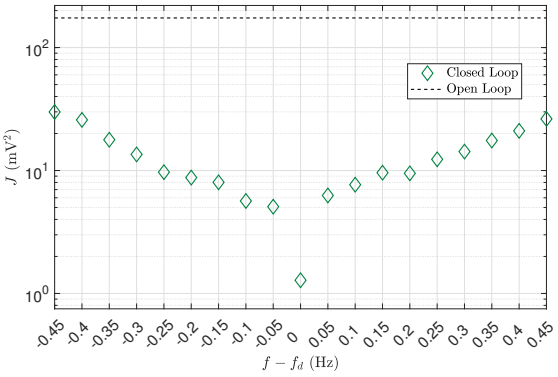

Figure 4.15: Average power for TDAHC.

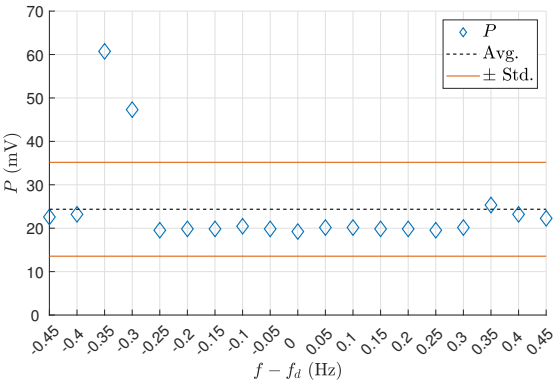

Figure 4.16: Magnitude of peak response for FDAHC.

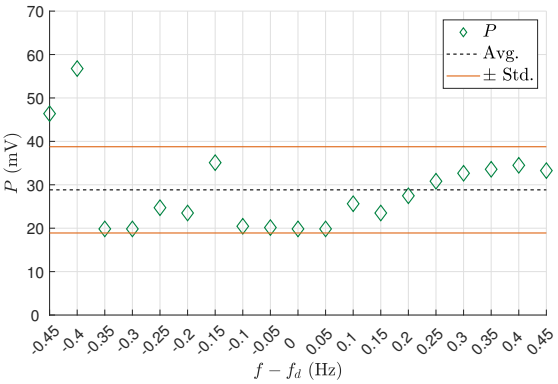

Figure 4.17: Magnitude of peak response for TDAHC.

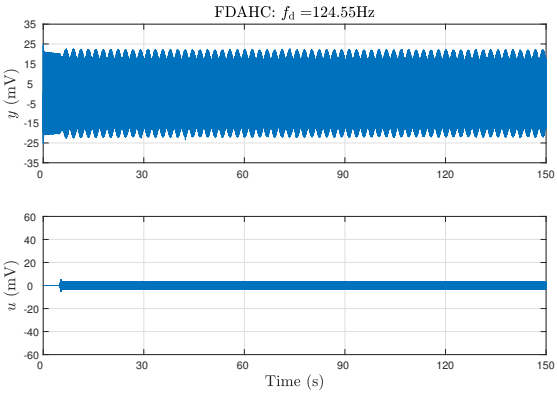

Figure 4.18: FDAHC for $f_{\mathrm{d}} = 124.55$ Hz.

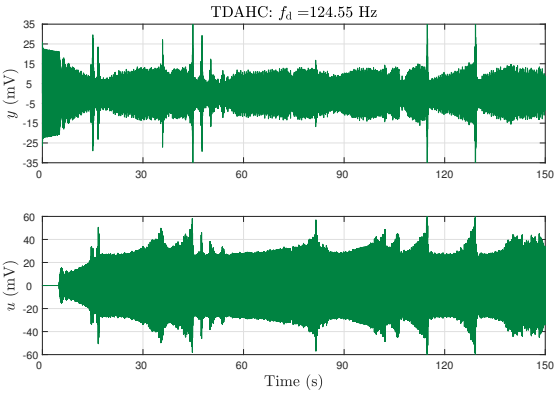

Figure 4.19: TDAHC for $f_{\mathrm{d}} = 124.55$ Hz.

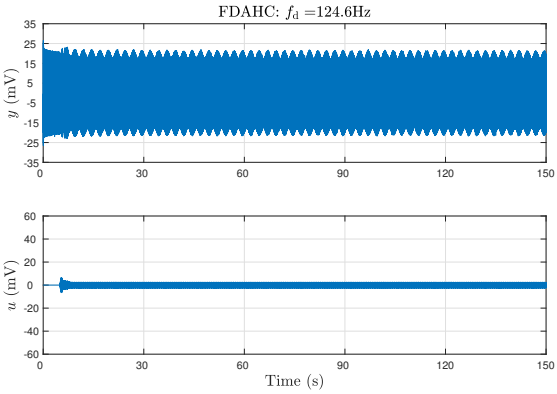

Figure 4.20: FDAHC for $f_{\mathrm{d}} = 124.6$ Hz.

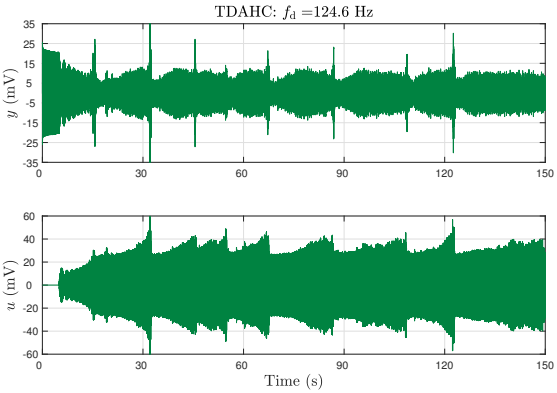

Figure 4.21: TDAHC for $f_{\mathrm{d}} = 124.6$ Hz.

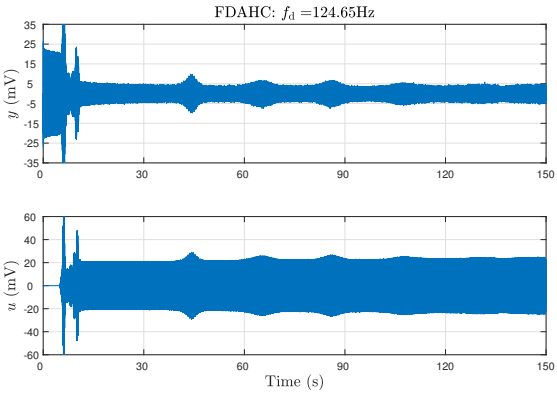

Figure 4.22: FDAHC for $f_{\mathrm{d}} = 124.65$ Hz.

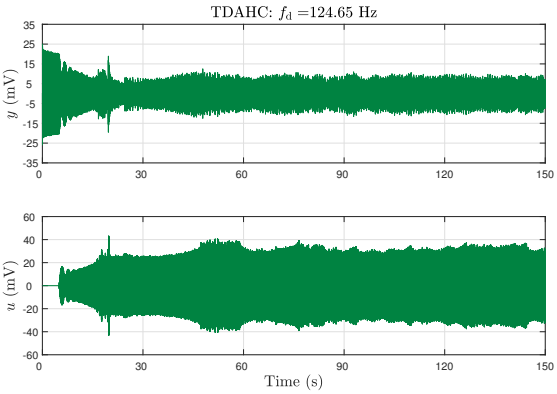

Figure 4.23: TDAHC for $f_{\mathrm{d}} = 124.65$ Hz.

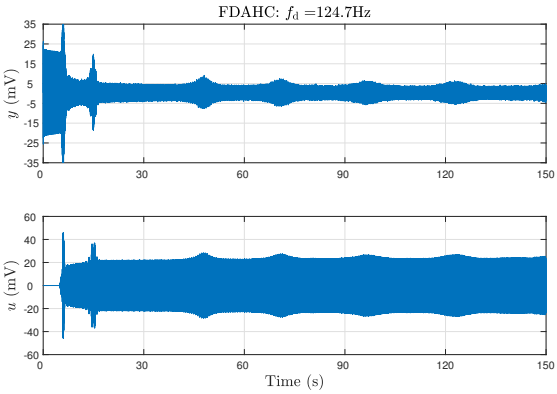

Figure 4.24: FDAHC for $f_{\mathrm{d}} = 124.7$ Hz.

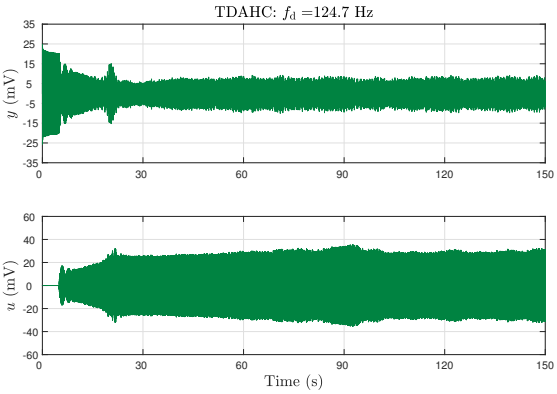

Figure 4.25: TDAHC for $f_{\mathrm{d}} = 124.7$ Hz.

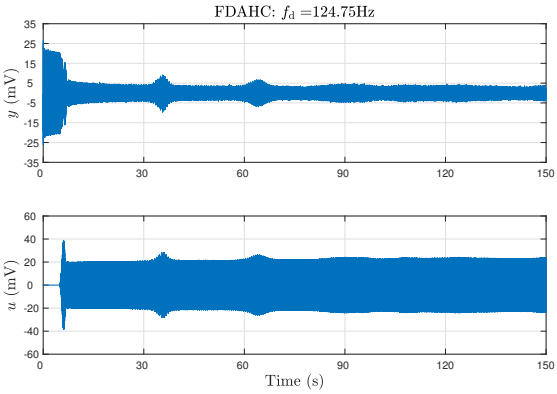

Figure 4.26: FDAHC for $f_{\mathrm{d}} = 124.75$ Hz.

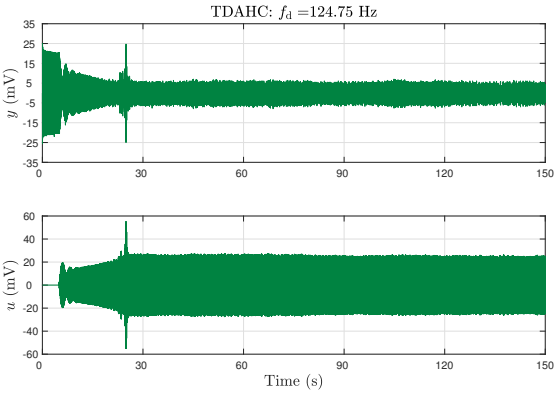

Figure 4.27: TDAHC for $f_{\mathrm{d}} = 124.75$ Hz.

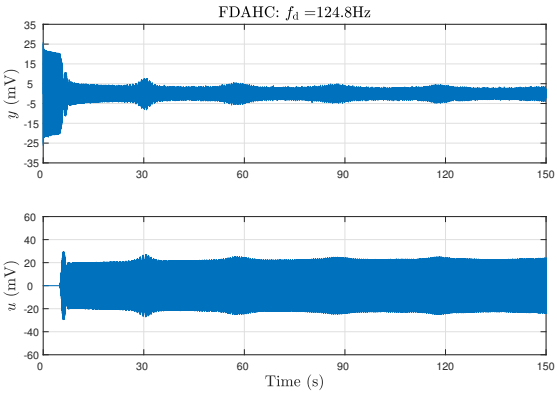

Figure 4.28: FDAHC for $f_{\mathrm{d}} = 124.8$ Hz.

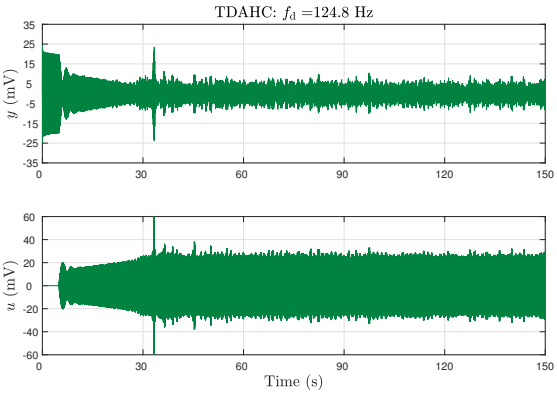

Figure 4.29: TDAHC for $f_{\mathrm{d}} = 124.8$ Hz.

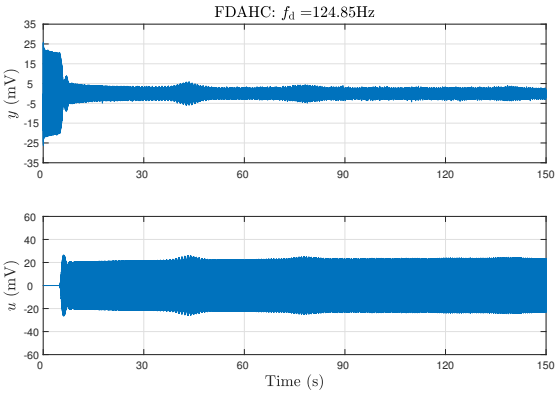

Figure 4.30: FDAHC for $f_{\mathrm{d}} = 124.85$ Hz.

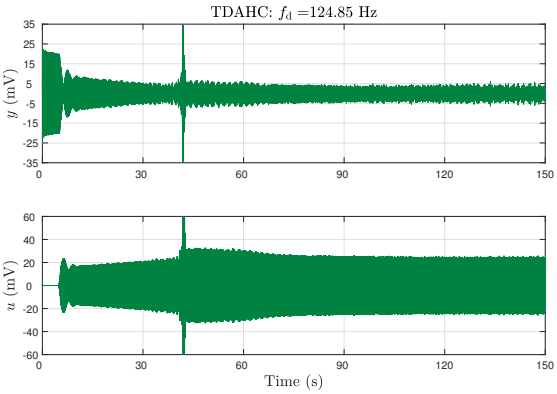

Figure 4.31: TDAHC for $f_{\mathrm{d}} = 124.85$ Hz.

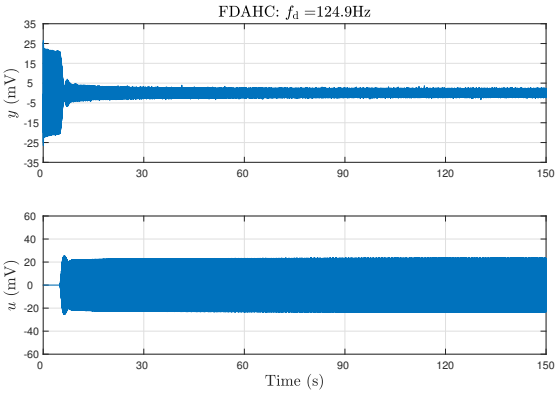

Figure 4.32: FDAHC for $f_{\mathrm{d}} = 124.9$ Hz.

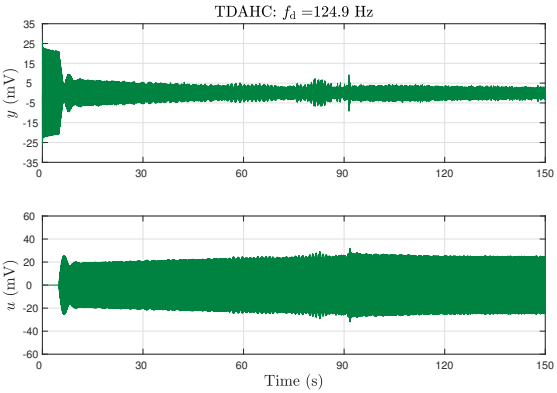

Figure 4.33: TDAHC for $f_{\mathrm{d}} = 124.9$ Hz.

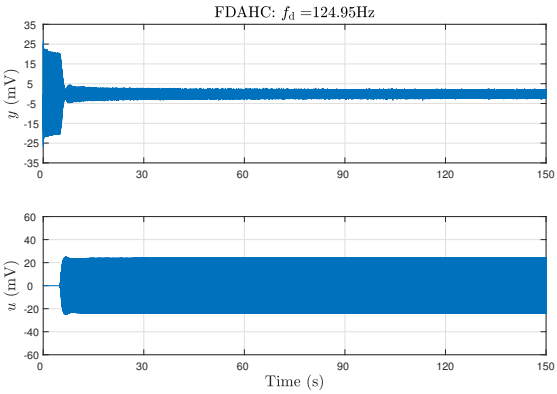

Figure 4.34: FDAHC for $f_{\mathrm{d}} = 124.95$ Hz.

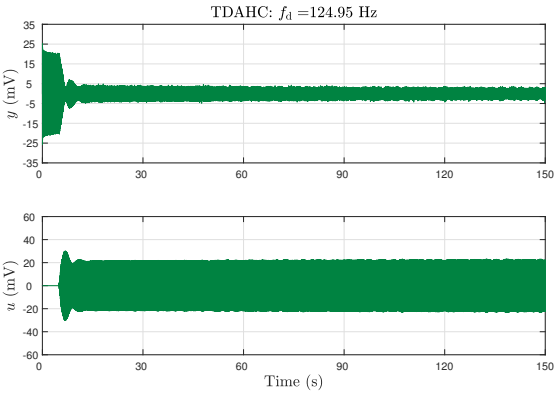

Figure 4.35: TDAHC for $f_{\mathrm{d}} = 124.95$ Hz.

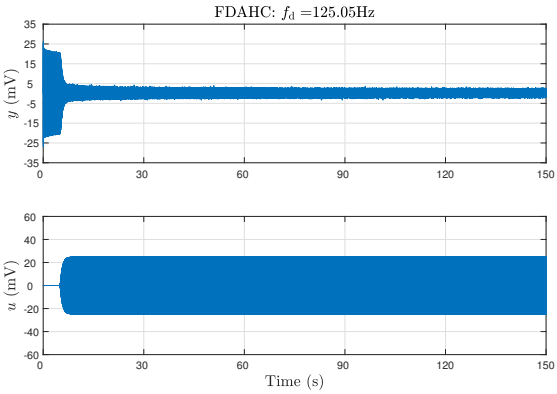

Figure 4.36: FDAHC for $f_{\mathrm{d}} = 125.05$ Hz.

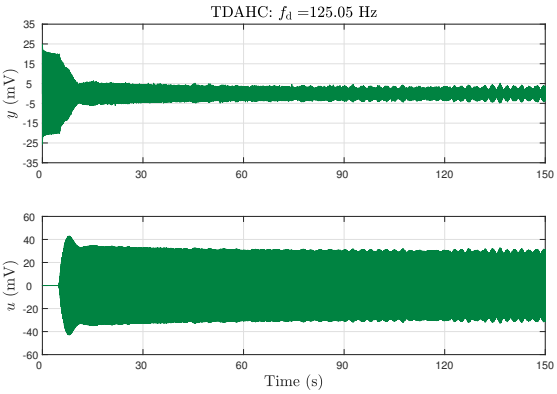

Figure 4.37: TDAHC for $f_{\mathrm{d}} = 125.05$ Hz.

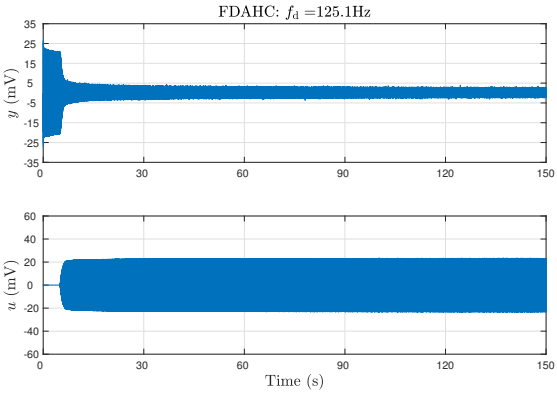

Figure 4.38: FDAHC for $f_{\mathrm{d}} = 125.1$ Hz.

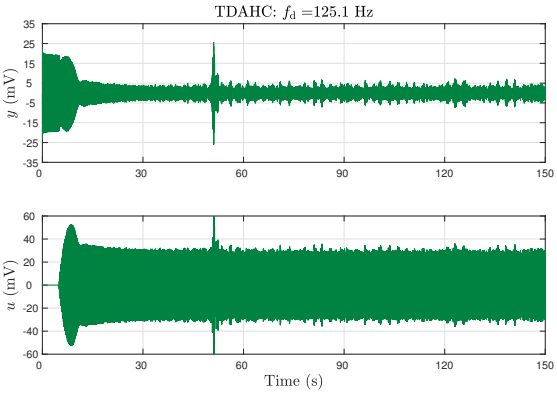

Figure 4.39: TDAHC for $f_{\mathrm{d}} = 125.1$ Hz.

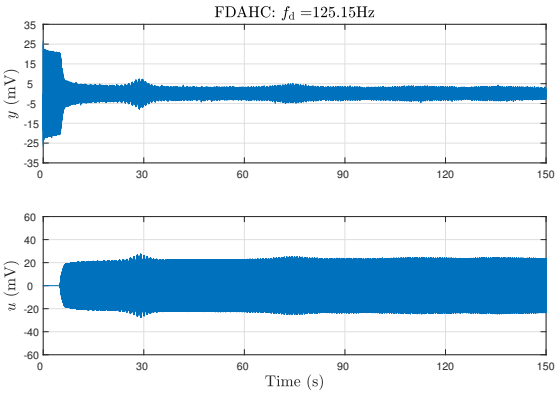

Figure 4.40: FDAHC for $f_{\mathrm{d}} = 125.15$ Hz.

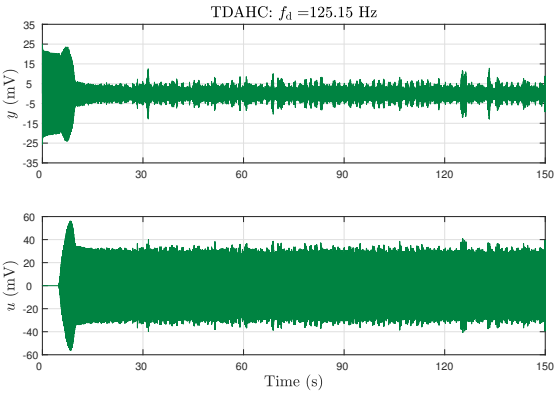

Figure 4.41: TDAHC for $f_{\mathrm{d}} = 125.15$ Hz.

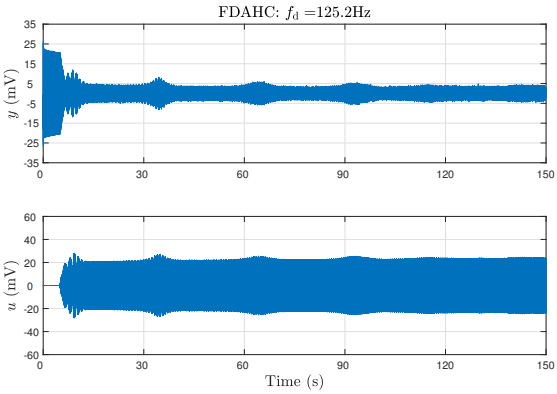

Figure 4.42: FDAHC for $f_\mathrm{d} = 125.2$ Hz.

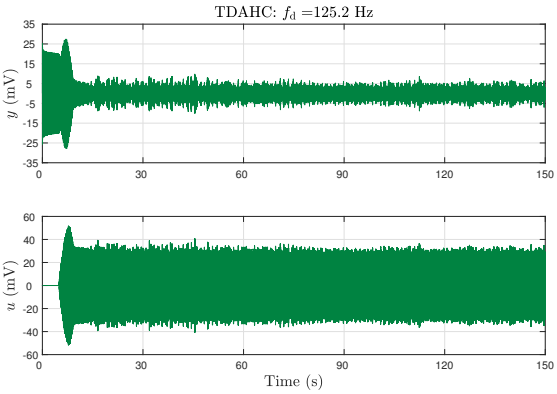

Figure 4.43: TDAHC for $f_\mathrm{d} = 125.2$ Hz.

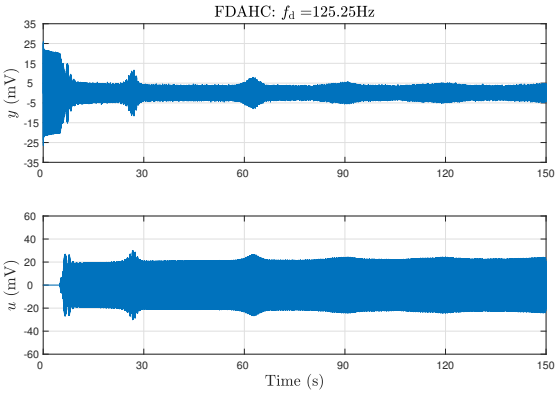

Figure 4.44: FDAHC for $f_\mathrm{d} = 125.25$ Hz and $f_c = 125$ Hz.

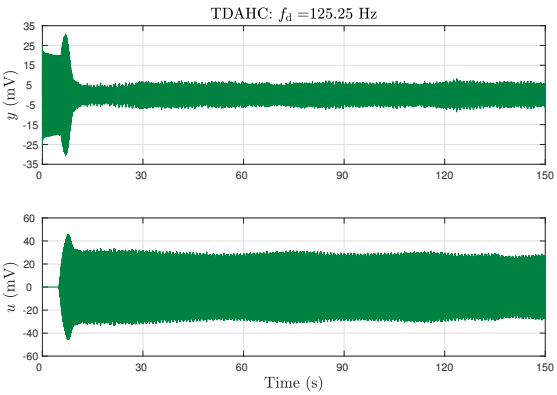

Figure 4.45: TDAHC for $f_\mathrm{d} = 125.25$ Hz.

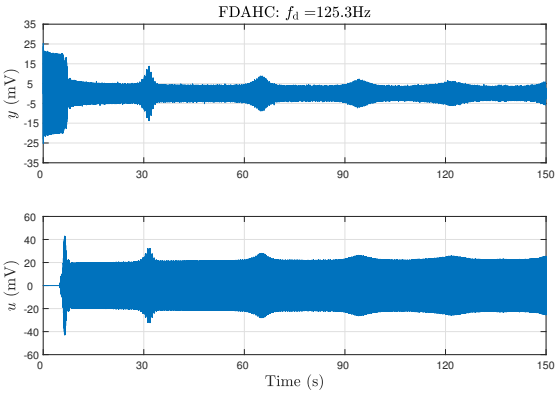

Figure 4.46: FDAHC for $f_\mathrm{d} = 125.3$ Hz.

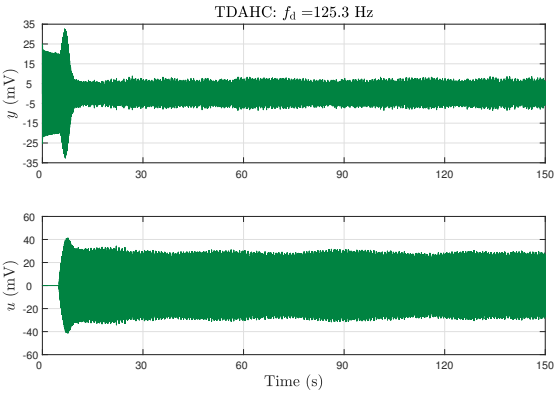

Figure 4.47: TDAHC for $f_\mathrm{d} = 125.3$ Hz.

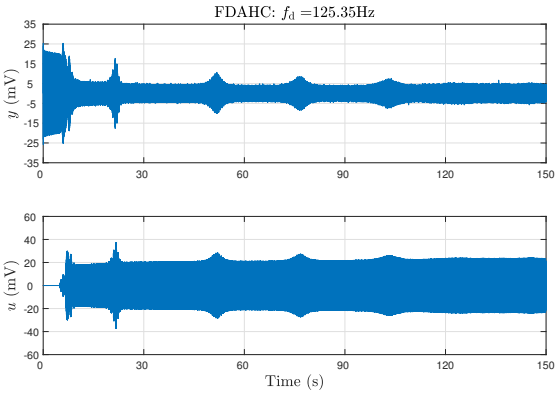

Figure 4.48: FDAHC for $f_\mathrm{d} = 125.35$ Hz.

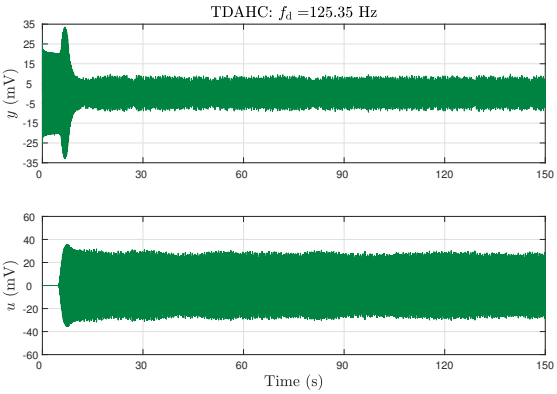

Figure 4.49: TDAHC for $f_\mathrm{d} = 125.35$ Hz.

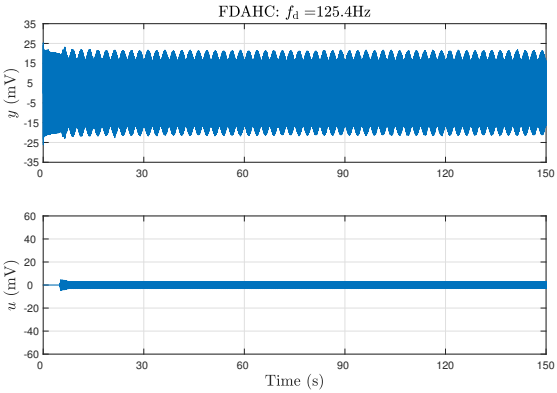

Figure 4.50: FDAHC for $f_\mathrm{d} = 125.4$ Hz.

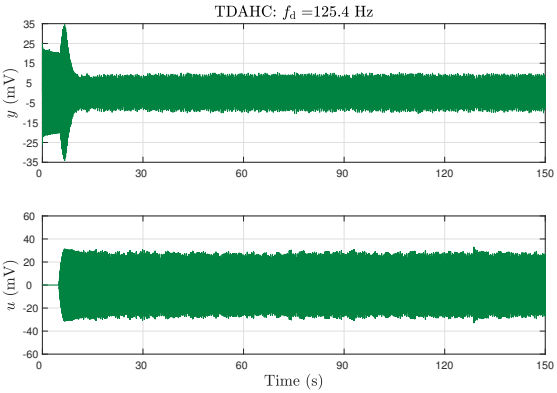

Figure 4.51: TDAHC for $f_\mathrm{d} = 125.4$ Hz.

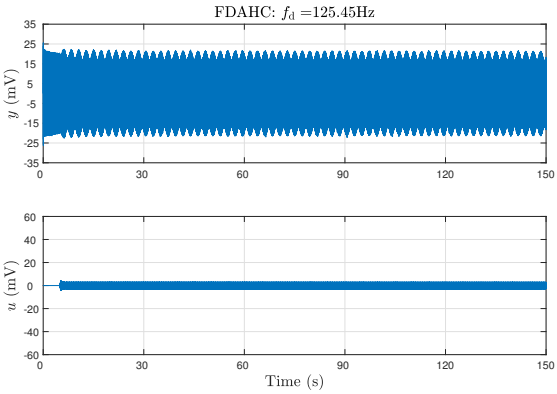

Figure 4.52: FDAHC for $f_\mathrm{d} = 125.45$ Hz.

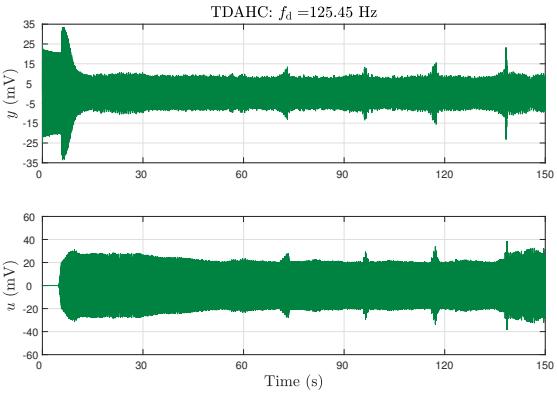

Figure 4.53: TDAHC for $f_\mathrm{d} = 125.45$ Hz.

Experiment 4.3. This experiment compares the convergence speed (i.e., time required to reach steady-state performance), average power, and magnitude of the peak response using FDAHC and TDAHC when tuned to yield the fastest possible convergence speed.

The configuration for this experiment is shown in Fig. 4.54. In this configuration, one microphone measures the response y, one speaker provides the control u, and one

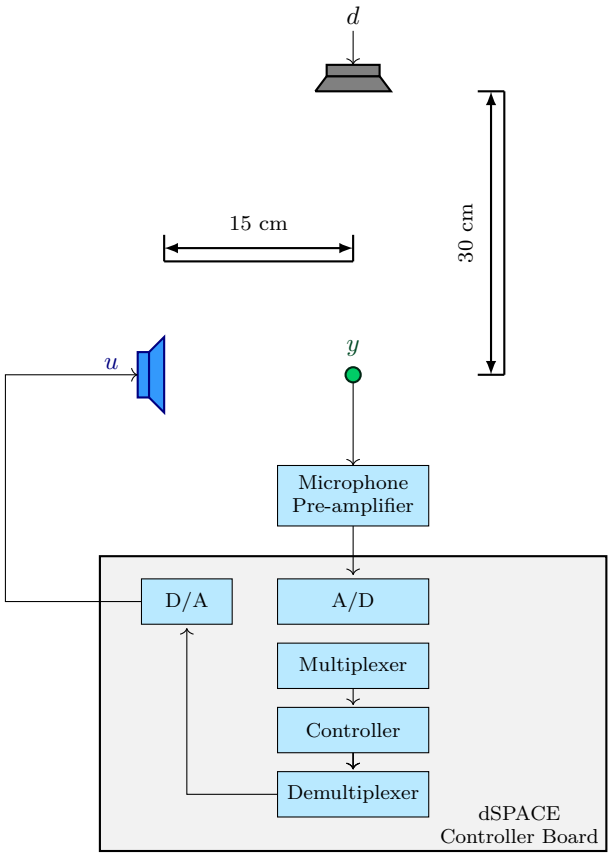

Figure 4.54: Experiment 4.3 configuration.

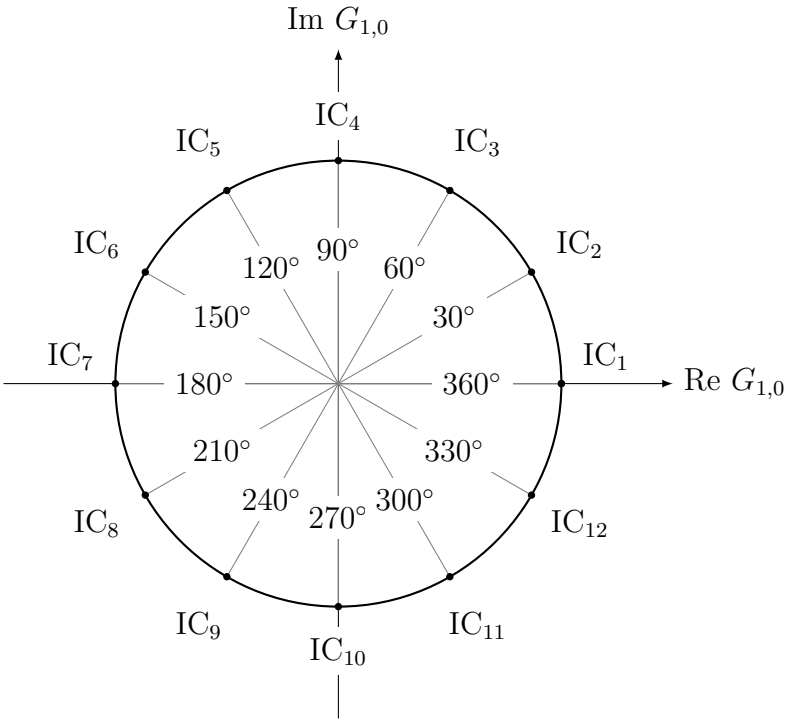

Figure 4.55: Initial conditions where $|G_{1,0}| = 0.04$.

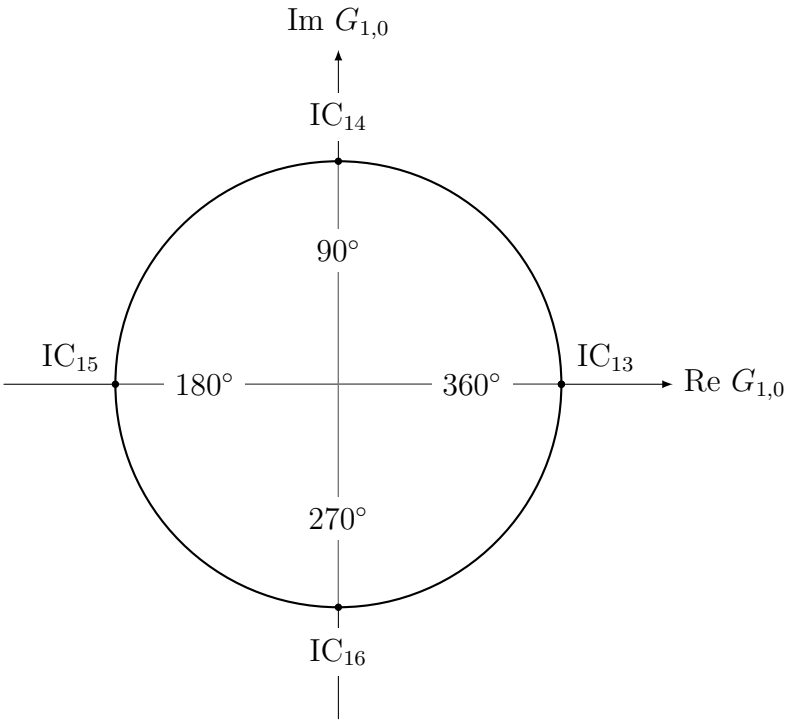

Figure 4.56: Initial conditions where $|G_{1,0}| = 0.02$.

Table 4.3: Control parameters for Experiment 4.3.

Parameter.	FDAHC	TDAHC
T_s	0.064 s	0.055 s
μ_1	0.25	1.1
γ_1	0.45	0.7
σ_1	10^{-10}	10^{-6}
ν_1	10^{-10}	10^{-6}

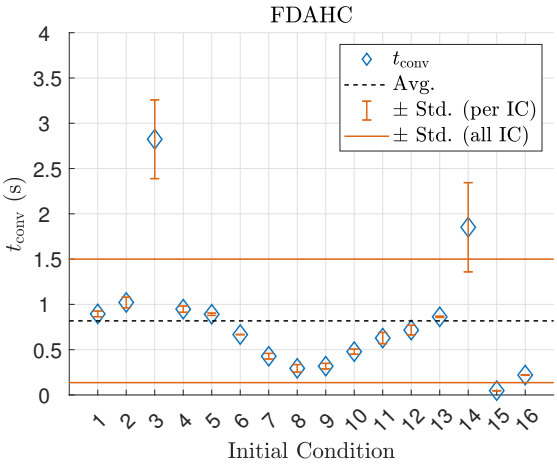

Figure 4.57: Convergence time of FDAHC.

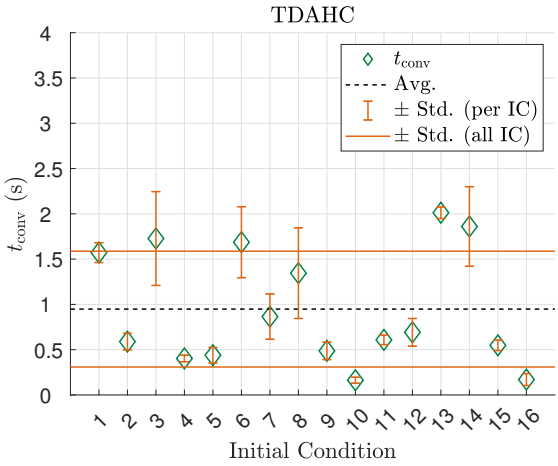

Figure 4.58: Convergence time of TDAHC.

speaker provides the disturbance d. The disturbance is $d(t) = 0.1 \sin \omega_1 t$, where $\omega_1 = 250\pi$ rad/s (i.e., 125 Hz). We use 16 initial conditions for $G_{1,0}$ that are distributed around circles of radius 0.04 and 0.02. For the first 12 initial conditions, we let $|G_{1,0}| = 0.04$. For the last 4 initial conditions, we let $|G_{1,0}| = 0.02$. For each initial condition, 4 trials are performed. A graphical representation of the initial conditions is presented in Figs. 4.55 and 4.56.

The algorithm parameters used in this experiment are in Table 4.3. The update time T_{s} and the DFT implementation in this experiment are the same as in Experiment 4.1.

Empirical testing suggests that the fastest possible convergence speed with this configuration occurs using $\mu_1 = 0.25$ and $\gamma_1 = 0.45$ for FDAHC, and $\mu_1 = 1.1$ and $\gamma_1 = 0.7$ for TDAHC. Similarly, empirical testing suggests that the fastest convergence speed with this experimental configuration occurs using $\sigma_1 = \nu_1 = 10^{-10}$ for FDAHC, and $\sigma_1 = \nu_1 = 10^{-6}$ for TDAHC.

Figures 4.57 and 4.58 show the convergence time using FDAHC and TDAHC. For each trial, convergence time $t_{\text{conv}} \geq 0$ is the smallest time such that

$$\min_{t \geq t_{\text{conv}}} |y(t)| \leq \delta_{\text{conv}},$$

where the threshold $\delta_{\text{conv}} = 0.5 \times 10^{-3}$ V is determined from that data noise level. Figures 4.57 and 4.58 show that FDAHC attenuates the disturbance more quickly than TDAHC. The convergence time averaged among all initial conditions is 0.82 s with FDAHC and 0.95 s with TDAHC. As an example, Figs. 4.59–4.60 show the response for IC_1 where FDAHC outperforms TDAHC. However, there are initial conditions where TDAHC outperforms FDAHC such as IC_3 shown in Figs. 4.61–4.62. The higher convergence time with TDAHC is primarily due to a higher magnitude of peak response on most initial conditions and the algorithm being more sensitive to sensor noise compared to FDAHC. Note that FDAHC utilizes a DFT which can have an averaging effect that can produce a smoother response.

Figures 4.63 and 4.64 show that the magnitude peak response of y using FDAHC and TDAHC for each of the 16 initial conditions tested. The magnitude of the peak

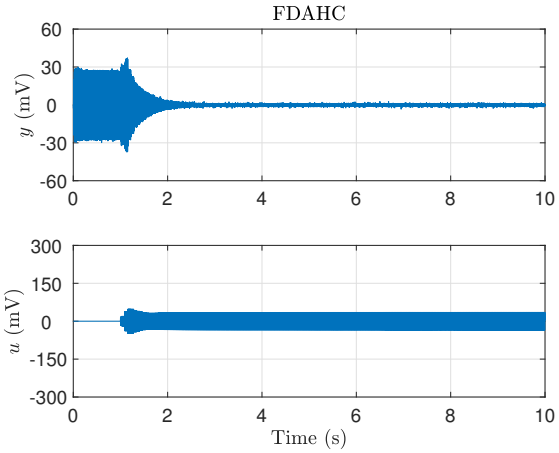

Figure 4.59: FDAHC with IC_1.

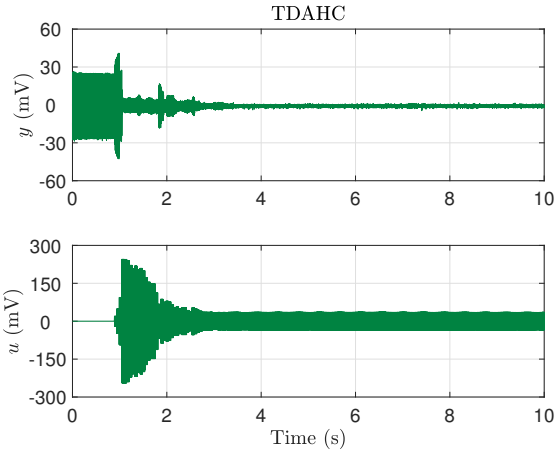

Figure 4.60: TDAHC with IC_1.

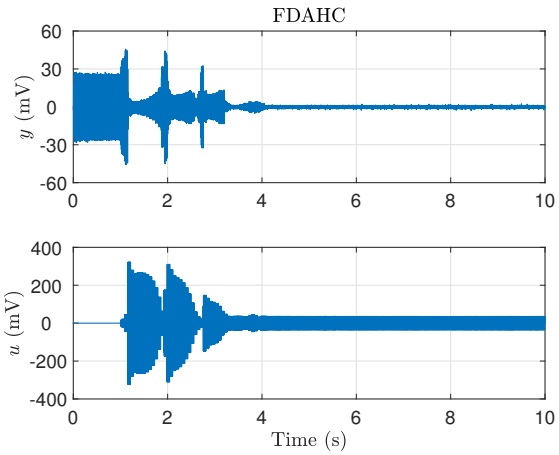

Figure 4.61: FDAHC with IC_3.

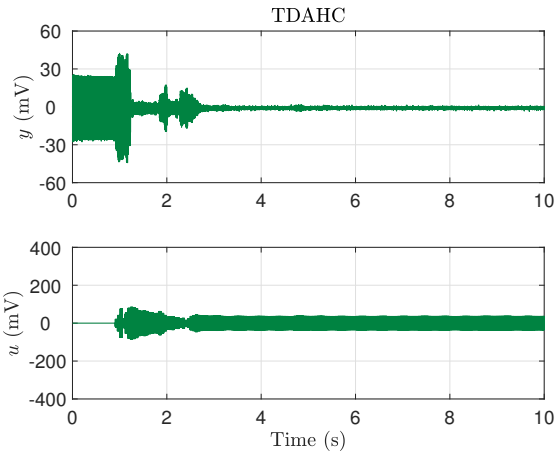

Figure 4.62: TDAHC with IC_3.

response is

$$P \triangleq \max_{k\in\{0,\ldots,N\}} |y(10^{-4}k)|,$$

where $N = 10 \times 10^4$ data points. The magnitude of the peak response averaged over the 16 initial conditions is 32 mV and 35 mV for FDAHC and for TDAHC. However, there are initial conditions (e.g., IC_2, IC_3, and IC_{10}) where TDAHC outperforms FDAHC. This suggests that implementing larger control gains with TDAHC comes at the cost of increasing the magnitude peak response which does not always lend itself to achieving faster convergence speeds.

Figures 4.65 and 4.66 show the average power of y using FDAHC and TDAHC for each of the 16 initial conditions tested. The average power of y for each initial condition is computed using 10 s of data, specifically,

$$J \triangleq \frac{1}{N+1}\sum_{k=0}^{N} \|y(10^{-4}k)\|^2,$$

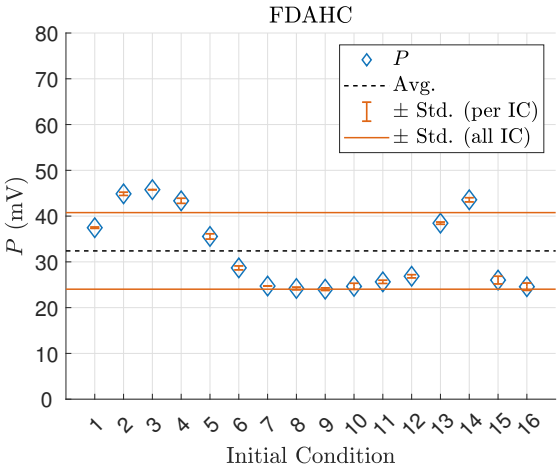

Figure 4.63: Magnitude of the peak response for FDAHC.

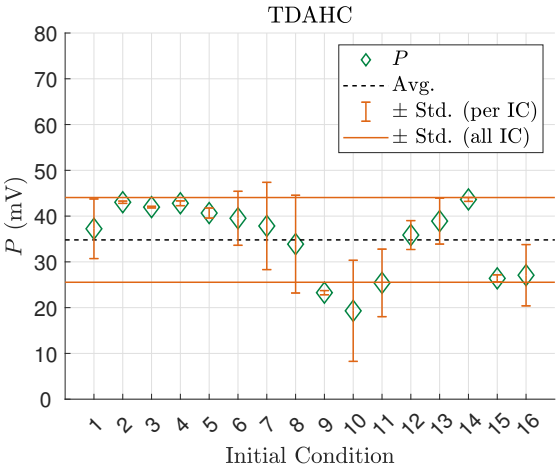

Figure 4.64: Magnitude of the peak response for TDAHC.

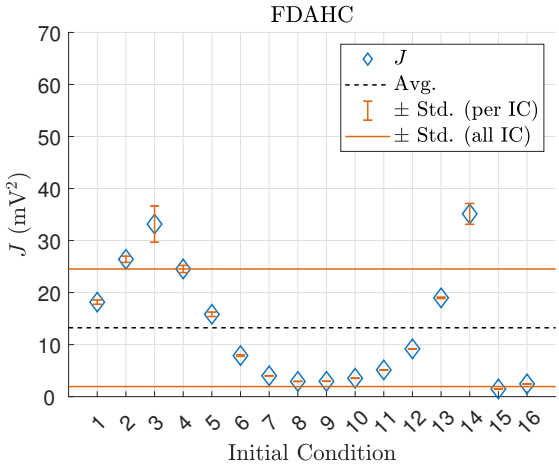

Figure 4.65: Average power for FDAHC.

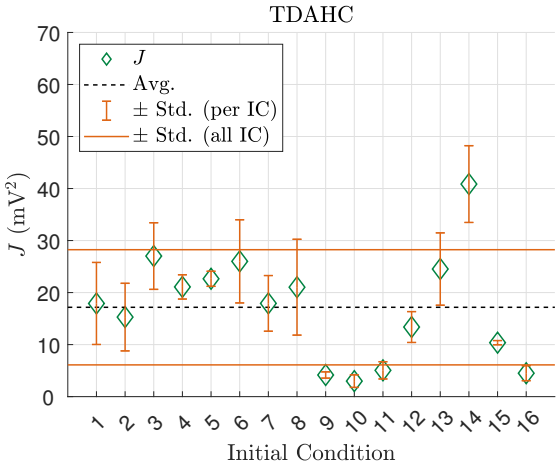

Figure 4.66: Average power for TDAHC.

Table 4.4: Experiment 4.3 summary of results.

Metric	FDAHC	TDAHC
Average Convergence Time (s)	0.82	0.95
Average Power (mV^2)	12	17
Magnitude of Peak Response (mV)	32	35

where $N = 10 \times 10^4$ data points. Figures 4.65 and 4.66 show that FDAHC generally has a lower average power compared to TDAHC. The average power among all trials is 12 mV^2 with FDAHC and 17 mV^2 with TDAHC.

Table 4.4 summarizes the average values among all trials for metrics of convergence time, average power, and peak of peak response. Based on the results in Figs. 4.57–4.58 and Figs. 4.63–4.66, we conclude that FDAHC tends to outperform TDAHC under this experiment configuration if convergence speed is the objective.

Table 4.5: Control parameters for Experiment 4.4.

Parameter.	FDAHC	TDAHC
T_{s}	0.1 s	0.061 s
$\mu_1 = \mu_2$	0.1	0.2
$\gamma_1 = \gamma_2$	0.5	0.8
$\sigma_1 = \sigma_2$	10^{-6}	10^{-6}
$\nu_1 = \nu_2$	10^{-6}	10^{-6}
R_{m}	100	100

Experiment 4.4. This experiment shows that FDAHC and TDAHC are capable of asymptotically rejecting a multi-tone (specifically, $q = 2$) disturbance acting on an unknown SISO system. We compare the performance of FDAHC and TDAHC using both a single-tone and multi-tone disturbance. We use two initial conditions for $G_{i,k}$, which have angles that are 180° apart. The 180° difference guarantees that one of the initial conditions satisfies the HHC stability condition (i.e., $G_{i,0}$ is within 90° of $G_{yu}(\jmath\omega_i)$), whereas the other initial condition does not satisfy the stability condition.

The configuration for this experiment is shown in Fig. 4.67. In this configuration, one microphone measures the response y, one speaker provides the control u, and one speaker provides the disturbance d_i. We use two disturbance frequencies for this test, let $f_1 = 180$ Hz and let $f_2 = 200$ Hz. For the case of a single-tone disturbance using f_1, we let

$$d(t) = \eta_1(t) \triangleq 0.0065 \sin 2\pi f_1 t + 0.0065 \cos 2\pi f_1 t.$$

For the case of a single-tone disturbance using f_2, we let

$$d(t) = \eta_2(t) \triangleq 0.0065 \sin 2\pi f_2 t + 0.0065 \cos 2\pi f_2 t.$$

For the case of a multi-tone disturbance using f_1 and f_2, we let

$$d(t) = \eta_3(t) \triangleq 0.0065 \sin 2\pi f_1 t + 0.0065 \cos 2\pi f_1 t + 0.0078 \sin 2\pi f_2 t + 0.0078 \cos 2\pi f_2 t.$$

We consider the initial condition $0.3 - \jmath 0.3$ and $-0.3 + \jmath 0.3$, which have angles that are 180° apart.

The parameters μ_i, γ_i, T_{s}, σ_i, ν_i are selected based on empirical testing to obtain good convergence speed and a low peak transient response. Table 4.5 shows the algorithm parameters used in this experiment.

The system response y and u is presented in Figs. 4.68–4.73 for FDAHC and TDAHC with $G_{i,0} = 0.3 - \jmath 0.3$ and $G_{i,0} = -0.3 + \jmath 0.3$, where $i \in \{1, 2\}$ as appropriate. Both FDAHC and TDAHC attenuate the single-tone and multi-tone disturbances yielding near-zero steady-state performance.

For each trial, convergence time $t_{\mathrm{conv}} \geq 0$ is the smallest time such that

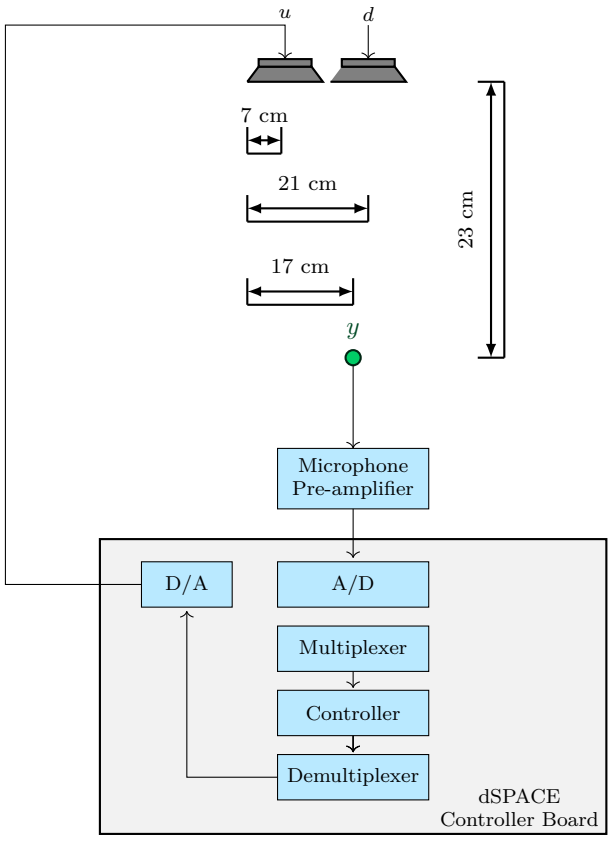

Figure 4.67: Experiment 4.4 configuration

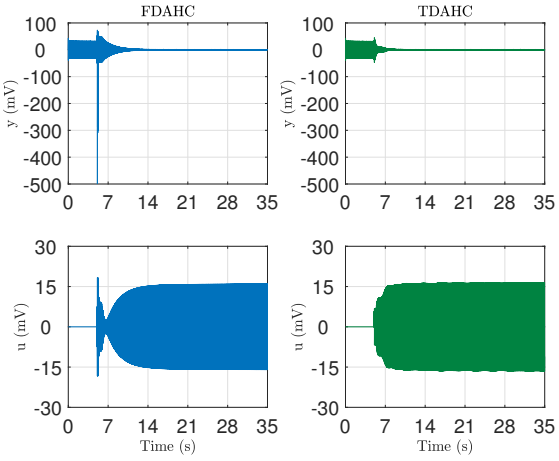

Figure 4.68: Response to single-tone disturbance $d = \eta_1$ using $G_{1,0} = 0.3 - \jmath 0.3$.

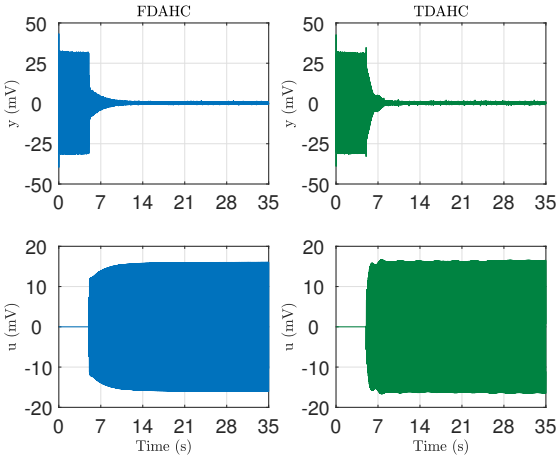

Figure 4.69: Response to single-tone disturbance $d = \eta_1$ using $G_{1,0} = -0.3 + \jmath 0.3$.

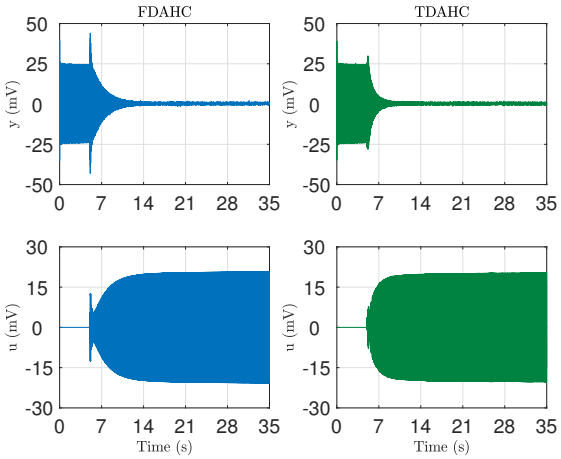

Figure 4.70: Response to single-tone disturbance $d = \eta_2$ using $G_{1,0} = 0.3 - \jmath 0.3$.

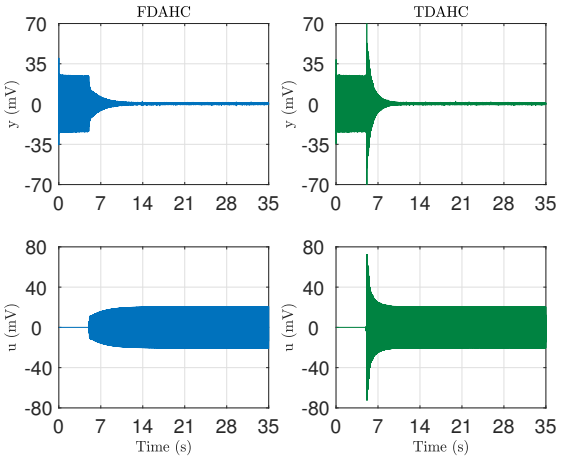

Figure 4.71: Response to single-tone disturbance $d = \eta_2$ using $G_{1,0} = -0.3 + \jmath 0.3$.

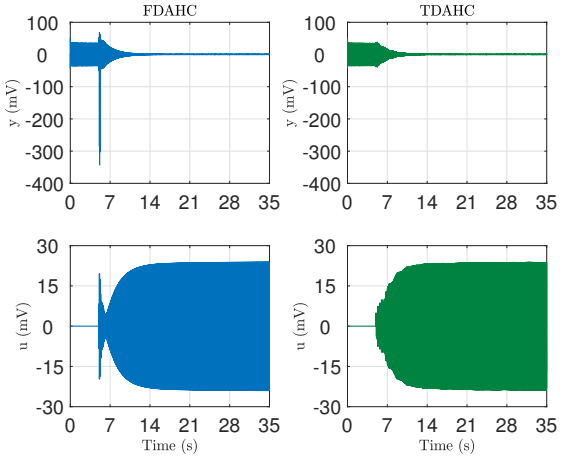

Figure 4.72: Response to multi-tone disturbance $d = \eta_3$ using $G_{1,0} = G_{2,0} = 0.3 - \jmath 0.3$.

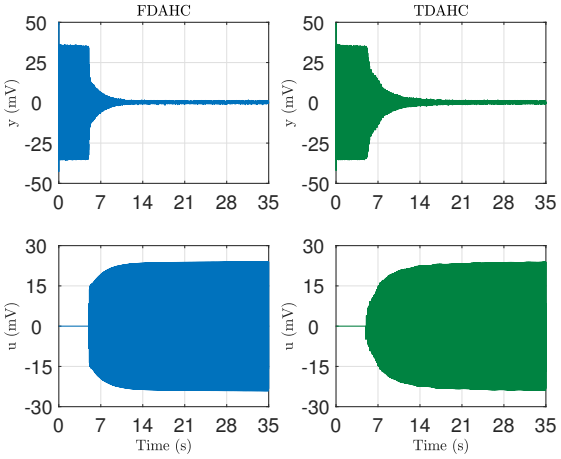

Figure 4.73: Response to multi-tone disturbance $d = \eta_3$ using $G_{1,0} = G_{2,0} = -0.3 + \jmath 0.3$.

Table 4.6: Convergence time.

	$G_{1,0} = 0.3 - \jmath 0.3$		$G_{1,0} = -0.3 + \jmath 0.3$	
	FDAHC	TDAHC	FDAHC	TDAHC
$d = \eta_1$	9.6 s	5.2 s	5.2 s	4.0 s
$d = \eta_2$	7.8 s	4.7 s	6.1 s	4.8 s
$d = \eta_3$	8.7 s	8.2 s	5.8 s	12.5 s

$$\min_{t \geq t_{\text{conv}}} |y(t)| \leq \delta_{\text{conv}},$$

where the threshold $\delta_{\text{conv}} = 0.5 \times 10^{-3}$ V is determined from that data noise level. A comparison of the single-tone disturbance response to the multi-tone disturbance response shows that FDAHC attenuates the single-tone and multi-tone disturbance in approximately the same time. In contrast, TDAHC attenuates the single-tones more quickly. Table 4.6 presents the convergence times. The average FDAHC convergence time with the single-tone disturbances is 7.2 s compared to 7.3 s with the multi-tone disturbance. In contrast, the average TDAHC convergence time with the single-tone disturbances is 4.7 s compared to 10.4 s with the multi-tone disturbance. This suggests that the number of disturbance tones has a small impact on FDAHC convergence time.

A comparison of the magnitude of the peak responses for each case shows that with FDAHC is generally higher than that with TDAHC magnitude of peak response. Table 4.7 presents the magnitude of peak response for each algorithm. The magnitude of the peak response is

$$P \triangleq \max_{k \in \{0,\ldots,N\}} |y(10^{-4}k)|,$$

where $N = 35 \times 10^4$ data points. The average single-tone FDAHC magnitude of peak response is 153 mV^2 while the average single-tone TDAHC magnitude of peak response is 46 mV^2. Similarly, a comparison of the multi-tone disturbance response shows that the FDAHC magnitude of peak response is generally higher than the TDAHC magnitude peak response. The average multi-tone FDAHC magnitude of peak response is 190 mV^2 while the average magnitude of peak response with TDAHC is 37 mV^2.

In conclusion, we note that the number of disturbance tones generally increases convergence times for TDAHC but does not significantly affect FDAHC convergence times. In addition, in contrast to FDAHC, the TDAHC magnitude of peak response is generally not affected by the number of disturbance tones. Note that empirical data suggests if the adaptive control gain γ_1 was selected smaller for each algorithm, the resulting magnitude of the peak response would have likely decreased into a similar range of values. This is because γ_1 directly affects the scaling of $G_{i,k}$ during

Table 4.7: Magnitude of the peak response.

	$G_{1,0} = 0.3 - \jmath 0.3$		$G_{1,0} = -0.3 + \jmath 0.3$	
	FDAHC	TDAHC	FDAHC	TDAHC
$d = \eta_1$	509 mV	47 mV	32 mV	35 mV
$d = \eta_2$	44 mV	30 mV	25 mV	74 mV
$d = \eta_3$	343 mV	39 mV	36 mV	36 mV

each update period and larger values can lead to more adaptation required to reach stability.

Chapter 5
Conclusions and Future Work

We reviewed two adaptive control techniques that address the problem of rejecting sinusoidal disturbances with known frequencies that act on a completely unknown asymptotically stable linear time-invariant (LTI) system. The first method is FDAHC introduced in [11] and the second method is TDAHC introduced in [12]. Modifications of the FDAHC and TDAHC algorithms were presented to address sensor noise and actuator saturation. We demonstrated the effectiveness of each algorithm through numerical simulations in Ch. 2 and Ch. 3. The main contribution in this thesis is presented in Ch. 4 where results from active noise control experiments are presented that examine the strengths and weaknesses of each algorithm when implementing in the real world.

5.1 Trade-offs for Adaptive Algorithms

We summarize the main characteristics and trade-offs of FDAHC and TDAHC in the list below:

1) FDAHC is less susceptible to measurement noise due to the DFT. Since the DFT performs batch processing, it has the effect of filtering out some sensor noise. In contrast, TDAHC does not utilize a DFT and is, thus, more susceptible to measurement noise.

2) FDHAC is less influenced by the transient response due to the averaging properties of the DFT. In contrast, TDAHC is generally more sensitive to the transient response.

3) TDAHC can be implemented with larger control gains which can yield faster steady-state performance convergence times compared to that of FDAHC. However, implementing larger control gains can increase the peak transient response.

4) FDAHC tends to outperform TDAHC when there is uncertainty in the disturbance frequency.

5) The convergence time using FDAHC is generally not affected by the number of disturbance tones. In contrast, TDAHC convergence times tend to increase with the number of disturbance tones. In addition, the magnitude of the peak response is generally larger with FDAHC compared to TDAHC when the number of disturbance tones is increased.

5.2 Recommendations for Future Work

In Ch. 4 we conducted experiments using a combination of speakers and microphones in a controlled environment. In the future, it may be beneficial to explore integrating these control methods into the design of buildings–an environment that is susceptible to noise generation from utilities and equipment. Further consideration should go into addressing the problems of noise that is generated inside ductwork and vibration emitted from mechanical equipment. Currently, these problems are addressed in the industry by over-sizing ductwork to reduce the velocity of the air, installing expensive internal acoustical insulation or sound attenuators, or designing vibration spring isolators. However, these strategies tend to increase building costs, add complexity to the design, and can reduce the space that is available to route other above ceiling utilities. For this reason, it is worth studying how to integrate these control methods into building design to improve the health of the building and happiness of the occupants.

Bibliography

[1] F. Peng, M. Gu, and H.-J. Niemann, "Sinusoidal reference strategy for adaptive feedforward vibration control: numerical simulation and experimental study," *Journal of Sound and Vibration*, vol. 265, no. 5, pp. 1047–1061, 2003.

[2] *ASHRAE Handbook: Heating, Ventilation, and Air Condition Applications*. Atlanta, GA: ASHRAE, 2012.

[3] J. Shaw and N. Albion, "Active control of the helicopter rotor for vibration reduction," *J. Amer. Helicopter Society*, vol. 26, no. 3, pp. 32–39, 1981.

[4] W. A. Welsh, "Helicopter vibration reduction," in *Morphing Wing Technologies*, A. Concilio, I. Dimino, L. Lecce, and R. Pecora, Eds. Butterworth-Heinemann, 2018, pp. 865 – 892.

[5] Y. Mizoshita, S. Hasegawa, and K. Takaishi, "Vibration minimized access control for disk drives," *IEEE Trans. Magnetics*, vol. 32, no. 3, pp. 1793–1798, 1996.

[6] T. Atsumi, T. Arisaka, T. Shimizu, and T. Yamaguchi, "Vibration servo control design for mechanical resonant modes of a hard-disk-drive actuator," *JSME Int. J. Series C Mechanical Systems, Machine Elements and Manufacturing*, vol. 46, no. 3, pp. 819–827, 2003.

[7] V. Patel, J. Cheer, and S. Fontana, "Design and implementation of an active noise control headphone with directional hear-through capability," *IEEE Transactions on Consumer Electronics*, vol. 66, no. 1, pp. 32–40, 2020.

[8] S. Kuo, S. Mitra, and W.-S. Gan, "Active noise control system for headphone applications," *IEEE Transactions on Control Systems Technology*, vol. 14, no. 2, pp. 331–335, 2006.

[9] M. Bodson, "Performance of an adaptive algorithm for sinusodial disturbance rejection in high noise," *Automatica*, vol. 37, pp. 1133–1140, 2001.

[10] Q. Hu and G. Ma, "Variable structure control and active vibration suppression of flexible spacecraft during attitude maneuver," *Aerospace Science and Technology*, vol. 9, no. 4, pp. 307–317, 2005.

[11] M. Kamaldar and J. B. Hoagg, "Adaptive harmonic steady-state control for rejection of sinusoidal disturbances acting on a completely unknown system," *International Journal of Adaptive Control and Signal Processing*, vol. 31, no. 9, pp. 1308–1326, 2017.

[12] ——, "Time-domain adaptive higher-harmonic control for rejection of sinusoidal disturbances," *Journal of Dynamic Systems, Measurement and Control*, vol. 143, no. 5, pp. 051 007.1–2, 2020.

[13] J. B. Hoagg, M. A. Santillo, and D. S. Bernstein, "Internal model control in the shift and delta domains," *IEEE Trans. Autom. Contr.*, vol. 53, pp. 1066–1072, 2008.

[14] B. A. Francis, A. Sebakhy, and W. M. Wonham, "Synthesis of multivariable regulators: The internal model principle," *J. Appl. Math. Optim.*, vol. 1, pp. 64–86, 1974.

[15] W.-H. Chen, J. Yang, L. Guo, and S. Li, "Disturbance-observer-based control and related methods–An overview," *IEEE Trans. Indust. Electr.*, vol. 63, no. 2, pp. 1083–1095, 2016.

[16] M. Bodson, "Rejection of periodic disturbances of unknown and time-varying frequencies," *Int. J. Adapt. Contr. Sig. Proc.*, vol. 19, pp. 67–88, 2005.

[17] L. Guo and W.-H. Chen, "Disturbance attenuation and rejection for systems with nonlinearity via DOBC approach," *Int. J. Robust Nonlin. Contr.*, vol. 15, no. 3, pp. 109–125, 2005.

[18] M. Bodson, A. Sacks, and P. Khosla, "Harmonic generation in adaptive feedforward cancellation schemes," *IEEE Trans. Autom. Contr.*, vol. 39, no. 9, pp. 1939–1944, 1994.

[19] W. Messner and M. Bodson, "Design of adaptive feedforward algorithms using internal model equivalence," *Int. J. Adapt. Contr. Sig. Proc.*, vol. 9, pp. 199–212, 1995.

[20] J.-P. Jiang and D.-x. Li, "Optimal placement and decentralized robust vibration control for spacecraft smart solar panel structures," *Smart Materials and Structures*, vol. 19, p. 085020, 07 2010.

[21] M. Kamaldar and J. B. Hoagg, "Centralized and decentralized adaptive harmonic control for sinusoidal disturbance rejection," *Control Engineering Practice*, vol. 112, p. 104814, 2021.

[22] D. Patt, J. Chandrasekar, D. S. Bernstein, and P. P. Friedmann, "Higher-harmonic-control algorithm for helicopter vibration reduction revisted," *J. Guid. Contr. Dyn.*, vol. 28, no. 5, pp. 918–930, 2005.

[23] P. P. Friedmann and T. A. Millott, "Vibration reduction in rotorcraft using active control: A comparision of various approaches," *J. Guid. Contr. Dyn.*, vol. 18, no. 4, pp. 664–673, 1995.

[24] J. T. Pearson, R. M. Goodall, and I. Lyndon, "Active control of helicopter vibration," *Computer Contr. Eng. J.*, vol. 5, pp. 277–284, 1994.

[25] C. R. Knospe, R. W. Hope, S. M. Tamer, and S. J. Fedigan, "Robustness of adaptive unbalance control of rotors with magnetic bearings," *J. Vibration Contr.*, vol. 2, no. 2, pp. 33–52, 1996.

[26] J. Chandrasekar, L. Liu, D. Patt, P. P. Friedmann, and D. S. Bernstein, "Adaptive harmonic steady-state control for disturbance rejection," *IEEE Trans. Contr. Sys. Tech.*, vol. 14, no. 6, pp. 993–1007, 2006.

[27] M. Kamaldar and J. B. Hoagg, "Adaptive control for rejection of a sinusoidal disturbance with unknown frequency acting on an unknown system," in *2017 American Control Conference (ACC)*, 2017, pp. 5696–5701.

[28] ——, "Adaptive harmonic control for rejection of sinusoidal disturbances acting on an unknown system," *IEEE Transactions on Control Systems Technology*, vol. 28, no. 2, pp. 277–290, 2020.

[29] J. Hong, J. C. Ackers, R. Venugopal, M. N. Lee, A. G. Sparks, P. D. Washabaugh, and D. S. Bernstein, "Modeling, identification, and feedback control of noise in an acoustic duct," *IEEE Trans. Contr. Sys. Tech.*, vol. 4, pp. 283–291, 1996.

[30] D. S. Bernstein and D. S. Bernstein, *Scalar, vector, and matrix mathematics: theory, facts, and formulas*. Princeton: Princeton University Press, 2018.

Vita

William Grayson Woods was born in Greensboro, NC. He received a B.S.M.E. degree from the University of Kentucky, Lexington, KY, in 2016. He currently works as a professionally licensed mechanical/electrical/plumbing design engineer.